nagra.

Arbeitsbericht NAB 21-22

TBO Bözberg-2-1: Data Report

Dossier V
Structural Geology

April 2022

National Cooperative
for the Disposal of
Radioactive Waste

Hardstrasse 73
P.O. Box 280
5430 Wettingen
Switzerland
Tel. +41 56 437 11 11

www.nagra.ch

nagra.

Arbeitsbericht NAB 21-22

TBO Bözberg-2-1: Data Report

Dossier V Structural Geology

April 2022

A. Ebert[1], L. Gregorczyk[1], S. Cioldi[1], E. Hägerstedt[1] & M. Gysi[2]

[1] Geologiegemeinschaft Strukturgeologie-Experten Nagra Tiefbohrungen

[2] Nagra

Keywords:
BOZ1-1, Jura Ost, TBO, deep drilling campaign, structural geology, goniometry, drill cores

National Cooperative for the Disposal of Radioactive Waste

Hardstrasse 73
P.O. Box 280
5430 Wettingen
Switzerland
Tel. +41 56 437 11 11

www.nagra.ch

Nagra Arbeitsberichte ("Working Reports") present the results of work in progress that have not necessarily been subject to a comprehensive review. They are intended to provide rapid dissemination of current information.

This NAB aims at reporting drilling results at an early stage. Additional borehole-specific data will be published elsewhere.

In the event of inconsistencies between dossiers of this NAB, the dossier addressing the specific topic takes priority. In the event of discrepancies between Nagra reports, the chronologically later report is generally considered to be correct. Data sets and interpretations laid out in this NAB may be revised in subsequent reports. The reasoning leading to these revisions will be detailed there.

This Dossier was prepared by a project team consisting of:
A. Ebert (core description, core photograph picking, core goniometry, writing and QC)
L. Gregorczyk (core description, core photograph picking, core goniometry, writing and QC)
S. Cioldi (core description, core photograph picking and core goniometry)
E. Hägerstedt (core description, core photograph picking and core goniometry)
M. Gysi (project management, conceptualisation and QC)

Editorial work: Geomecon, P. Blaser and M. Unger

The Dossier has greatly benefitted from technical discussions with, and reviews by, external and internal experts. Their input and work are very much appreciated.

"Copyright © 2022 by Nagra, Wettingen (Switzerland) / All rights reserved.
All parts of this work are protected by copyright. Any utilisation outwith the remit of the copyright law is unlawful and liable to prosecution. This applies in particular to translations, storage and processing in electronic systems and programs, microfilms, reproductions, etc."

Table of Contents

Table of Contents I

List of Tables II

List of Figures III

List of Appendices VIII

1 Introduction 1
1.1 Context 1
1.2 Location and specifications of the borehole 2
1.3 Documentation structure for the BOZ2-1 borehole 6
1.4 Scope and objectives of this dossier 7
1.5 Petrophysical logs and preliminary log analysis available 7
1.6 Borehole deviation 8

2 Methodology 9
2.1 Core goniometry 9
2.1.1 Introduction 9
2.1.2 Workflow 9
2.1.3 Dip picking and dip type classification 11
2.1.4 Dip data for non-oriented and missing cores 14
2.1.5 Goniometry confidence assessment and uncertainties 16
2.2 Structural work 20
2.3 Geo-statistical evaluation 27

3 Inventory of structure types 29
3.1 Examples of fault planes 29
3.2 Examples of fault zones 36
3.3 Examples of joints 37
3.4 Examples of veins / tension gashes 39
3.5 Examples of stylolites 40
3.6 Examples of open pores 42
3.7 Examples of drilling-induced fractures 45

4 Geo-statistical evaluation: results 49
4.1 Entire cored borehole section (260.00 m to 829.88 m MD [log depth]) 49
4.1.1 Basic structural dip evaluation 49
4.1.2 Natural structural discontinuities 53
4.1.3 Fracture density (P32) and distribution 62
4.1.4 Kinematic indicators 62
4.2 Malm 67
4.2.1 Wildegg Formation 67

4.3 Dogger 74
4.3.1 Hauptrogenstein to Ifenthal Formation 74
4.3.2 Passwang Formation 80
4.3.3 Opalinus Clay 86
4.4 Lias (Staffelegg Formation) 91
4.5 Keuper 98
4.5.1 Klettgau Formation 98
4.5.2 Bänkerjoch Formation 104
4.6 Muschelkalk 110
4.6.1 Schinznach Formation 110
4.6.2 Zeglingen Formation 116

5 Main structural findings 117
5.1 Single fracture at 351.70 m MD 117
5.2 Deformation zone in the Opalinus Clay between 509.03 m and 510.74 m MD 118
5.3 Deformation zone in the Opalinus Clay between 530.51 m and 533.22 m MD 123

6 References 129

List of Tables

Tab. 1-1: General information about the BOZ2-1 borehole 2
Tab. 1-2: Core and log depth for the main lithostratigraphic boundaries in the BOZ2-1 borehole 5
Tab. 1-3: List of dossiers included in NAB 21-22 6
Tab. 2-1: Core goniometry confidence assessment of the analysed borehole interval 16
Tab. 2-2: Types of structural discontinuities identified in this study 21
Tab. 2-3: Systematically recorded parameters for the investigated structures 24
Tab. 4-1: Vector means of orientation values for bedding planes and structural discontinuities (Azim: dip azimuth) 49
Tab. 4-2: List of interpreted fault zones, mirror-like fault planes (MirFP) and associated FDC 55
Tab. 4-3: List of all kinematic indicators in oriented and non-oriented cores 63

List of Figures

Fig. 1-1: Tectonic overview map with the three siting regions under investigation 1
Fig. 1-2: Overview map of the investigation area in the Jura Ost siting region with the location of the BOZ2-1 borehole in relation to the boreholes Riniken and BOZ1-1 3
Fig. 1-3: Lithostratigraphic profile and casing scheme for the BOZ2-1 borehole 4
Fig. 1-4: Borehole deviation within the cored section 8
Fig. 2-1: Using a goniometer to determine kinematic indicators along faults 11
Fig. 2-2: Symbols for dip types, fracture density classes and kinematic data used for this study 12
Fig. 2-3: Two fault planes identified at 272.67 m and 273.00 m MD (log depth) in the Wildegg Formation 13
Fig. 2-4: Example of dip data in a non-oriented core interval 14
Fig. 2-5: Interval without 360° core photographs from 626.65 m to 627.72 m MD (log depth) in the Klettgau Formation 15
Fig. 2-6: Core – FMI / UBI correlation for a fault at 508.04 m MD (log depth) in the Opalinus Clay 17
Fig. 2-7: Core – FMI / UBI correlation from 575.80 m to 576.80 m MD (log depth) in the Staffelegg Formation 18
Fig. 2-8: Core – FMI / UBI correlation for subhorizontal to shallow dipping bedding 19
Fig. 2-9: The five main groups of structural discontinuities 21
Fig. 2-10: Completed DIN A3 sheet of primary record of the detailed structural core analysis 26
Fig. 3-1: Fault plane 29
Fig. 3-2: Fault plane 30
Fig. 3-3: Mirror-like fault plane 31
Fig. 3-4: Mirror-like fault plane 32
Fig. 3-5: Stylolitic fault plane 33
Fig. 3-6: Stylolitic fault plane 34
Fig. 3-7: Synsedimentary faults 35
Fig. 3-8: Fault zone with FDC 3 36
Fig. 3-9: Fault zone with FDC 3 36
Fig. 3-10: Joint 37
Fig. 3-11: Joint 38
Fig. 3-12: Joint 38
Fig. 3-13: Vein / tension gash 39
Fig. 3-14: Vein / tension gash 39

Fig. 3-15: Vein / tension gash 40
Fig. 3-16: Stylolite 40
Fig. 3-17: Stylolite 41
Fig. 3-18: Open pores 42
Fig. 3-19: Open pores 43
Fig. 3-20: Open pores 44
Fig. 3-21: Petal fractures, indicated by yellow arrows 45
Fig. 3-22: Drilling-induced fractures 45
Fig. 3-23: Discing 46
Fig. 3-24: Discing 47
Fig. 4-1: Stereogram and depth plot for bedding planes (n = 352) for the entire cored borehole section 50
Fig. 4-2: Dip azimuth rose diagram, dip histogram and depth plot for bedding planes (n = 352) for the entire cored borehole section 51
Fig. 4-3: Vector azimuth (or walkout) plot with bedding dips (n = 352) in oriented cores 52
Fig. 4-4: Overview plot showing P32 fracture densities along the BOZ2-1 borehole 54
Fig. 4-5: Stereogram and depth plot of fault planes for the entire cored interval 56
Fig. 4-6: Dip azimuth rose diagram, dip histogram and depth plot for fault planes in the entire cored interval 57
Fig. 4-7: Stereogram and depth plot for tension gashes / veins, unassigned fractures and joints in the entire cored interval 58
Fig. 4-8: Dip azimuth rose diagram of tension gashes / veins, unassigned fractures and joints in the entire cored interval 59
Fig. 4-9: Stereogram and depth plot for stylolites (n = 580) along the cored BOZ2-1 borehole 60
Fig. 4-10: Dip azimuth rose diagram and depth plot for stylolites in the entire cored interval 61
Fig. 4-11: Plunge azimuth of striations along fault planes in the entire cored interval 63
Fig. 4-12: Stereogram of striations on all oriented fault planes (including multiple lineations on a single fault plane) and associated kinematic data 64
Fig. 4-13: Stereogram with striations of oriented thrust / reverse fault planes (including multiple lineations on a single fault plane) 64
Fig. 4-14: Stereogram of striations on all oriented normal fault planes (including multiple lineations on a single fault plane) 65
Fig. 4-15: Stereogram of striations on all oriented strike-slip fault planes 65
Fig. 4-16: Stereogram of striations on all fault planes with unknown shear sense (including multiple lineations on a single fault plane) 66
Fig. 4-17: Stereogram and depth plot of fault planes (Wildegg Formation) 67

Fig. 4-18: Dip azimuth rose diagram, dip histogram and depth plot of fault planes (Wildegg Formation) 68

Fig. 4-19: Stereogram and depth plot of tension gashes / veins and unassigned fractures (Wildegg Formation) 69

Fig. 4-20: Dip azimuth rose diagram, dip histogram and depth plot of tension gashes / veins, joints and unassigned fractures (Wildegg Formation) 70

Fig. 4-21: Stereogram and depth plot of stylolites (Wildegg Formation; n = 23) 71

Fig. 4-22: Dip azimuth rose diagram, dip histogram and depth plot of stylolites (Wildegg Formation; n = 23) 72

Fig. 4-23: Stereogram of striations on fault planes, including multiple lineations on a single fault plane (Wildegg Formation; n = 21) 73

Fig. 4-24: Stereogram and depth plot of fault planes (Hauptrogenstein to Ifenthal Formation) 74

Fig. 4-25: Dip azimuth rose diagram, dip histogram and depth plot of fault planes (Hauptrogenstein to Ifenthal Formation) 75

Fig. 4-26: Stereogram and depth plot of tension gashes / veins, joints and unassigned fractures (Hauptrogenstein to Ifenthal Formation) 76

Fig. 4-27: Stereogram and depth plot of stylolites (Hauptrogenstein to Ifenthal Formation; n = 274) 77

Fig. 4-28: Dip azimuth rose diagram, dip histogram and depth plot of stylolites (Hauptrogenstein to Ifenthal Formation; n = 274) 78

Fig. 4-29: Stereogram of striations on fault planes, including multiple lineations on a single fault plane (Hauptrogenstein to Ifenthal Formation; n = 38) 79

Fig. 4-30: Stereogram and depth plot of fault planes (Passwang Formation) 80

Fig. 4-31: Stereogram and depth plot of tension gashes / veins, joints and unassigned fractures (Passwang Formation) 81

Fig. 4-32: Dip azimuth rose diagram, dip histogram and depth plot of tension gashes / veins, joints and unassigned fractures (Passwang Formation) 82

Fig. 4-33: Stereogram and depth plot of stylolites (Passwang Formation; n = 15) 83

Fig. 4-34: Dip azimuth rose diagram, dip histogram and depth plot of stylolites (Passwang Formation; n = 15) 84

Fig. 4-35: Stereogram of striations on fault planes (including multiple lineations on a single fault plane) (Passwang Formation; n = 10) 85

Fig. 4-36: Stereogram and depth plot of fault planes (Opalinus Clay) 86

Fig. 4-37: Dip azimuth rose diagram, dip histogram and depth plot of fault planes (Opalinus Clay) 87

Fig. 4-38: Stereogram and depth plot of tension gashes / veins, joints and unassigned fractures (Opalinus Clay) 88

Fig. 4-39: Dip azimuth rose diagram, dip histogram and depth plot of tension gashes / veins, joints and unassigned fractures (Opalinus Clay) 89

Fig. 4-40: Stereogram of striations on fault planes, including multiple lineations on a single fault plane (Opalinus Clay; n = 114) 90

Fig. 4-41: Stereogram and depth plot of fault planes (Lias) 91
Fig. 4-42: Dip azimuth rose diagram, dip histogram and depth plot of fault planes (Lias) 92
Fig. 4-43: Stereogram and depth plot of tension gashes / veins, joints and unassigned fractures (Lias) 93
Fig. 4-44: Dip azimuth rose diagram, dip histogram and depth plot of tension gashes / veins, joints and unassigned fractures (Lias) 94
Fig. 4-45: Stereogram and depth plot of stylolites (Lias; n = 20) 95
Fig. 4-46: Dip azimuth rose diagram, dip histogram and depth plot of stylolites (Lias; n = 20) 96
Fig. 4-47: Stereogram of striations on fault planes (Lias; n = 16) 97
Fig. 4-48: Stereogram and depth plot of faults (Klettgau Formation) 98
Fig. 4-49: Dip azimuth rose diagram, dip histogram and depth plot of faults (Klettgau Formation) 99
Fig. 4-50: Stereogram and depth plot of tension gashes / veins, joints and unassigned fractures (Klettgau Formation) 100
Fig. 4-51: Dip azimuth rose diagram, dip histogram and depth plot of tension gashes / veins, joints and unassigned fractures (Klettgau Formation) 101
Fig. 4-52: Stereogram and depth plot of stylolites (Klettgau Formation; n = 2) 102
Fig. 4-53: Stereogram of striations on fault planes, including multiple lineations on a single fault plane (Klettgau Formation; n = 93) 103
Fig. 4-54: Stereogram and depth plot of faults (Bänkerjoch Formation) 104
Fig. 4-55: Dip azimuth rose diagram, dip histogram and depth plot of faults (Bänkerjoch Formation) 105
Fig. 4-56: Stereogram and depth plot of tension gashes / veins, joints and unassigned fractures (Bänkerjoch Formation) 106
Fig. 4-57: Dip azimuth rose diagram, dip histogram and depth plot of tension gashes / veins, joints and unassigned fractures (Bänkerjoch Formation) 107
Fig. 4-58: Stereogram and depth plot of stylolites (Bänkerjoch Formation; n = 3) 108
Fig. 4-59: Stereogram of striations on fault planes, including multiple lineations on a single fault plane (Bänkerjoch Formation; n = 250) 109
Fig. 4-60: Stereogram and depth plot of fault planes (Schinznach Formation) 110
Fig. 4-61: Dip azimuth rose diagram, dip histogram and depth plot of fault planes (Schinznach Formation) 111
Fig. 4-62: Stereogram and depth plot of tension gashes / veins, joints and unassigned fractures (Schinznach Formation) 112
Fig. 4-63: Dip azimuth rose diagram, dip histogram and depth plot of tension gashes / veins, joints and unassigned fractures (Schinznach Formation) 113
Fig. 4-64: Stereogram and depth plot of stylolites (Schinznach Formation; n = 243) 114
Fig. 4-65: Dip azimuth rose diagram, dip histogram and depth plot of stylolites (Schinznach Formation; n = 243) 115

Fig. 4-66: Stereogram of striations of fault planes, including multiple lineations on a single fault plane (Schinznach Formation; n = 41) 116

Fig. 5-1: Single joint at 351.70 m MD (log depth)..... 117

Fig. 5-2: Overview plot of the Opalinus Clay with the well visible deformation zone from 509.03 m to 510.74 m MD (log depth) 119

Fig. 5-3: Stereogram and depth plot of fault planes from the depth interval 507.7 m to 512.2 m MD (log depth)..... 120

Fig. 5-4: Dip azimuth rose diagrams showing dip directions and depth plot of fault planes from the depth interval 507.7 m to 512.2 m MD (log depth)..... 121

Fig. 5-5: Stereogram of fault planes and associated striations within (red) and around (black) the deformation zone..... 122

Fig. 5-6: Overview plot of the deformed Opalinus Clay from 530.51 m to 533.22 m MD (log depth) 124

Fig. 5-7: Example of mineralised fault plane within the Opalinus Clay at 531.9 m MD (log depth) 125

Fig. 5-8: Stereogram of fault planes and bedding around and within the deformed Opalinus Clay, from the depth interval 529.6 m to 534.6 m MD (log depth)..... 126

Fig. 5-9: Dip azimuth rose diagram, dip histogram and depth plot of fault planes within the deformed Opalinus Clay from the depth interval 529.6 m to 534.6 m MD (log depth)..... 127

Fig. 5-10: Stereogram of fault planes and associated striations within the deformation zone..... 128

List of Appendices

App. A: Lithostratigraphy profile Bözberg-2-1, 1:2'500, 0.00 m to 829.11 m MD core depth

App. B: Structural geology profile Bözberg-2-1, 1:1'000, 250.00 m to 829.88 m MD log depth

App. C-1: Structural geology profile Bözberg-2-1, 1:100, 250.00 m to 525.00 m MD log depth

App. C-2: Structural geology profile Bözberg-2-1, 1:100, 500.00 m to 775.00 m MD log depth

App. C-3: Structural geology profile Bözberg-2-1, 1:100, 750.00 m to 829.88 m MD log depth

App. D-1: Overview plot of stereograms and rose diagrams: Villigen to Klettgau Fm.

App. D-2: Overview plot of stereograms and rose diagrams: Bänkerjoch to Schinznach Fm.

App. E-1: Core goniometry depth shift table

App. E-2: Core goniometry rotation angle table

App. F: Lithostratigraphy patterns, colours, weathering index and symbols for lithostratigraphy

Note: In the digital version of this report the appendices can be found under the paper clip symbol.

1 Introduction

1.1 Context

To provide input for site selection and the safety case for deep geological repositories for radioactive waste, Nagra has drilled a series of deep boreholes ("Tiefbohrungen", TBO) in Northern Switzerland. The aim of the drilling campaign is to characterise the deep underground of the three remaining siting regions located at the edge of the Northern Alpine Molasse Basin (Fig. 1-1).

In this report, we present the results from the Bözberg-2-1 borehole.

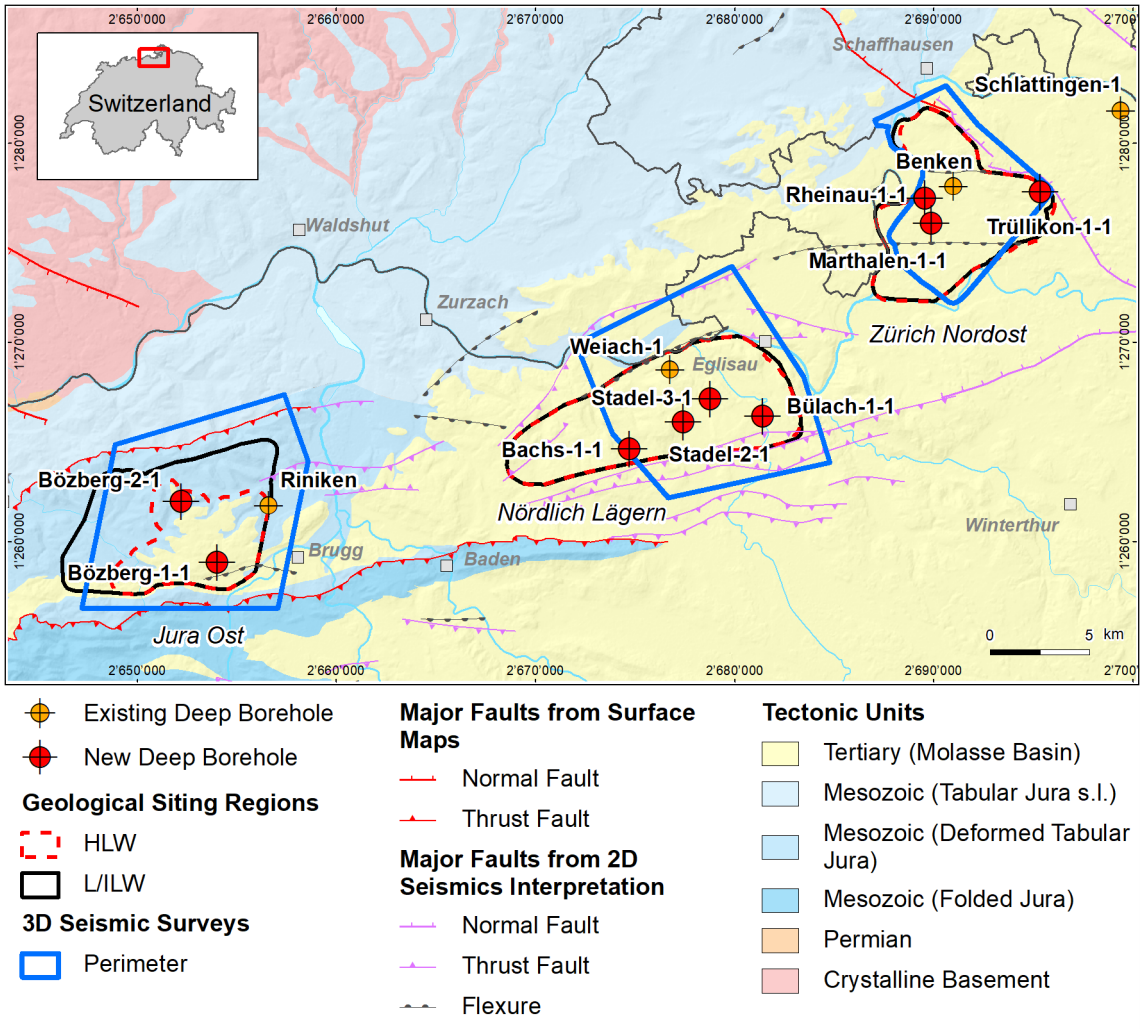

Fig. 1-1: Tectonic overview map with the three siting regions under investigation

1.2 Location and specifications of the borehole

The Bözberg-2-1 (BOZ2-1) exploratory borehole is the fifth borehole drilled within the framework of the TBO project. The drill site is located in the northern part of the Jura Ost siting region (Fig. 1-2). The vertical borehole reached a final depth of 829.11 m (MD)[1]. The borehole specifications are provided in Tab. 1-1.

Tab. 1-1: General information about the BOZ2-1 borehole

Siting region	Jura Ost
Municipality	Bözberg (Canton Aargau / AG), Switzerland
Drill site	Bözberg-2 (BOZ2)
Borehole	Bözberg-2-1 (BOZ2-1)
Coordinates	LV95: 2'652'218.764 / 1'261'985.437
Elevation	Ground level = top of rig cellar: 624.33 m above sea level (asl)
Borehole depth	829.11 m measured depth (MD) below ground level (bgl)
Drilling period	11th August – 14th December 2020 (spud date to end of rig release)
Drilling company	Daldrup & Söhne AG
Drilling rig	Wirth B 152t
Drilling fluid	Water-based mud with various amounts of different components such as[2]: 0 – 370 m: Bentonite & polymers 370 – 615 m: Potassium silicate & polymers 615 – 829.11 m: Pure-Bore®

The lithostratigraphic profile and the casing scheme are shown in Fig. 1-3. The comparison of the core versus log depth[3] of the main lithostratigraphic boundaries in the BOZ2-1 borehole is shown in Tab. 1-2.

[1] Measured depth (MD) refers to the position along the borehole trajectory, starting at ground level, which for this borehole is the top of the rig cellar. For a perfectly vertical borehole, MD below ground level (bgl) and true vertical depth (TVD) are the same. In all Dossiers depth refers to MD unless stated otherwise.

[2] For detailed information see Dossier I.

[3] Core depth refers to the depth marked on the drill cores. Log depth results from the depth observed during geophysical wireline logging. Note that the petrophysical logs have not been shifted to core depth, hence log depth differs from core depth.

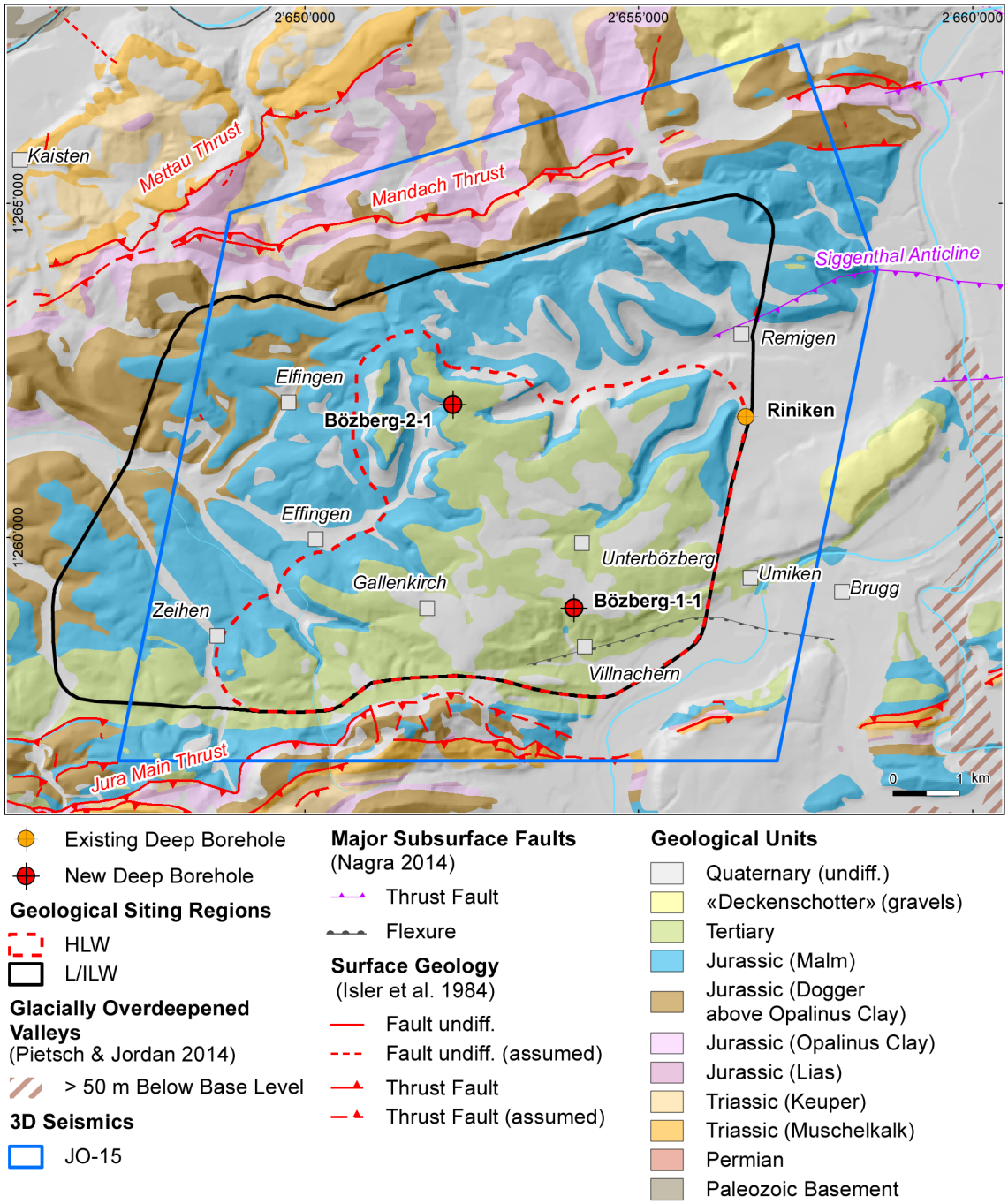

Fig. 1-2: Overview map of the investigation area in the Jura Ost siting region with the location of the BOZ2-1 borehole in relation to the boreholes Riniken and BOZ1-1

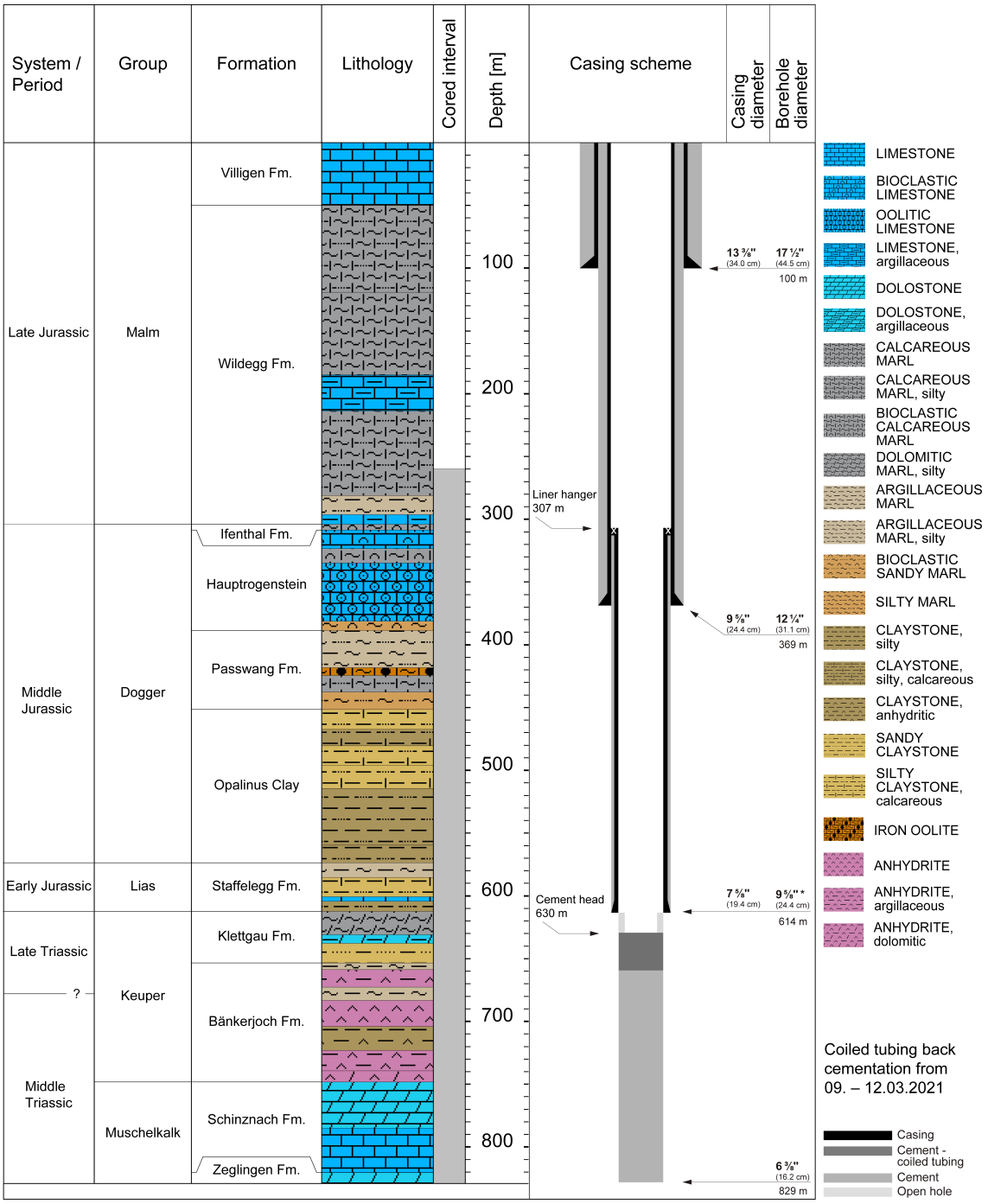

Fig. 1-3: Lithostratigraphic profile and casing scheme for the BOZ2-1 borehole[4]

[4] For detailed information see Dossier I and III.

Tab. 1-2: Core and log depth for the main lithostratigraphic boundaries in the BOZ2-1 borehole[5]

System / Period	Group	Formation	Core depth in m (MD)	Log depth in m (MD)	
Jurassic	Malm	Villigen Formation	50.0		—
		Wildegg Formation	303.95	304.38	—
	Dogger	Ifenthal Formation	308.70	309.07	—
		Hauptrogenstein	388.54	388.97	—
		Passwang Formation	451.54	451.90	—
		Opalinus Clay	573.68	573.89	—
	Lias	Staffelegg Formation	**612.46**	**612.76**	—
Triassic	Keuper	Klettgau Formation	653.45	654.70	—
		Bänkerjoch Formation	748.27	749.52	—
	Muschelkalk	Schinznach Formation	820.32	821.09	—
		Zeglingen Formation	829.11 final depth	829.88	—

[5] For details regarding lithostratigraphic boundaries see Dossier III and IV; for details about depth shifts (core goniometry) see Section 2.1.

1.3 Documentation structure for the BOZ2-1 borehole

NAB 21-22 documents the majority of the investigations carried out in the BOZ2-1 borehole, including laboratory investigations on core material. The NAB comprises a series of stand-alone dossiers addressing individual topics and a final dossier with a summary composite plot (Tab. 1-3).

This documentation aims at early publication of the data collected in the BOZ2-1 borehole. It includes most of the data available approximately one year after completion of the borehole. Some analyses are still ongoing (e.g. diffusion experiments, analysis of veins, hydrochemical interpretation of water samples) and results will be published in separate reports.

The current borehole report will provide an important basis for the integration of datasets from different boreholes. The integration and interpretation of the results in the wider geological context will be documented later in separate geoscientific reports.

Tab. 1-3: List of dossiers included in NAB 21-22

Black indicates the dossier at hand.

Dossier	Title	Authors
I	TBO Bözberg-2-1: Drilling	P. Hinterholzer-Reisegger
II	TBO Bözberg-2-1: Core Photography	D. Kaehr & M. Gysi
III	TBO Bözberg-2-1: Lithostratigraphy	P. Jordan, P. Schürch, H. Naef, M. Schwarz, R. Felber, T. Ibele & M. Gysi
IV	TBO Bözberg-2-1: Microfacies, Bio- and Chemostratigraphic Analyses	S. Wohlwend, H.R. Bläsi, S. Feist-Burkhardt, B. Hostettler, U. Menkveld-Gfeller, V. Dietze & G. Deplazes
V	TBO Bözberg-2-1: Structural Geology	A. Ebert, L. Gregorczyk, S. Cioldi, E. Hägerstedt & M. Gysi
VI	TBO Bözberg-2-1: Wireline Logging, Micro-hydraulic Fracturing and Pressure-meter Testing	J. Gonus, E. Bailey, J. Desroches & R. Garrard
VII	TBO Bözberg-2-1: Hydraulic Packer Testing	R. Schwarz, M. Willmann, S. Reinhardt, S.M.L. Hardie, M. Voß & A. Pechstein
VIII	TBO Bözberg-2-1: Rock Properties, Porewater Characterisation and Natural Tracer Profiles	T. Gimmi, L. Aschwanden, L. Camesi, E. Gaucher, A. Jenni, M. Kiczka, U. Mäder, M. Mazurek, D. Rufer, H.N. Waber, P. Wersin, C. Zwahlen & D. Traber
IX	TBO Bözberg-2-1: Rock-mechanical and Geomechanical Laboratory Testing	E. Crisci, L. Laloui & S. Giger
X	TBO Bözberg-2-1: Petrophysical Log Analysis	S. Marnat & J.K. Becker
	TBO Bözberg-2-1: Summary Plot	Nagra

1.4 Scope and objectives of this dossier

The dossier at hand (Dossier V) documents the work of the structural geology experts. The objectives of the report are:

- core goniometry to reset drill cores to the correct depth and original orientation based on high resolution borehole images and high resolution 360° core photographs (Appendices E-1 and E-2)
- structural discontinuities identification on high resolution 360° core photographs and drill cores
- true dip and dip azimuth analysis of structures and bedding planes on high resolution 360° photographs in TerraStation II and/or manual measurements with a geological compass on drill cores
- documentation of recorded structures and their relevant parameters
- visualisation of structural geology data as profiles and overview plots:
  - profile 1:1'000: Appendix B
  - profile 1:100: Appendices C-1 to C-3
  - overview plot of stereograms and rose diagrams: Appendices D-1 and D-2

The level of detail in this dossier is limited by the data availability at data cut-off two months after the end of drilling operations. The lithostratigraphic subdivision used in this report is in line with the finding in Dossier III.

1.5 Petrophysical logs and preliminary log analysis available

The petrophysical logs and preliminary log analysis listed below were available at the data-freeze and considered as a supplementary source of information for this report (for more details, see Dossier VI):

- total natural gamma ray borehole and potassium corrected (GR)
- caliper / radius (RD1 to RD6)
- near / array corrected limestone porosity (APLC)
- high resolution formation density (RHO8)
- high resolution formation photoelectric factor (PEF8)
- array laterolog apparent resistivity from computed focusing mode 0 to 5 (RLA1 to RLA5)
- formation micro imager (FMI)
- ultrasonic borehole image (UBI)
- borehole breakouts and centreline fractures analysis based on FMI and UBI images

1.6 Borehole deviation

The cored section of BOZ2-1 is almost vertical, with a slight deviation towards the NNW. The maximum horizontal deviation at TD of 828.88 m MD (log depth) is about 7 m to the NNW (Fig. 2-1).

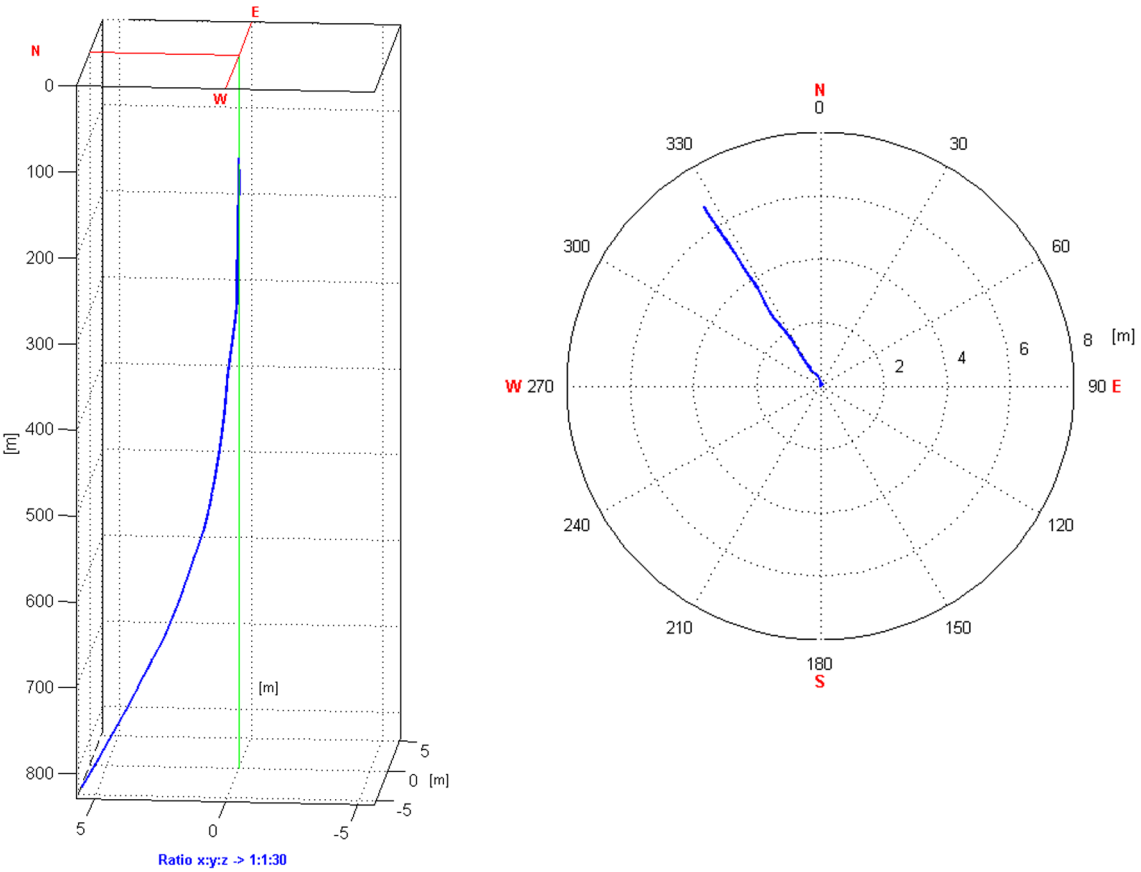

Fig. 1-4: Borehole deviation within the cored section

The left image visualises the borehole path in 3D with a compressed z-axis compared to the x- and y-axes. The borehole azimuth is shown on the right.

2 Methodology

2.1 Core goniometry

2.1.1 Introduction

A structural analysis was performed on drill cores along with circumferential and planar drill core photographs. Using the reference line on the core surface, positioned at an azimuth of 0° during core photography, most drill cores could be oriented using borehole image logs.

For this study, high-resolution 360° and planar photographs were available for most of the cored interval from 260.00 m to 829.88 m MD (log depth). The data were delivered as 905 circumferential and 927 planar photographs in TIF format. However, the original photographs with a resolution of 10 pixels/mm were too large to be handled with TerraStation II (TERRASCIENCES Inc.). Therefore, the original photographs were compressed by 25% and exported with a resolution of 300 dpi. In addition, FMI and UBI logs were available. Both were of good to excellent quality. Further relevant data included auxiliary borehole data, core orientation line and core section listings, lithostratigraphic boundaries and petrophysical logs.

2.1.2 Workflow

This section describes the methodology used for extracting the directional information from 360° core photographs. The following steps were tailored for efficient core goniometry using the TerraStation II software:

1. Quality control of core photographs:

   Prior to loading the data, it was ensured that the core orientation line (red) on the 360° core photographs was set to 0°.

   Note: the core orientation line (COL) represents a continuous reference line set to an azimuth of 0° to fix the relative orientation of drill cores. The COL was drawn on the core surface immediately after core retrieval at the drill site. The line lengths vary widely from a few centimetres up to several metres and therefore sometimes continue over several core sections, depending on whether each individual core section could be fitted together along the core edges or not. If core sections could not be merged, a new COL was determined. The coherent COL was then used to orient the drill core using borehole image logs.

2. Data loading:

   All 360° core photographs were loaded as mirror images in order to simulate the view of the borehole image log looking from inside the borehole. A constant value of 95 mm (3.74") was added as image diameter.

   The processed FMI and UBI logs as well as the auxiliary petrophysical logs were imported into TerraStation II. It was checked that the depth of the petrophysical logs, especially the first GR (gamma ray) run, matched the depth of the FMI data.

3. Depth shifting:

   The 360° core photographs were shifted to FMI logs using distinct, correlated planar and/or non-planar features. For the purpose of simplicity and consistency, only one shift value was applied for each individual core section (generally 3 m per section). This resulted in minor data gaps and / or overlaps at core section boundaries of a few centimetres maximum. In total, 191 distinct depth shift values were applied for the core sections of the entire cored borehole; these varied from + 0.17 m to + 1.37 m. The defined values are listed in Appendix E-1.

4. Core orientation:

   The core was oriented using correlated geological features (e.g. faults / fractures, inclined / deformed bedding, nodules etc.) which were matched with the orientation on the FMI by rotating the 360° core photographs clockwise around the borehole axis.

   The obtained angle of rotation was then applied to the entire core section with a continuous COL. Simultaneously, the validity across other geological features was checked. Note that the length of a linked COL segment was highly variable and could continue across several core sections. All COLs and the applied angles of rotation of the individual COLs are listed in Appendix E-2. To highlight the uncertainties related to core orientation, an uncertainty assessment was carried out and visualised using three confidence classes.

5. Quality control of core goniometry:

   Prior to the structural recording of the drill cores, the depth shifts, the core correlation with the FMI / UBI combination and the core orientations were reviewed.

The following steps do not belong to classical core goniometry. However, they played a key role in the coherent workflow of the structural core analysis and are thus mentioned here:

6. Dip picking on oriented 360° core photographs:

   Bedding-related planes were picked manually for a structural dip evaluation.

   Structural elements on drill cores were picked manually and characterised in detail with respect to relevant parameters.

7. Recording of kinematic features:

   Kinematic indicators along fault surfaces such as slickensides, striations, shear sense indicators and (fault) offsets were identified and measured on the cores. To determine the lineation plunge azimuth and plunge and / or planes not visible in the photographs, a goniometer constructed by Geo Explorers was used. The drill core was placed in the goniometer facing up-hole and rotated around the vertical axis by the angle of rotation determined from the COL. Subequently, the plunge azimuth and plunge of the striation were measured using a geological compass (see Fig. 2-1).

8. Examination of angular differences:

   Using the TectonicsFP software, the angular differences between the striation plunge azimuths / plunges and the orientation of associated fault planes were checked. If the angular offset exceeded 15°, the fault plane and lineation were remeasured.

9. Quality control:

   A final quality control was performed with the main focus on consistency (between TerraStation, primary records of the structural core analysis and the structural inventory meta-data), completeness of records and the accurate characterisation of the recorded tectonic features.

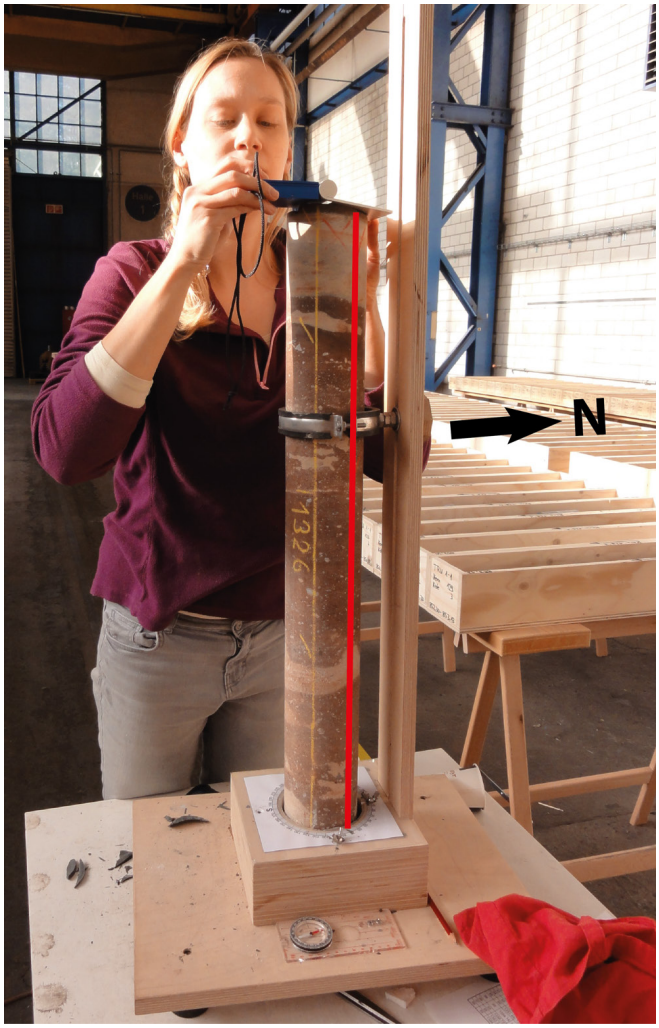

Fig. 2-1: Using a goniometer to determine kinematic indicators along faults

Note the red core orientation line defining the position of the drill core in the goniometer.

2.1.3 Dip picking and dip type classification

Due to higher accuracy and reliability compared to automated methods, a manual sinusoid method and a point-to-point method were used to pick all relevant features on the 360° core photographs. In a cylindrical borehole, a perfect plane will appear as a sine wave on the circumferential core photograph and its amplitude reflects the dip relative to the borehole axis.

Different dip classes were defined for the different structure types. For this study, a total of 15 different dip types were defined in TerraStation II (Fig. 2-2).

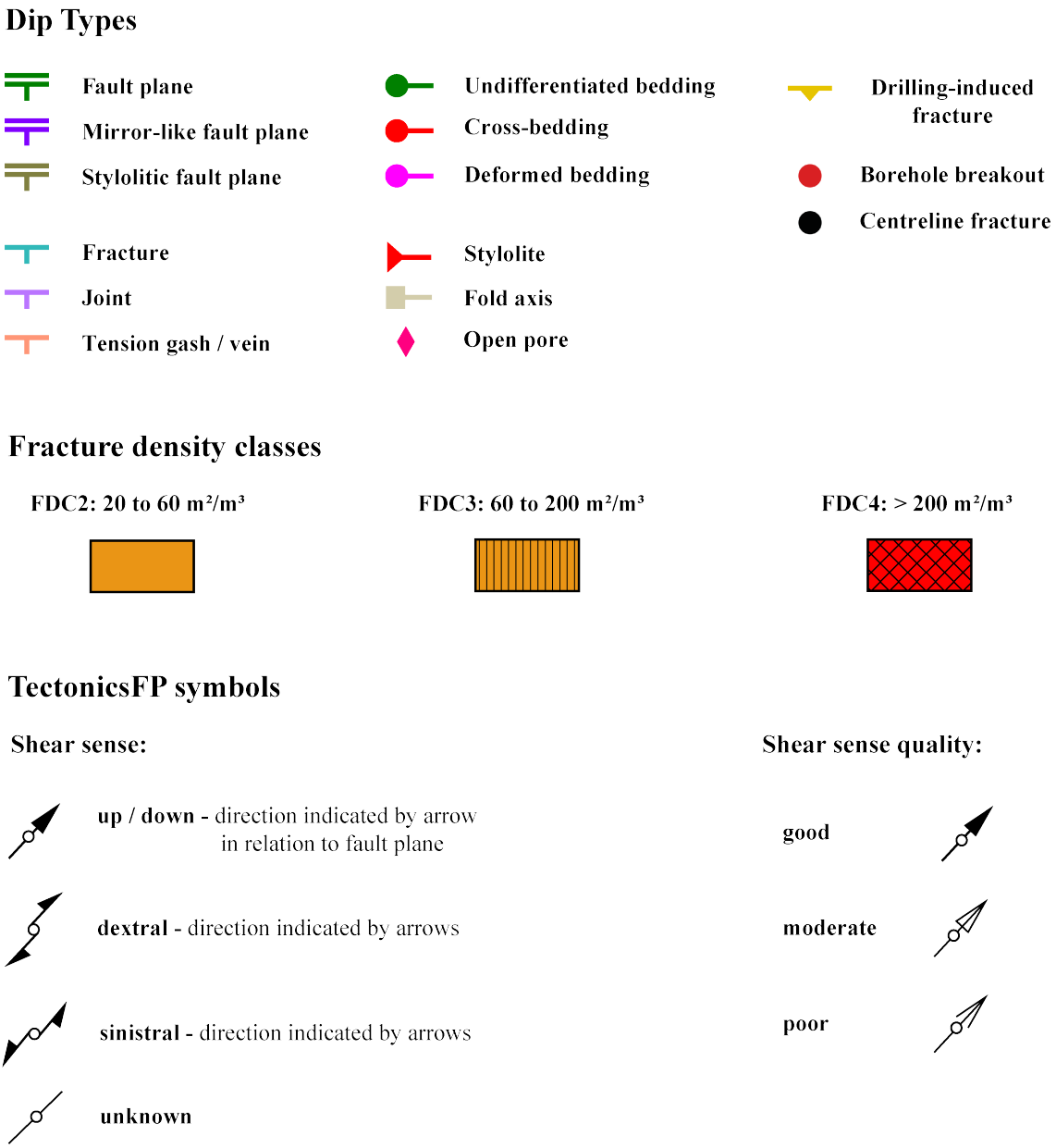

Fig. 2-2: Symbols for dip types, fracture density classes and kinematic data used for this study

Some structures were only visible on planes not outcropping at the rim of the core and were not visible on the 360° core photographs. The orientation of these structures was obtained with a geological compass as described above and the data were subsequently imported into the digital dip dataset. Consequently, the associated dip sine waves did not fit with any visible traces and/or were simply not visible at this depth level, as exemplified in Fig. 2-3.

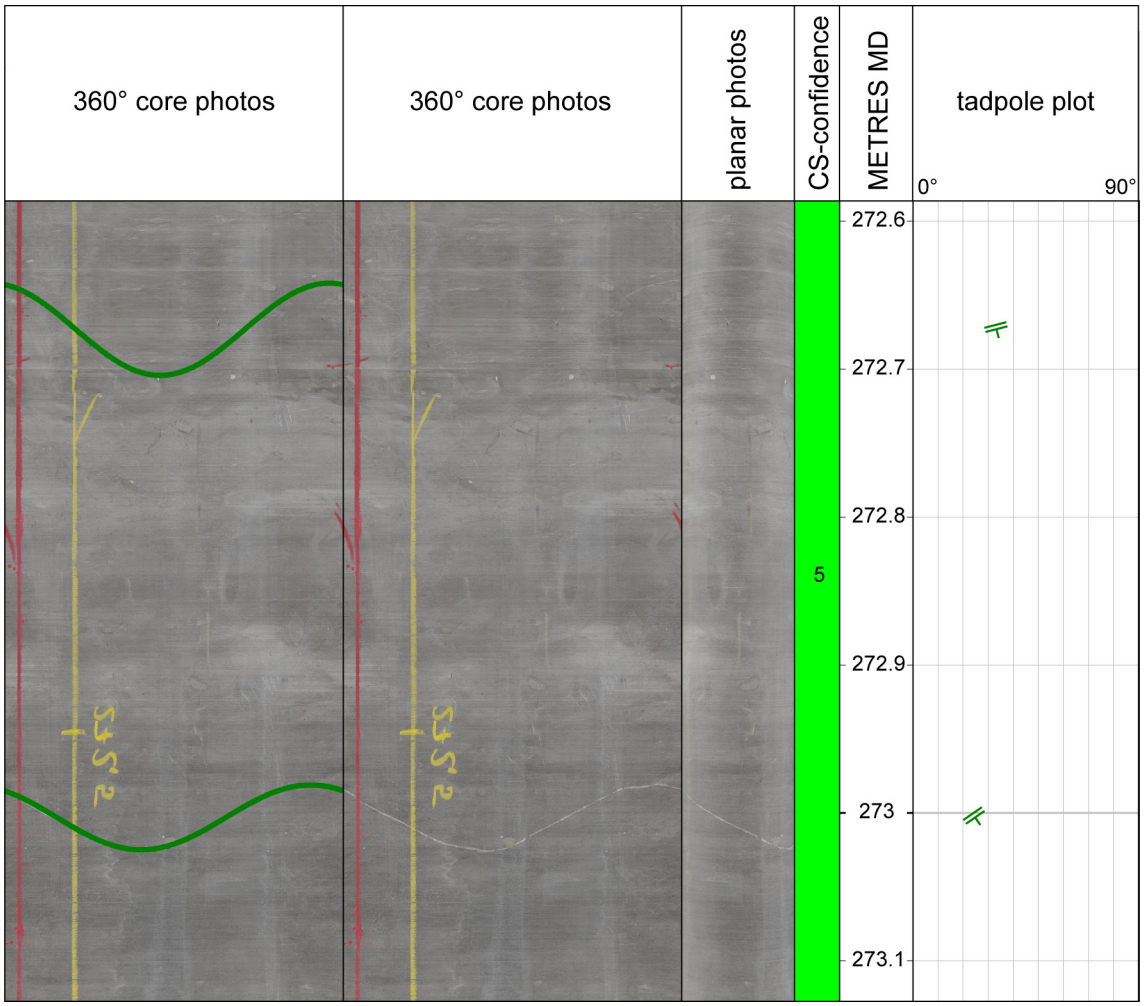

Fig. 2-3: Two fault planes identified at 272.67 m and 273.00 m MD (log depth) in the Wildegg Formation

The upper one was determined only within the drill core.

From left to right: shifted and oriented 360° core photograph with (left) and without (right) picked sine waves, followed by depth-shifted planar core photographs, core section numbering in the coloured bar displaying the goniometry confidence ranking, depth track showing the position and length of the currently displayed window, tadpole plot. Note that the displayed sine wave of the structure at 272.67 m MD (log depth) is not visible in the 360° core photograph of the dark layer. The fault plane was implemented from the core analysis and the orientation obtained from a compass measurement.

2.1.4 Dip data for non-oriented and missing cores

Due to a lack of correlated features, poor data quality or missing image log data, 42.75 m of the available drill cores remained non-oriented. Within these non-oriented drill cores, a total of 25 bedding planes and 159 tectonic / drilling-induced discontinuities could be observed and picked. The structural planes were nevertheless measured manually with a geological compass and included in Terrastation II or picked digitally on 360° core photographs. For non-oriented drill cores and core photographs, the red COL was set to 0°. Because the dip measurements of these features are correct, but the dip azimuth measurements are affected by the lack of orientation, the non-oriented dataset can only be used for fracture density calculations.

To highlight incorrect dip azimuth measurements of these features, a quality indicator of 0 was assigned and open tadpoles were used for visualisation (Fig. 2-4). A quality indicator of 1 was assigned to all correctly oriented features.

For intervals with missing 360° core photographs, short drill core sections could still be oriented using the coherent COL, which sometimes continued across several cores. The depth and orientation of the structures were then measured on the core, and the dip data were subsequently imported into the digital database of TerraStation II (see Fig. 2-5).

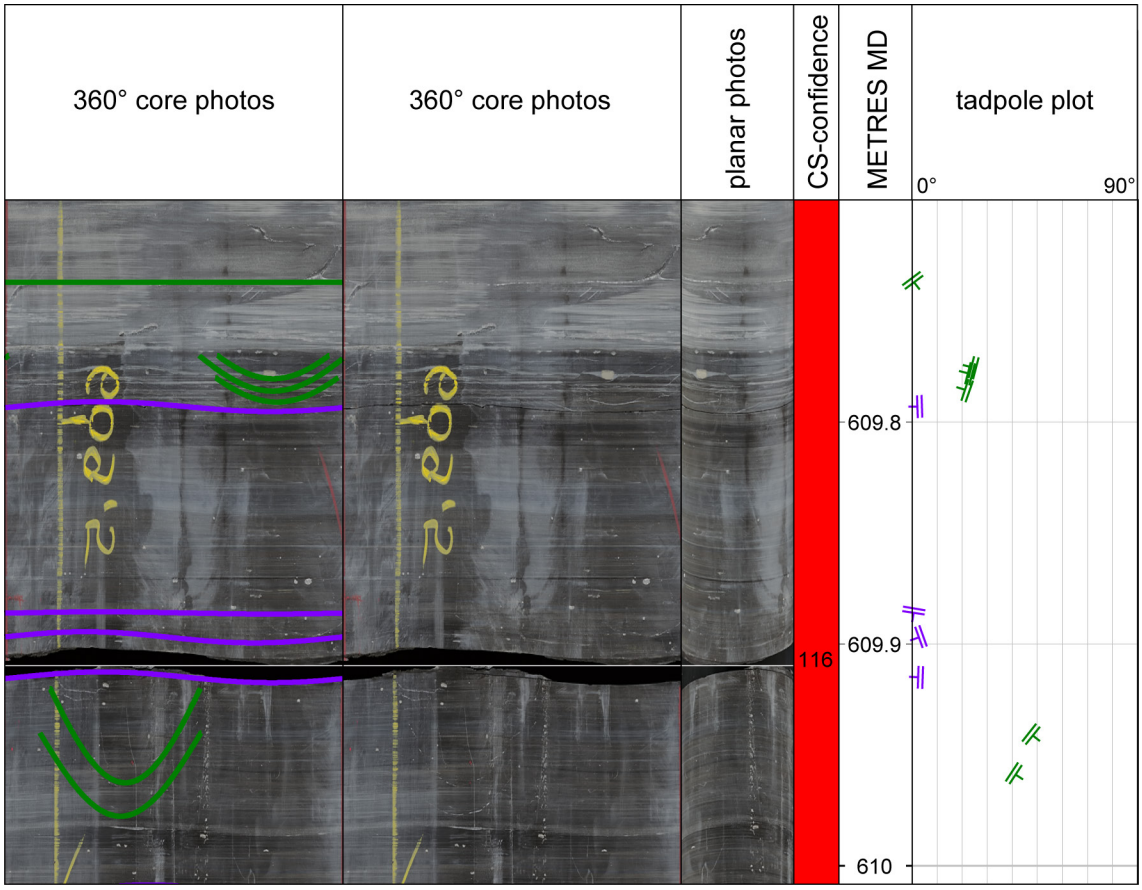

Fig. 2-4: Example of dip data in a non-oriented core interval

The goniometry confidence is set to "core not oriented" (red). Example from the Staffelegg Formation from 609.70 m to 610.01 m MD (log depth).

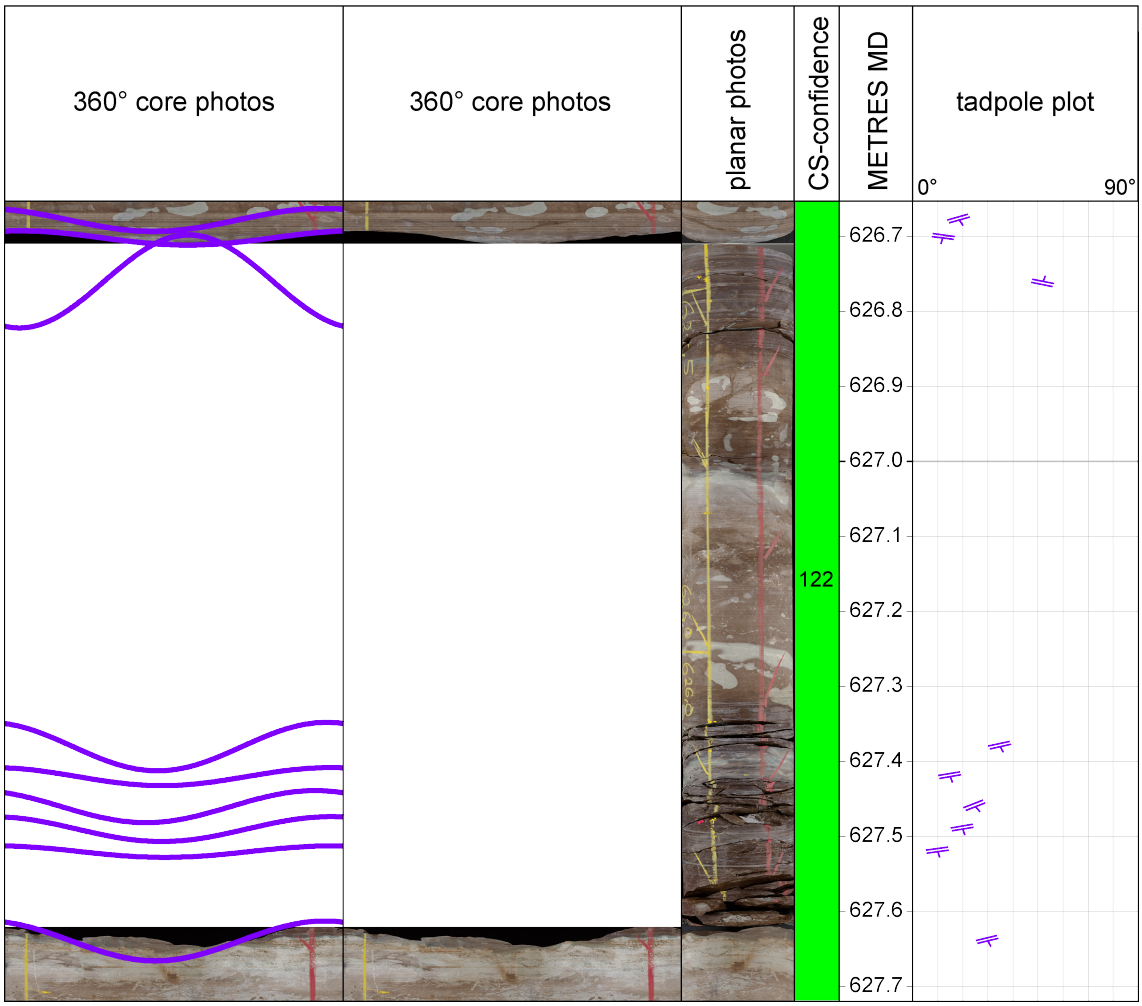

Fig. 2-5: Interval without 360° core photographs from 626.65 m to 627.72 m MD (log depth) in the Klettgau Formation

In this example, the core goniometry and structural analysis were performed directly on the drill core. The orientation data were determined with a geological compass and subsequently imported into the digital dip database of TerraStation II. The goniometry confidence for this core section is high (green).

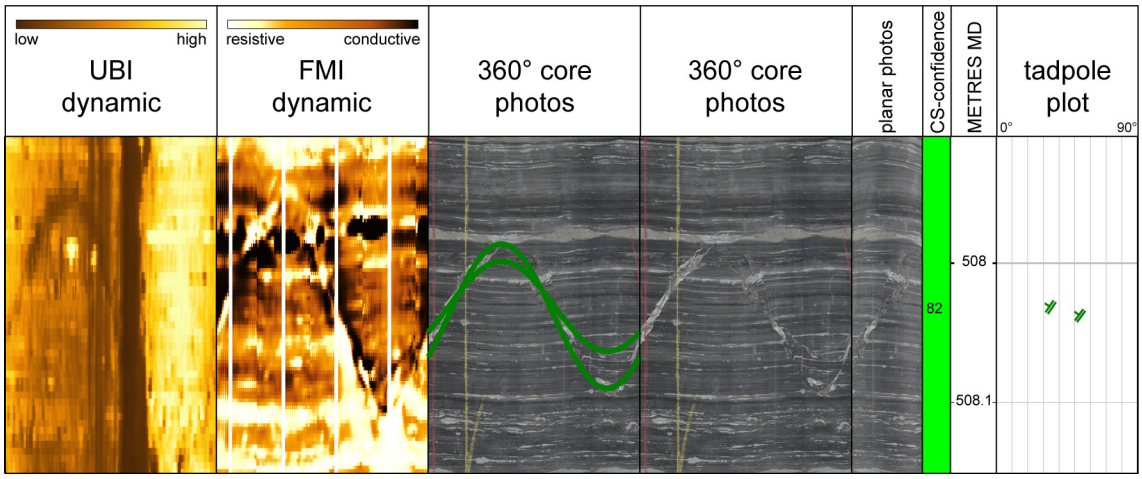

Fig. 2-6: Core – FMI / UBI correlation for a fault at 508.04 m MD (log depth) in the Opalinus Clay

This prominent NW-dipping fault was unequivocally correlated across the UBI and FMI logs and the core photographs, and therefore represents a high-confidence indicator for the core orientation. From left to right: dynamic normalised acoustic UBI image log, dynamic normalised FMI images, shifted and oriented 360° core photographs with (left) and without (right) sine waves, followed by shifted planar core photographs. The core section numbering is shown in the coloured bar displaying the goniometry confidence ranking (high – green, moderate – yellow, red – not oriented). The depth track shows the position and length of the currently displayed window. A tadpole plot with true orientations of manually picked planes is also displayed.

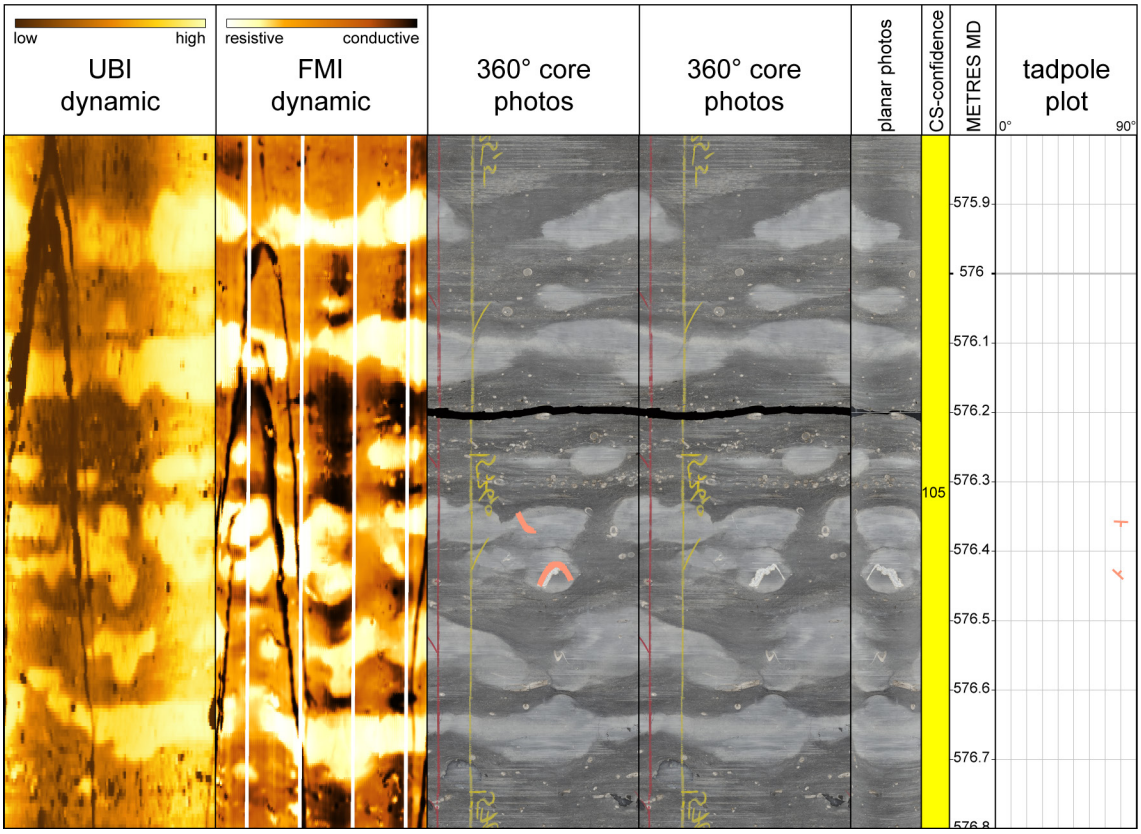

Fig. 2-7: Core – FMI / UBI correlation from 575.80 m to 576.80 m MD (log depth) in the Staffelegg Formation

These unique structures represent nodules which appear bright (high amplitude) on the UBI and resistive on the FMI images. They were used to shift and orient core section 105. Due to their heterogeneous nature, they are considered as indicators of limited quality for the core goniometry and assigned a moderate confidence level (yellow).

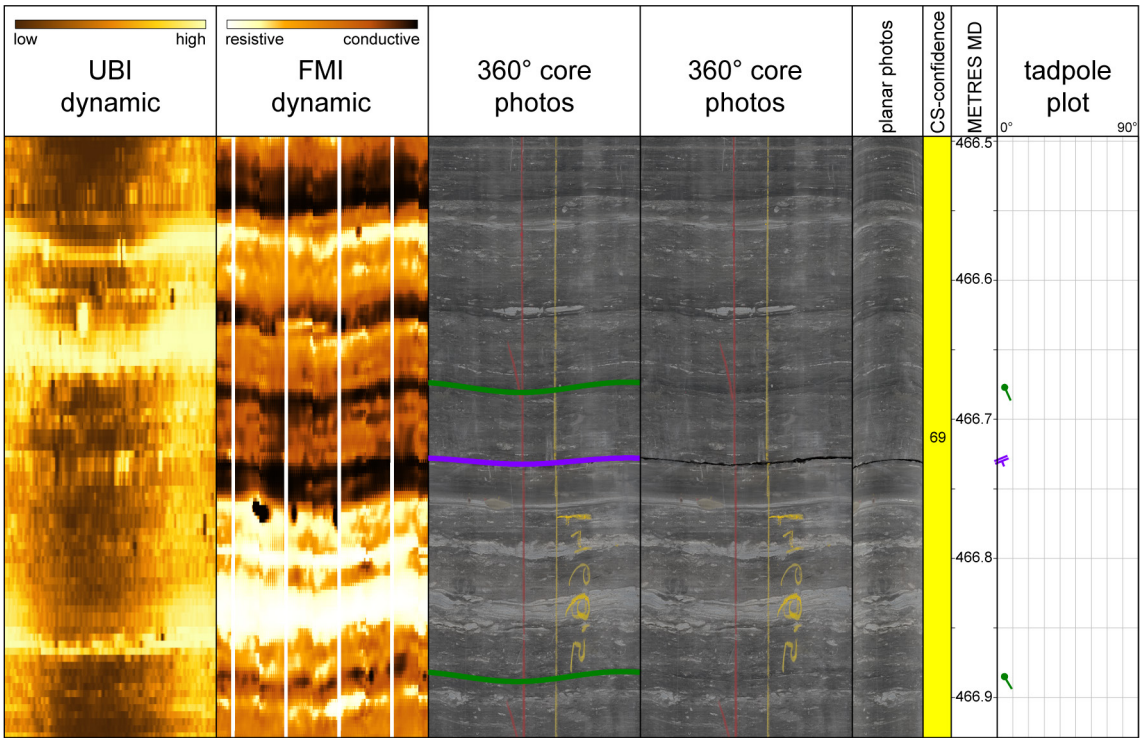

Fig. 2-8: Core – FMI / UBI correlation for subhorizontal to shallow dipping bedding

The FMI and the core photograph match within the well-bedded strata in the Opalinus Clay from 466.50 m to 466.92 m MD (log depth). Although the bedding planes are clearly visible on the FMI and core photographs, the relatively low dip angles (< 10°) imply some angular uncertainty and are therefore considered as moderate indicators for core goniometry (yellow).

Project-specific uncertainties

A number of unavoidable limitations and uncertainties were associated with the work performed and may have affected the accuracy of the results. These factors are evaluated below:

- angular uncertainty is associated with the core goniometry and is reflected by the confidence scheme. It particularly implies an angular error for the azimuth
- errors related to compass measurements on drill cores: to explore the measurement-related error, multiple measurements of the same structure were performed by different users. The reproducibility was 5° for the dip magnitudes and 5° to 10° for the dip azimuths. Considering that most geological compasses have an error margin within 2° for dip azimuth and magnitude, it can be concluded that the above-mentioned goniometer has an acceptable error margin and can safely be used for accurate structural core analysis
- dip picking on 360° photographs: the pixel resolution of the screen defines the angular uncertainty of the dip picks in 3D space and is 1° to 2° for the dip angle and 2° to 4° for the dip azimuth
  - core photographs: although the 360° core photographs covered almost the entire studied interval (260.00 m to 829.88 m MD [log depth]), some data gaps occurred, e.g. from 370.16 m to 372.00 m MD (core depth), from 561.60 m to 562.26 m MD (core depth), from 615.40 m to 617.24 m MD (core depth), from 617.85 m to 619.66 m MD (core depth), from 625.45 m to 626.36 m MD (core depth), from 638.68 m to 639.21 m MD

(core depth), from 753.56 m to 754.30 m MD (core depth), and from 805.04 m to 805.60 m MD (core depth). The missing core photographs are either due to pilot holes for formation integrity tests (no core photographs could be taken) or in case of highly fractured intervals or disintegrated cores, 360° core photography have not been recorded as these intervals were not suitable for circumferential photography

- in some core intervals the core orientation line was discontinuous. This was mainly related to uncertainties in the assembly of individual core pieces / sections at the drill site. In such cases, the non-coherent core sections were treated separately (see Appendix E)
- due to the presence of steel in the Nagra core storage facility in Würenlingen, a site-specific magnetic field disturbance was recognised. Consequently, the goniometer needed to be carefully aligned towards relative north to obtain the correct orientations of the geological features (mainly lineations) measured with a compass. This always had to be kept in mind when moving the equipment across the core store.

2.2 Structural work

This section describes (A) how the structural recording and characterisation of drill cores was carried out, (B) which structure types were distinguished, and (C) which structural parameters were defined. Details with regard to the structural core analysis are given in the structural analysis manual and enclosed factsheets and templates (Ebert & Decker 2019).

A) After the core goniometry was finalised, all deformation structures were recorded on the drill cores. The recording was usually finalised within a few weeks.

The overall core quality was excellent. Only cores from clay-rich lithologies (particularly the Dogger) were affected by progressive discing but were still suitable for structural analysis. Due to 401 samples with lengths of up to 50 cm being taken at the drill site (e.g. for porewater or geomechanical analyses), there were gaps within the core sections. Samplers were strictly advised not to sample core intervals containing tectonic structures. The completeness of the structural record is therefore not biased or limited by sampling. Furthermore, it can be assumed that the complete structural inventory was recorded because high-resolution core photographs were taken from all cores, including the sampled core sections.

Most of the structural work was performed by two people. A structural geology expert defined all visible structure types along with their relevant parameters for each core section, which was usually 3 m long. At the same time, the other colleague manually picked the structures on the 360° core photographs in TerraStation II. The structures and their parameters such as mineralisation, thickness or shear sense were documented on a DIN A3 template with content previously defined in Ebert & Decker (2019). The log depth was determined in metres MD along with the true orientation of the structures on oriented 360° core photographs. The difference in depth between the core and log depth mostly varied between +0.17 m and +1.37 m and depended on the dynamic depth shift of the core photographs with regard to the FMI used as the main depth reference data. Striations on slickensides recognised on surfaces of broken cores were measured with a geological compass (Fig. 2-1). As soon as a core section was completely analysed, all entries from the DIN A3 template were digitised and data QC was carried out.

B) Depending on rock rheology and the type and degree of deformation, different types of structural discontinuities may develop. Based on this, the structures were subdivided into five main groups of discontinuities (Fig. 2-9). In total, 11 types of structures were distinguished in this study (Tab. 2-2) and are illustrated with numerous examples in Chapter 3. Detailed definitions and information on the origin of the structures can be found in the structural manual of Ebert & Decker (2019).

C) Additionally, parameters such as mineralisation, shear sense and thickness (listed in Tab. 2-3) were determined and documented for each individual structure on the DIN A3 template (Fig. 2-10). In addition, each structure was sketched and labelled with a consecutive number on the designed grid with a scale of 1:10.

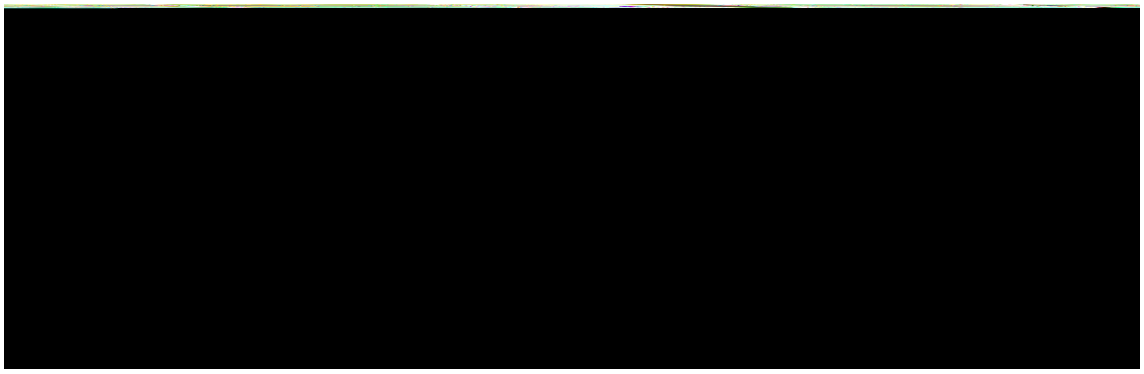

Fig. 2-9: The five main groups of structural discontinuities

Tab. 2-2: Types of structural discontinuities identified in this study

For more details see Ebert & Decker (2019).

Discontinuity group	**Structure type**	**Characteristics**
Brittle structures with shear indications	Fault plane	Planes of shear failure, i.e. planes along which there has been movement parallel to the plane (Peacock et al. 2016). Single, thin, planar and sharp structural discontinuities with shear indications (e.g. striations or slickenfibres).
	Mirror-like fault plane	A fault plane with a smoothed, polished or shiny slip surface.
	Stylolitic fault plane	A fault plane with dissolution seams and stylolite-bearing columns which are oblique or parallel to the plane (modified from Hancock 1985).
	Fault zone	A fault zone is defined as a zone with a volume which includes interacting and linked fault segments, densely fractured rock and / or fault rocks; zones are typically bounded by subparallel margins or fault planes (modified from Peacock et al. 2016).

Tab. 2-2: continued

Discontinuity group	**Structure type**	**Characteristics**
Drilling-induced fractures (DIF)	Drilling-induced fractures	Collective term for fractures created by forces associated with drilling and coring procedures. Depending on load on drill bit, mud weight and rock properties, drilling-induced fractures develop during drilling or shortly thereafter. Based on the aperture, fracture surface and geometric relationships, drilling-induced fractures can be distinguished from natural fractures. Drilling-induced fractures are always open and never mineralised.
	Petal fracture	Drilling-induced fracture with convex-up geometry cutting a core downwards starting from its perimeter. Petal fractures form immediately ahead of the drill bit as a result of excessive bit weight during coring. They propagate downhole.
	Centreline fracture	Drilling-induced fracture that typically splits a core approximately in half.
	Core discing	The formation of discs of relatively uniform thickness which fracture on surfaces approximately normal to the axis of the core.
Additional features / dip types	Undifferentiated bedding	Planar surface representing either the boundary between two different lithological units or internal bedding. Thought to reflect original horizontal and planar surfaces.
	Deformed bedding	Bedding planes occurring in narrow zones in any lithology with moderate to steep dip angles (> 15°) which differ from the general structural dip. They have been subject to deformation due to faulting and / or folding.
	Cross-bedding	Inclined foreset surfaces in sandstone occurring in sets and bounded by set boundaries. These sedimentary features may be used as paleocurrent indicators. Upper truncation by the next set is diagnostic.
	Fold (axis)	One or a stack of originally flat and planar surfaces, such as sedimentary rocks, that are bent or curved due to applied external stress. Folds appear in various scales and shapes.
	Fracture density	Numerical value that reflects a quantitative measure of the abundance of fractures in rock mass (e.g. fractures per metre, fracture area per rock volume).

Tab. 2-3: Systematically recorded parameters for the investigated structures

Parameter	**Definition of parameters and procedure for defining these parameters**
Depth	All types of structures are recorded quantitatively along the scanline of the core axis. The depth of the structure is measured at the point where it cuts the core axis. For steeply dipping planes, the depth should be determined half-way between the top edge and the base of the intersection ellipse of the structure. If a zone is recorded (e.g. fault zone, shear band, fracture density class), the top (Top MD) and the base (Bottom MD) of the zone are specified in the corresponding columns.
Core orientation line number	After the extraction of the core from the inner tube, the core pieces are juxtaposed whenever possible. Continuous sections without drilling breaks, demarcated by grinding, crushed or core loss zones, are marked with a core orientation line and denoted with a consecutive number. This number enables linking of the recorded structure with the key structure of this orientation line section that was identified on the borehole image.
Depth shift between core and FMI	The depth shift is defined using correlated structures visible on both the FMI and core.
Correlation with log	Assessment of whether each individual structure can be clearly identified on FMI / UBI and core. "yes" indicates that the structure can be correlated with the image log, and "no" indicates structures which cannot be correlated, or which are not shown by the image log. In addition, a correlation quality ranking is carried out (1 – good, 2 – moderate, 3 – no correlation).
Dip direction and dip	Measured dip direction and dip of the structure.
Structure type	The abbreviations of structure types according to Tab. 2-2 are entered into the paper template.
Length of structure	The length of the long axis of the intersection ellipse is measured for structures which cut the core axis at acute angles (dipping with more than about 70°) and structures which do not cut through the entire core diameter. The measured length will be used for the calculation of fracture density P32. Measurements are required to reduce the inaccuracy resulting from calculating fracture areas solely from the angle between the structure and the core axis.
Plunge azimuth and plunge of lineation	Measured plunge azimuth and plunge of the lineation observed on the measured plane.
Shear sense and quality	Shear sense of fault planes and shear bands using up (reverse fault), down (normal fault), dex (dextral strike slip) or sin (sinistral strike slip), and reliability indicators (good, fair, poor) of the shear sense observation.
Mineralisation / fault rock type	Any type of filling, mineralisation or fault rock associated with the structure (e.g. CC for calcite of a vein filling, synCC for mineralisation of slickenfibres).

Tab. 2-3: continued

Parameter	**Definition of parameters and procedure for defining these parameters**
Open / closed and width / length of open structures	Information on whether a tension gash / vein is open (displaying a continuous aperture), partly open (displaying a discontinuous aperture) or closed at the observation scale (i.e. the naked eye), including the width of the aperture and the observed lengths of open streaks for partly open structures.
Roughness	Roughness classification of a structure using the joint roughness coefficient (JRC). The JRC gives a picture of the classification of fracture smoothness and waviness (planarity) along 10 cm length of the fracture (Barton 1976, Barton & Choubey 1977). The scale of the JRC is from 0 (very smooth and planar) to 20 (very rough and wavy).
Fracture condition	Specifies whether the core is broken naturally or artificially at the structure under consideration or intact. If it cannot be specified whether the fracture occurred naturally or artificially, broken should be used.
Fracture density class (FDC)	In cases where cores or parts of a core are heavily disintegrated and order cannot be restored, the density of natural fractures cannot be calculated accurately. Fracture density should be estimated using the classification scheme of Bauer et al. (2016): fracture density class 2 (spacing of fractures = 5 cm to 10 cm), fracture density class 3 (spacing of fractures = 1 cm to 5 cm) or fracture density class 4 (spacing of fractures < 1 cm).
Additional remarks	Offsets or displacements as well as crosscutting relations are documented under "remarks". Further remarks are, e.g. karstification, the shape and length of the teeth of stylolites, alterations, recrystallisation phenomena or whether a structure is of synsedimentary origin.

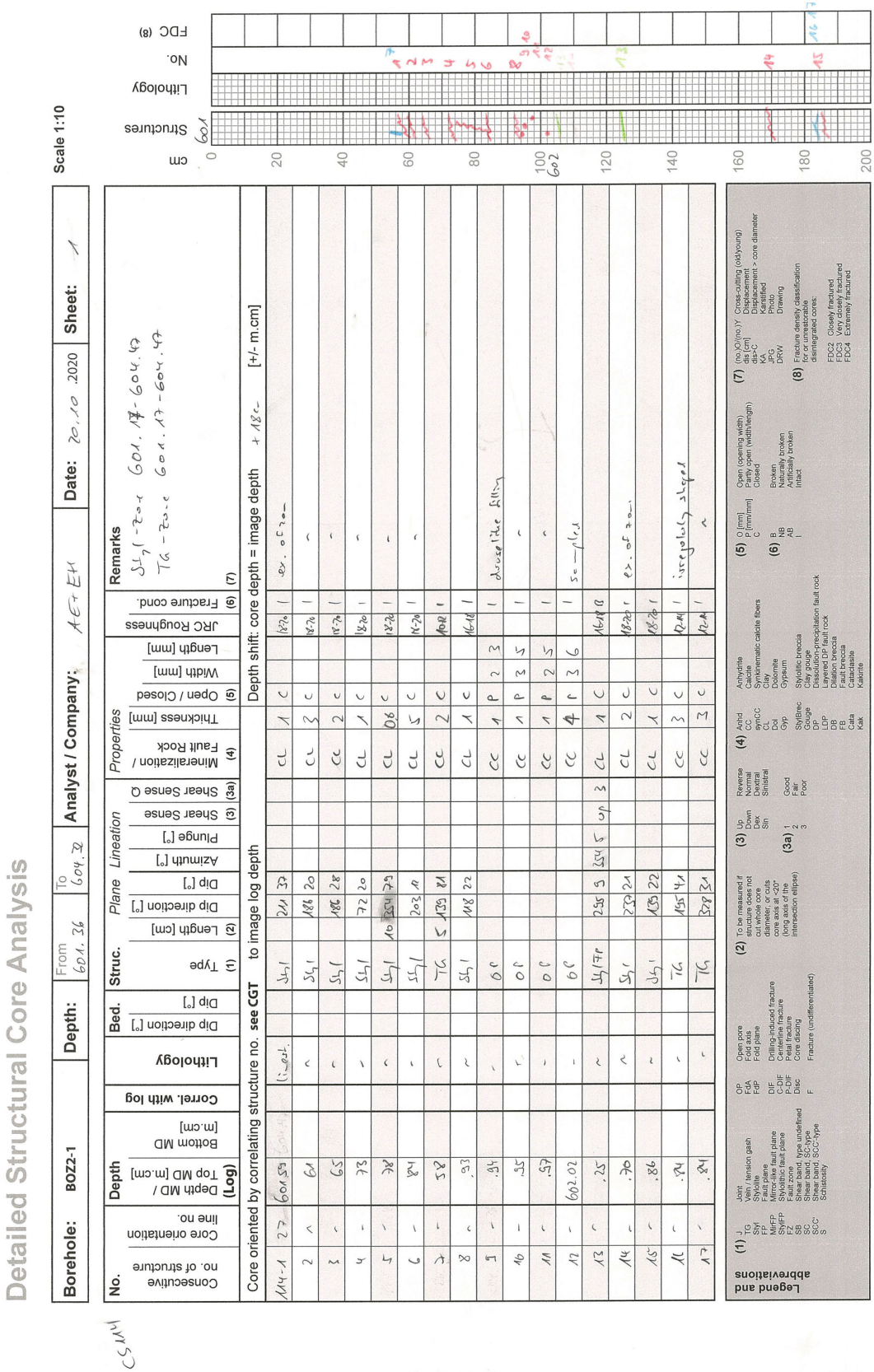

Fig. 2-10: Completed DIN A3 sheet of primary record of the detailed structural core analysis Example of core section 114 (601.36 m to 604.32 m MD core depth).

2.3 Geo-statistical evaluation

For the geo-statistical evaluation presented in Chapter 4, different structural tools and techniques were applied to analyse the available dip dataset. Most of the work was performed with TerraStation II (TERRASCIENCES, Inc.). This provides several advanced modules for the import, processing, visualisation and analysis of all types of available borehole data such as petrophysical logs, borehole images, core data and stratigraphic information.

For the structural evaluation of the different lithostratigraphic units and the different types of structural discontinuities, a series of figures was compiled:

- stereograms (Schmidt projection, lower hemisphere)
  - poles of the planes were displayed to examine the spatial orientation of bedding and structural planes
  - dip azimuth rose diagrams were compiled for planar features (bedding and fractures). The diagrams show the dip azimuth of the planes under consideration. The rose diagram is a circular histogram summarising orientation measurements. The radius of each segment of a rose diagram is proportional to the number of observations that occur within the angular range of that segment. Dip azimuth rose diagrams are displayed with cumulative petals, resulting in staked petals for different dip categories. For the directional statistics in Chapter 4, a minimum threshold of 10 structures was set for the rose diagrams
- dip histograms visualise the dip angle distribution and clustering for a given dip dataset
- vector means for representative clusters of the different structure types were calculated in stereograms
- the vector azimuth plot (dip walkout plot) reflects the along-borehole dip azimuth variations and was compiled for bedding-related dips only (deformed dips and crossbedding were excluded). Here, the dip azimuth of a plane was plotted in a nose-to-tail fashion pointing in the direction of dip. The length of an interval is related to the number of picked dips and not to the thickness of lithostratigraphic units
- fracture density (P32 curves) reflects the fracture area per unit of rock volume (m^2/m^3). The algorithm computes the area of each fracture and creates a sum of the areas across the defined window of 1 m core length and steps of 0.1524 m. The lengths of subvertical fractures are incorporated, whereas truncated parts of fractures are discarded. The computation of the area accounts for borehole ellipticity. The total area of fractures is then divided by the borehole volume (or volume of the rock mass) of the selected window. See Ebert & Decker (2019) and the literature therein for a more detailed discussion on P32 fracture density calculation. For this study, P32 fracture densities were calculated for all structural discontinuities as well as for each individual group:
  - fault planes, mirror-like fault planes and stylolitic fault planes
  - unassigned fractures, joints and tension gashes / veins
  - stylolites

The recorded kinematic indicators were analysed using TectonicsFP software. The fault and kinematic data were plotted in the stereographic Angelier projection, where the symbols and colours reflect the different shear senses (up, down, sinistral or dextral) and the observed shear sense reliability (good, moderate, poor). All Angelier plots in this report show corrected datasets in which the data points of the lineations are projected onto the great circle of the corresponding fault plane, even if they have an angular offset of < 15°.

3 Inventory of structure types

The different structure types identified in the drill cores of BOZ2-1 and their relevant characteristics were described in Section 2.2. In this chapter, these structures are visualised with examples. The diameter of the cores in the following figures (Fig. 3-1 to 3-24) is 95 mm.

3.1 Examples of fault planes



Fig. 3-1: Fault plane

Characteristics: Example of a fault plane with striation and mm-thick synkinematic calcite fibres. Shear sense is top up (reverse fault).

Formation: Opalinus Clay, depth: 482.76 m MD (core depth)



Fig. 3-2: Fault plane

Characteristics: Example of a subhorizontal fault plane with striation and mm-thick syn-kinematic calcite. Shear sense is top up (reverse fault).

Formation: Opalinus Clay, depth: 523.69 m MD (core depth)



Fig. 3-3: Mirror-like fault plane

Characteristics: A shallow-dipping non-planar fault plane with a polished, mirror-like slip surface and striation.

Formation: Opalinus Clay, depth: 484.70 m MD (core depth)



Fig. 3-4: Mirror-like fault plane

Characteristics: Example of a subhorizontal fault plane with a smooth mirror-like slip surface and striation.

Formation: Opalinus Clay, depth: 526.43 m MD (core depth)



Fig. 3-5: Stylolitic fault plane

Characteristics: Example of a stylolitic fault plane with striation generated by carbonate dissolution and displacement subparallel to the plane.

Formation: Staffelegg Formation, depth: 603.70 m MD (core depth)



Fig. 3-6: Stylolitic fault plane

Characteristics: Example of a stylolitic fault plane with subhorizontal striation generated by carbonate dissolution and displacement subparallel to the plane.

Formation: Staffelegg Formation, depth: 602.07 m MD (core depth)



Fig. 3-7: Synsedimentary faults

Characteristics: Example of a synsedimentary fault filled with black claystone limited to an individual sedimentary boundary between claystone and dolostone.

Formation: Schinznach Formation, depth: 752.07 m MD (core depth)

3.2 Examples of fault zones



Fig. 3-8: Fault zone with FDC 3

Characteristics: Example of a fault zone with numerous intersecting mirror-like fault planes and fault planes with synkinematic calcite. The core disintegration level corresponds to fracture density class 3.

Formation: Staffelegg Formation, depth: 604.29 m to 604.31 m MD (core depth)

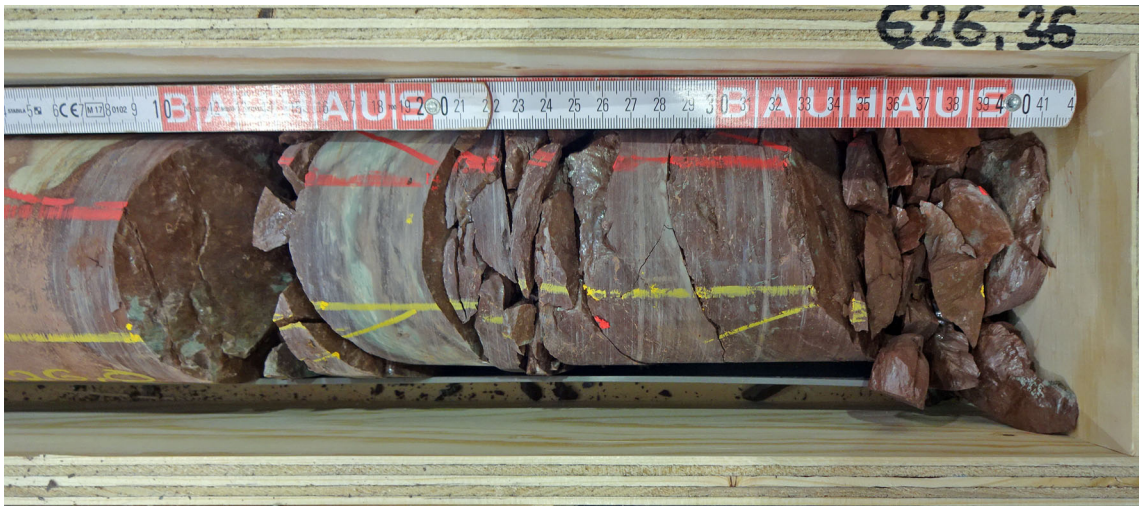

Fig. 3-9: Fault zone with FDC 3

Characteristics: Example of a 26 cm thick fault zone with numerous intersecting subhorizontal mirror-like fault planes. The core disintegration level corresponds to fracture density class 3.

Formation: Bänkerjoch Formation, depth: 626.12 m to 626.40 m MD (core depth)

3.3 Examples of joints



Fig. 3-10: Joint

Characteristics: A 24 cm long, subvertical joint characterised by a rough surface and the absence of slip indications.

Formation: Hauptrogenstein, depth: 340.35 m MD (core depth)



Fig. 3-11: Joint

Characteristics: A 33 cm long, subvertical joint characterised by the absence of slip indications.

Formation: Staffelegg Formation, depth: 577.56 m MD (core depth)



Fig. 3-12: Joint

Characteristics: A 105 cm long, subvertical joint characterised by the absence of slip indications.

Formation: Schinznach Formation, depth: 753.79 m MD (core depth)

3.4 Examples of veins / tension gashes

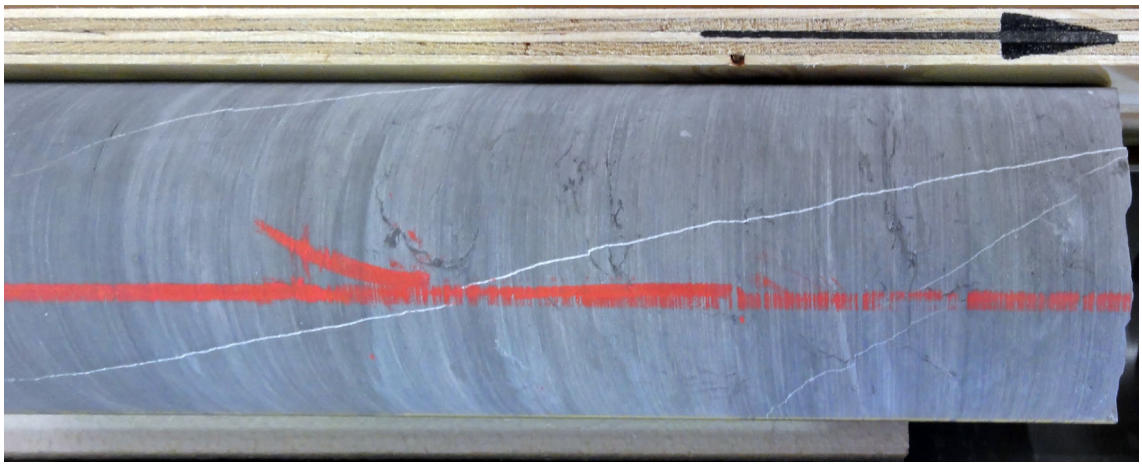

Fig. 3-13: Vein / tension gash

Characteristics: Example of thin, steeply dipping calcite-filled tension gashes.

Formation: Wildegg Formation, depth: 269.55 m (core depth)



Fig. 3-14: Vein / tension gash

Characteristics: Example of a subvertical, several millimetre-thick and undulating calcite-filled tension gash.

Formation: Passwang Formation, depth: 395.57 m MD (core depth)



Fig. 3-15: Vein / tension gash

Characteristics: Example of a thick tension gash filled with anhydrite.

Formation: Bänkerjoch Formation, depth: 654.41 m MD (core depth)

3.5 Examples of stylolites

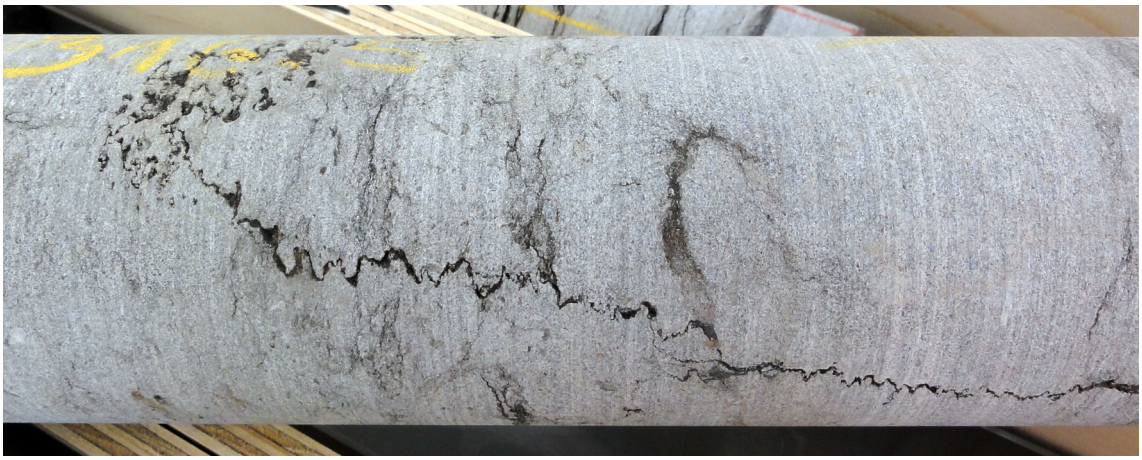

Fig. 3-16: Stylolite

Characteristics: Example of a subvertical stylolite with mm-long subhorizontal teeth.

Formation: Hauptrogenstein, depth: 316.68 m MD (core depth)

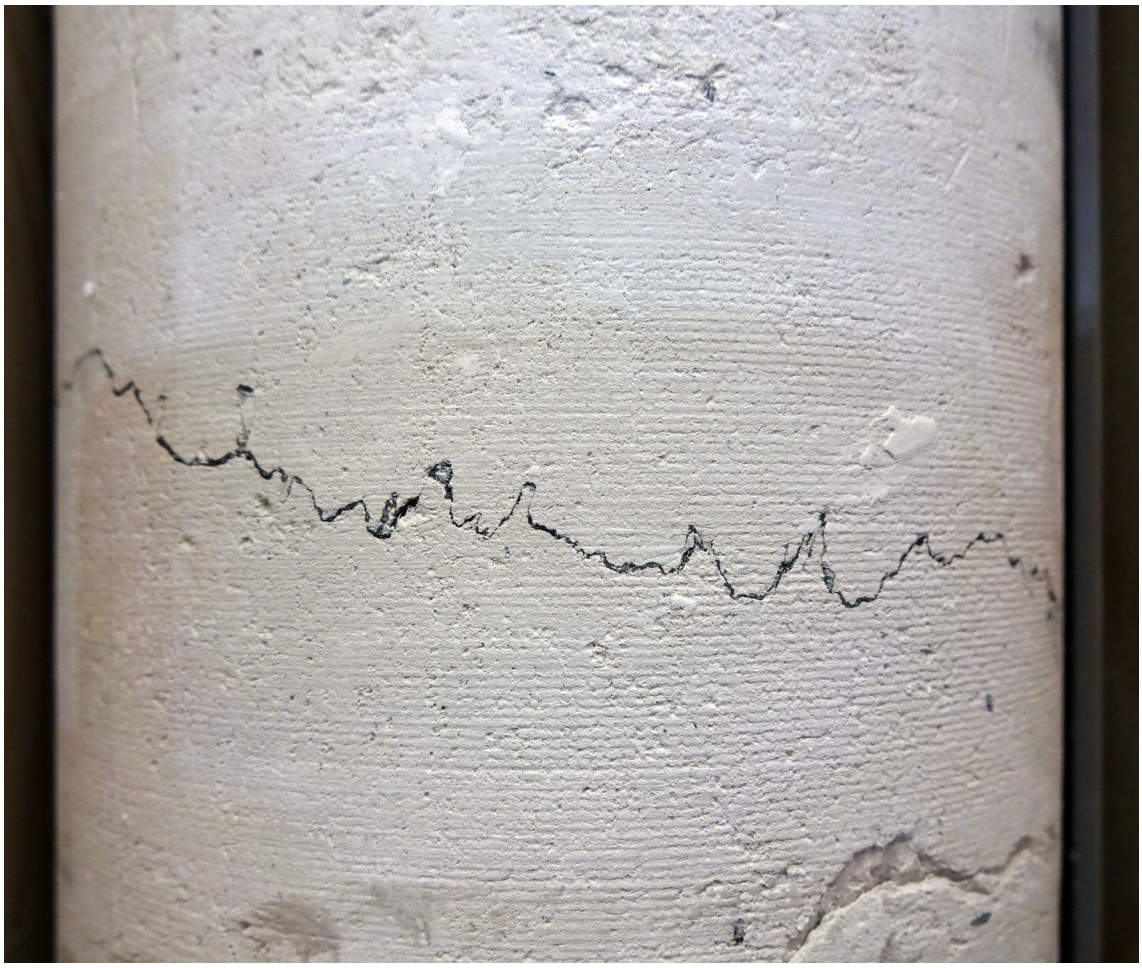

Fig. 3-17: Stylolite

Characteristics: Example of a subhorizontal stylolite with mm-long subvertical teeth.

Formation: Schinznach Formation, depth: 756.38 m MD (core depth)

3.6 Examples of open pores

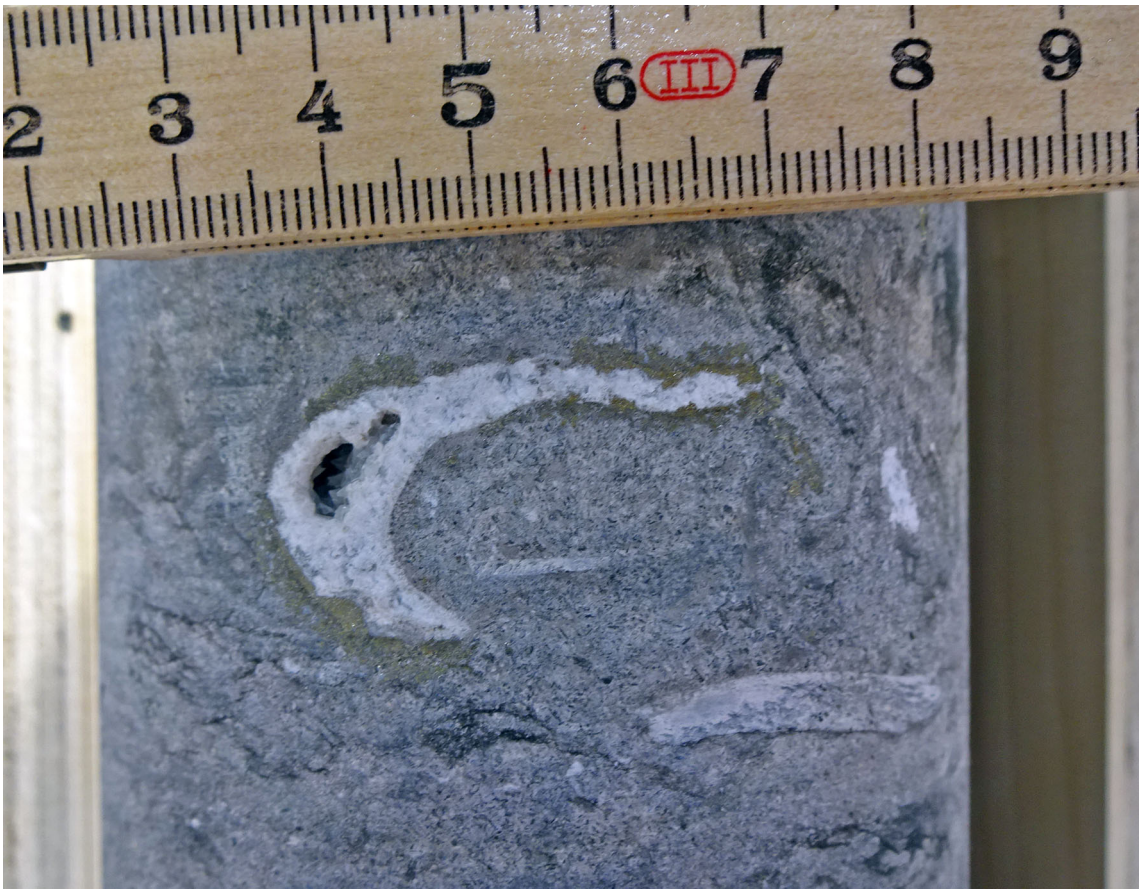

Fig. 3-18: Open pores

Characteristics: Example of an open pore with idiomorphic calcite crystals within a shell.

Formation: Staffelegg Formation, depth: 601.05 m MD (core depth)



Fig. 3-19: Open pores

Characteristics: Example of open pores in a layer typically found in the Triassic dolostone with a dense network of mm- to cm-sized open pores either with thin mineral coatings or without mineralisation.

Formation: Klettgau Formation, depth: 637.41 m MD to 637.62 m MD (core depth)

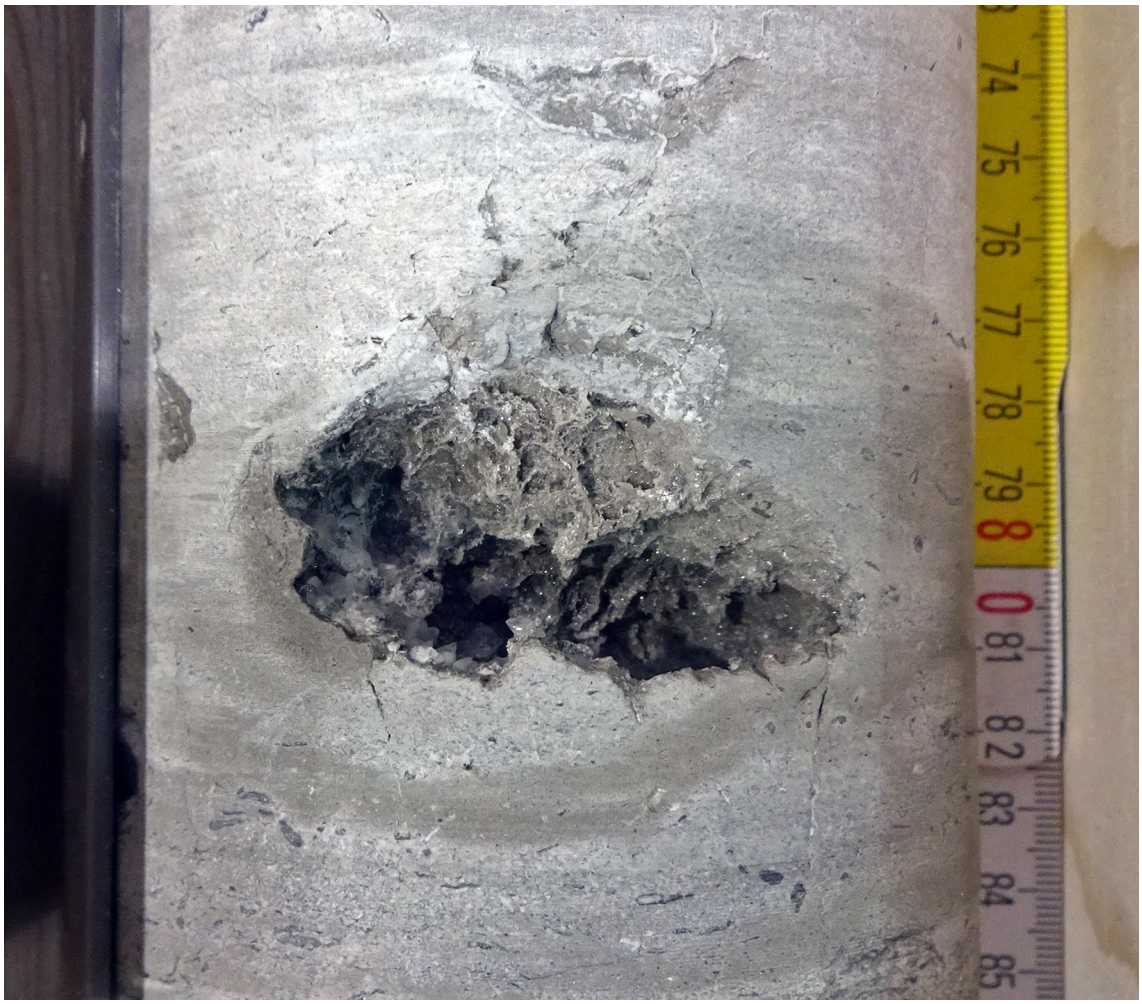

Fig. 3-20: Open pores

Characteristics: Example of a 7 cm large open pore in the Triassic dolostone with a thin coating of mineralisation.

Formation: Schinznach Formation, depth: 780.80 m MD (core depth)

3.7 Examples of drilling-induced fractures



Fig. 3-21: Petal fractures, indicated by yellow arrows

Characteristics: Sets of typical petal fractures of small, curved and broken core pieces with dip azimuths towards ENE and WSW (360° core photograph).

Formation: Klettgau Formation, depth: 653.12 m to 653.30 m MD (core depth)

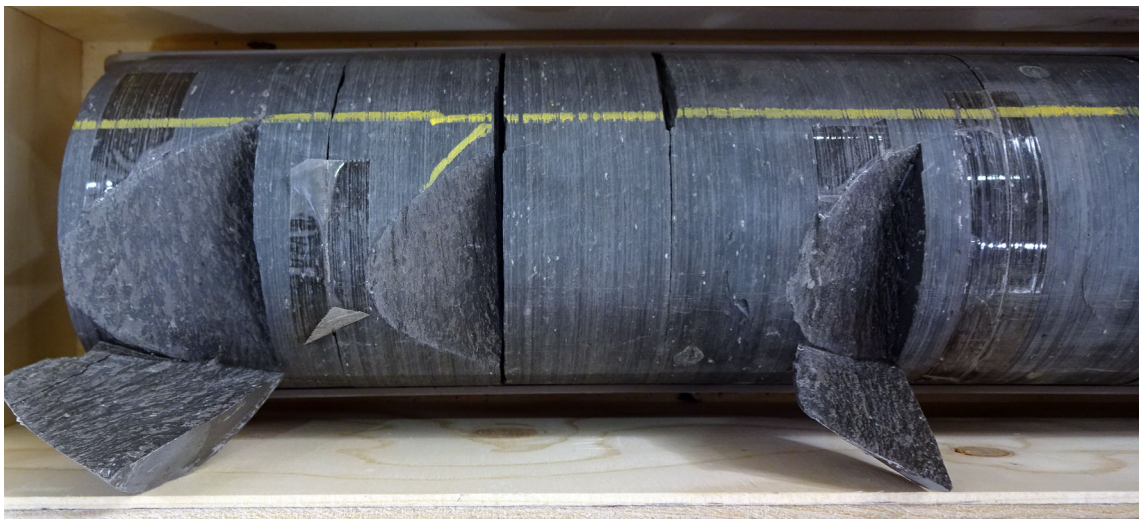

Fig. 3-22: Drilling-induced fractures

Characteristics: Sets of similar drilling-induced fractures of small, curved and broken core pieces (probably petal fractures).

Formation: Opalinus Clay, depth: 560.72 m, 560.78 m and 560.89 m MD (core depth)



Fig. 3-23: Discing

Characteristics: Example of discing in claystone, splitting the core into discs with typical parallel fractures. Discs are oriented perpendicular to the core axis and (sub-) parallel to the bedding.

Formation: Klettgau Formation, depth: 650.06 m MD (core depth)



Fig. 3-24: Discing

Characteristics: Example of discing in claystone, splitting the core into several discs with typical parallel fractures. Discs are oriented perpendicular to the core axis and (sub-) parallel to the bedding. Here, fracturing nucleated from the ammonite in the centre of the core.

Formation: Opalinus Clay, depth: 563.26 m MD (core depth)

4 Geo-statistical evaluation: results

Vector means of orientation values (dip direction and dip angle) of bedding planes and planar structural discontinuities were calculated for different data clusters in a stereographic projection (see Tab. 4-1). Bedding dips and structural discontinuities recorded in non-oriented cores (n = 184) were excluded from the following stereographic evaluation unless otherwise specified. However, they were included in the fracture density calculations (P32 curves) presented in Section 4.1.3.

Tab. 4-1: Vector means of orientation values for bedding planes and structural discontinuities (Azim: dip azimuth)

	Cluster 1 (main)			**Cluster 2 (subordinate)**			**Cluster 3 (subordinate)**		
	Azim	**Dip**	**No.**	**Azim**	**Dip**	**No.**	**Azim**	**Dip**	**No.**
Bedding	140	04	290						
Faults	158	04	423						
Tension gashes, joints, unassigned fractures	164	07	65						
Stylolites	158	04	336						

4.1 Entire cored borehole section (260.00 m to 829.88 m MD [log depth])

A total of 2'790 individual planar and non-planar features were identified during the core analysis and manual dip picking of the 565.11 m of core material. They are visualised at different scales in the structural composite plots of Appendices B and C1 – C3 and are evaluated briefly below.

4.1.1 Basic structural dip evaluation

Bedding dips, particularly in lithologies of a plane-parallel nature such as in claystone, marl and siltstone sequences, are the best indicators for structural dip and its variation with depth. The dip variations along the current borehole are well reflected in the stereograms of Figs. 4-1 and 4-2 and in the vector azimuth plot in Fig. 4-3.

The studied borehole interval (260.00 m to 829.88 m MD log depth) ranging from the Malm to the Zeglingen Formation reveals a subhorizontal to shallow (1° to 10°) structural dip towards the SE that is consistent throughout the studied borehole section. The overall mean structural dip of the bedding is 140/04 [dip direction / dip angle] (n = 290; see cluster 1 in Tab. 4-1). However, a number of local, abrupt changes in dip orientation were associated with evident faults / fault zones within the borehole, e.g. from 527.05 m to 541.80 m MD (log depth) and from 746.19 m to 752.52 m MD (log depth). These dip changes are well reflected and highlighted in the dip vector azimuth plot of Fig. 4-3.

Further significant dip anomalies were observed in the Opalinus Clay from 495.30 m to 502.40 m MD (log depth) and from 509.03 m to 510.74 m MD (log depth). These borehole intervals are partly characterised by bedding dips up to 20° and with variable dip directions. These dip changes are most likely linked to faulting and soft-sediment deformation. However, a more detailed structural dip evaluation is beyond the scope of this study.

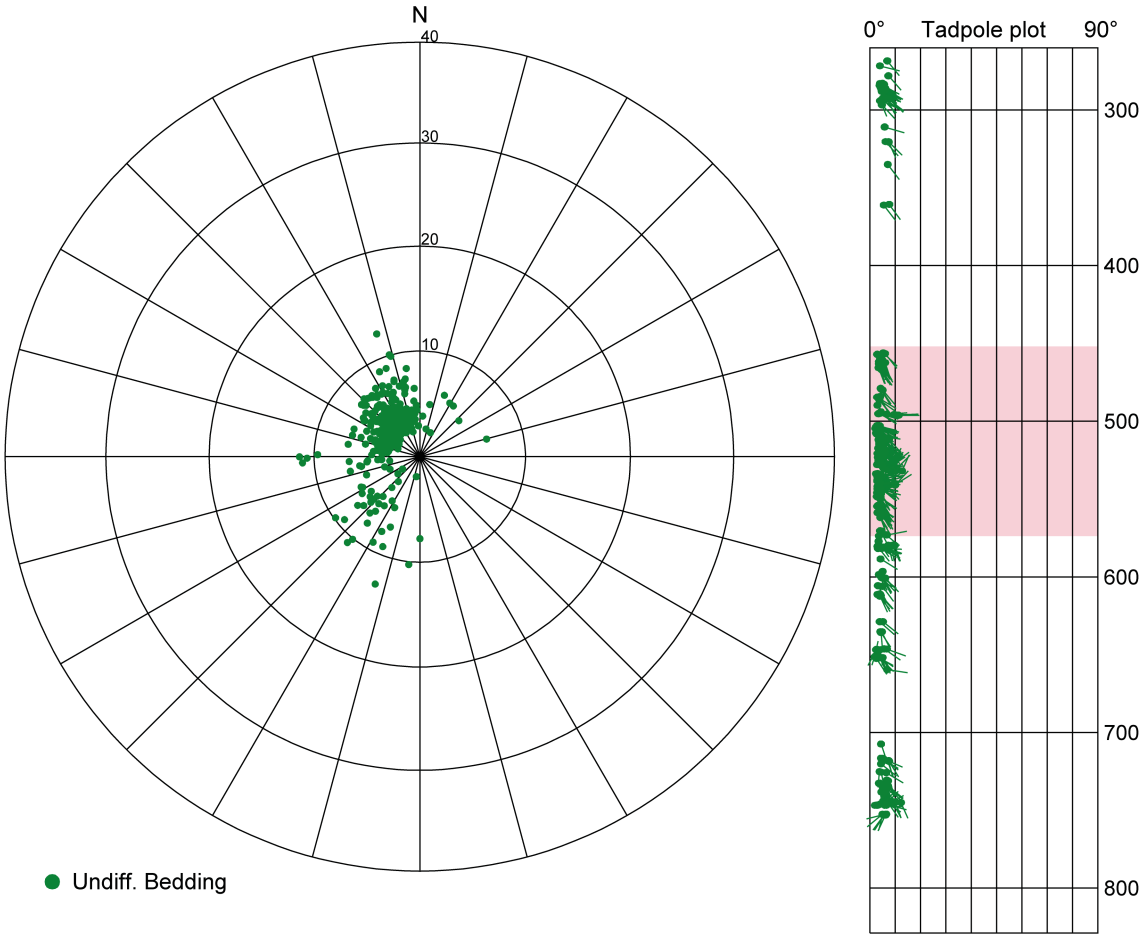

Fig. 4-1: Stereogram and depth plot for bedding planes (n = 352) for the entire cored borehole section

Note the predominance of 0° to 10° SE-directed dips with an overall mean of 140/04 (n = 290). Depth range is 260.00 m to 829.88 m MD (log depth). The Opalinus Clay interval is indicated by the red bar in the tadpole plot. The perimeter of the stereogram corresponds to 40° dip.

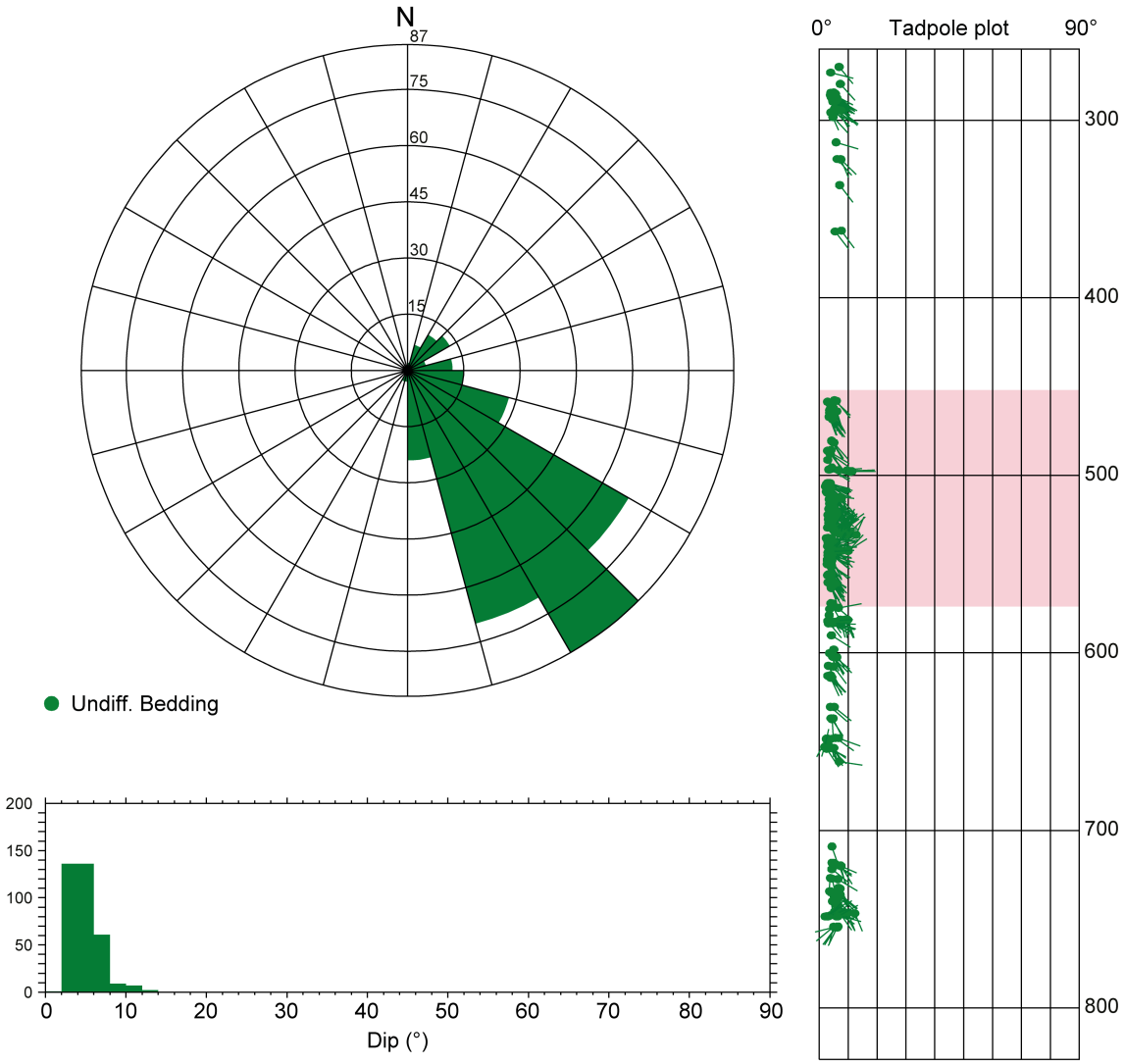

Fig. 4-2: Dip azimuth rose diagram, dip histogram and depth plot for bedding planes (n = 352) for the entire cored borehole section

Note the predominance of dip directions towards the SE. Depth range is 260.00 m to 829.88 m MD (log depth). The Opalinus Clay interval is indicated by the red bar in the tad-pole plot.

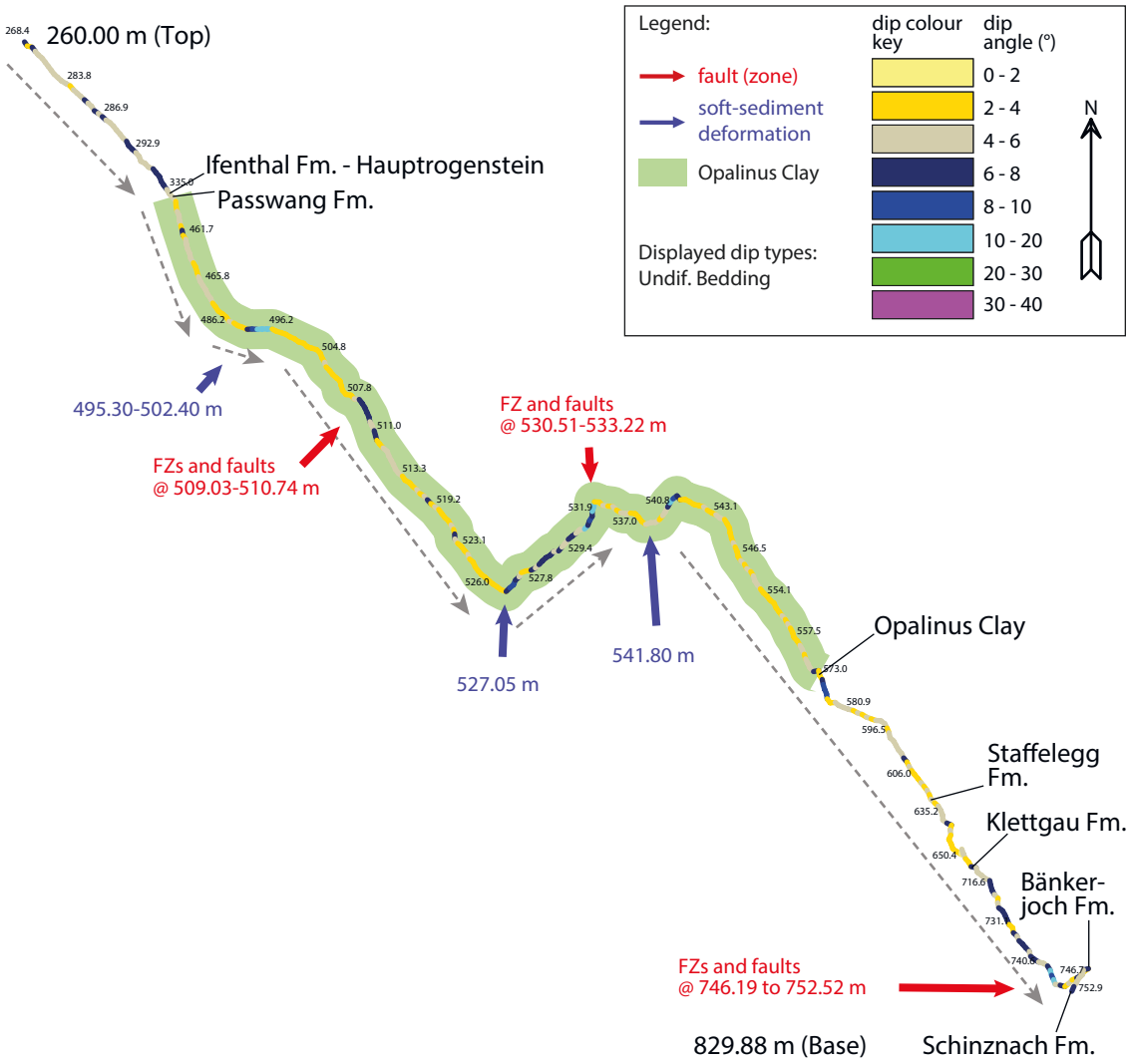

Fig. 4-3: Vector azimuth (or walkout) plot with bedding dips (n = 352) in oriented cores

The colour-coding reflects the dip angle. The horizontal distance has no meaning and only represents the number of bedding planes in the corresponding section. Grey arrows point in the direction of the overall dip direction. Lithostratigraphic formation boundaries (bottoms) are indicated as well as faults / fault zones (red arrows) and zones with possible soft-sediment deformation (blue arrows). The Opalinus Clay interval is shaded in green. Steeply dipping, deformed bedding planes and those from non-oriented cores are excluded from this plot. Depths are given in metres MD (log depth).

4.1.2 Natural structural discontinuities

Fault planes

In total, 892 individual faults were recorded in the BOZ2-1 borehole. Faults are planes of shear failure, i.e. planes with plane-parallel movement (Ebert & Decker 2019). Depending on their appearance in the drill core, three types were distinguished: (1) fault planes (n = 262), (2) mirror-like fault planes (n = 612) and (3) stylolitic fault planes (n = 18). Out of all recorded faults, 815 (91%) were detected in oriented cores and are included in this evaluation.

Several structurally complex intervals along the borehole were interpreted as fault zones. They are commonly associated with intense fracturing and high fracture densities. The latter correspond to the different fracture density classes (FDC) defined by Ebert & Decker (2019). In total, 16 individual fault zones were defined for the entire cored interval along with their FDC in some zones (see Tab. 4-2).

Faults are unevenly distributed along the borehole as shown in Fig. 4-4 and are discussed in more detail in Section 4.1.4. At certain depths faults are absent, whereas at other depths they occur as swarms with a large number of individual fault planes causing heavily fractured and disintegrated rock. Such fault zones and core intervals are described using FDC.

The orientations of all recorded faults are displayed in the stereograms of Figs. 4-5 and 4-6. Faults show a scattered orientation with variable dip directions and dip angles ranging from horizontal to subvertical (1° to 87°). However, there is a predominance of bedding-subparallel and SE-dipping faults with an overall mean of 158/04 (n = 423; mean of selected cluster). Associated kinematic data could be defined on 252 fault planes out of 892 and are further evaluated in Section 4.1.4.

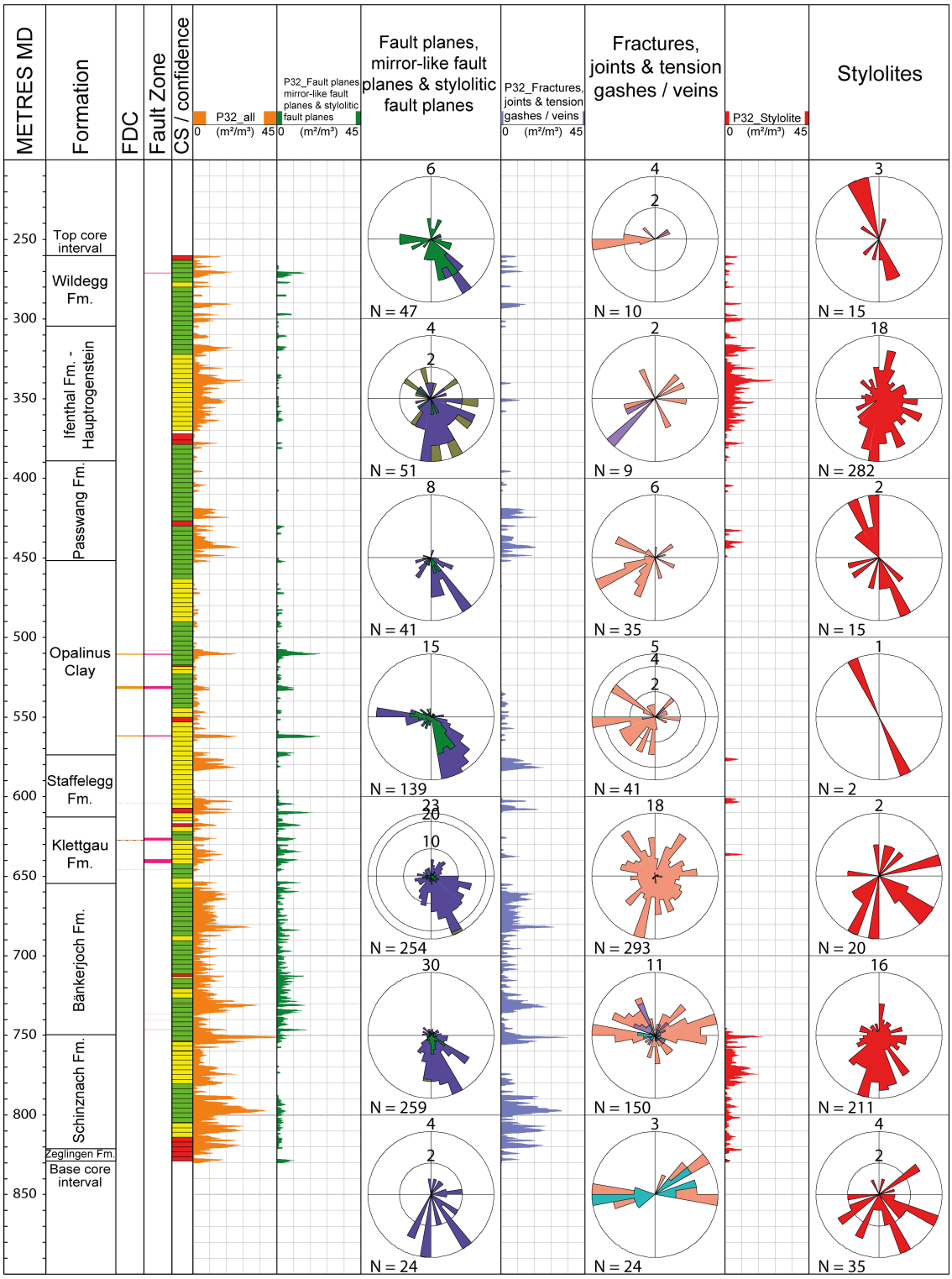

Fig. 4-4: Overview plot showing P32 fracture densities along the BOZ2-1 borehole

In addition to the lithostratigraphic subdivision, core sections and goniometry confidence as well as fault zones associated with intense fracturing (expressed as FDC; see Tab. 4-2 below) are shown. The rose diagrams with the respective number of planes are displayed for 100 m intervals, except for the top- and bottommost diagrams which cover an interval of 40 m and 30 m, respectively.

Tab. 4-2: List of interpreted fault zones, mirror-like fault planes (MirFP) and associated FDC

Fault zones				**FDC**
Top [m MD log depth]	**Bottom** [m MD log depth]	**Thickness** [m]	**Type**	**Type**
270.84	271.28	0.44	Fault zone	
508.03	508.04	0.01	Fault zone	
510.26	510.74	0.48	Fault zone	FDC 2
530.51	532.25	1.74	Fault zone	FDC 2
561.65	562.22	0.57	Fault zone	FDC 2
562.42	562.47	0.05	Fault zone	FDC 2
604.47	604.49	0.02	Fault zone	FDC 3
625.85	627.66	1.81	MirFP zone	
627.38	627.66	0.28	Fault zone	FDC 3
639.31	641.73	2.42	MirFP zone	
645.73	645.75	0.02	Fault zone	FDC 3
736.67	736.68	0.01	Fault zone	
740.31	740.36	0.05	Fault zone	
746.19	746.22	0.03	Fault zone	
746.42	746.43	0.01	Fault zone	
746.46	746.50	0.04	Fault zone	

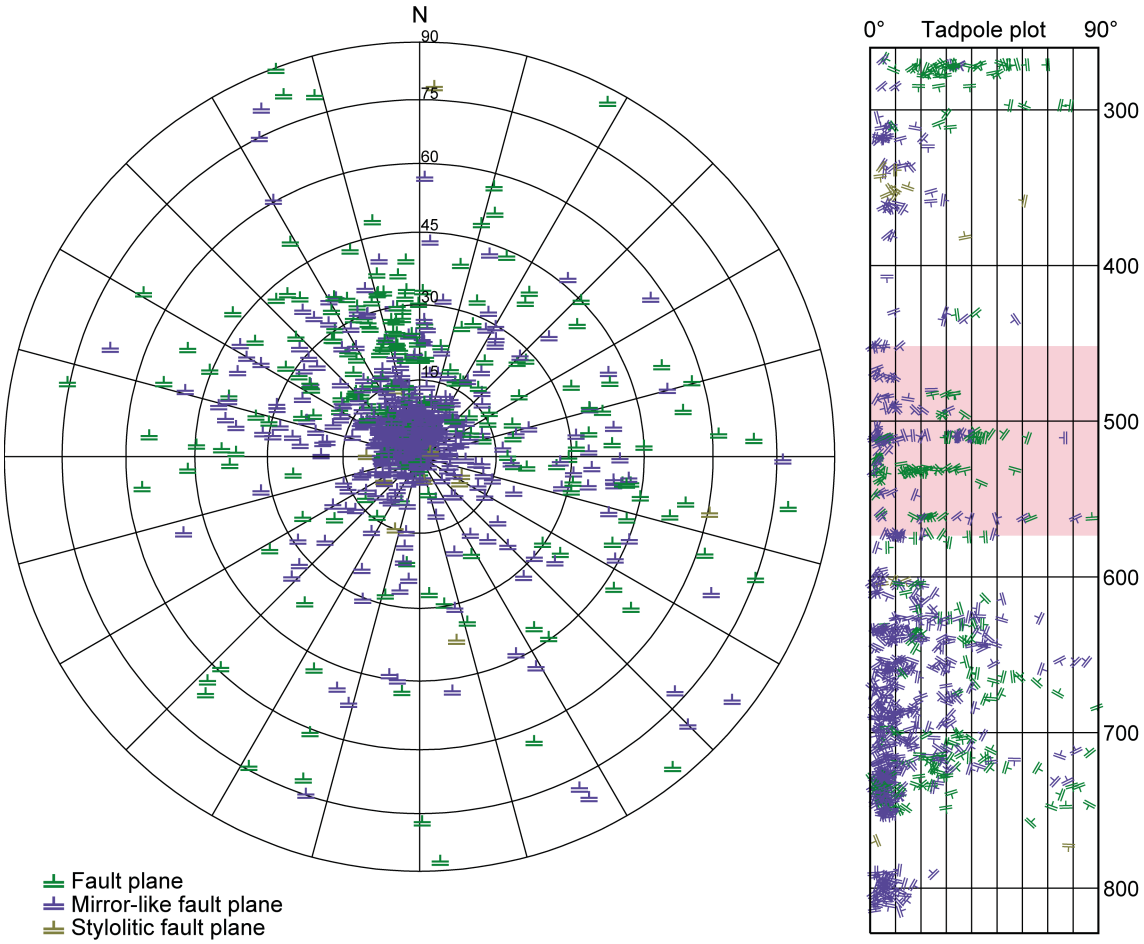

Fig. 4-5: Stereogram and depth plot of fault planes for the entire cored interval

A total 815 fault planes in oriented cores are plotted: fault planes (n = 241), mirror-like fault planes (n = 559) and stylolitic fault planes (n = 15). Depth range is 260.00 m to 829.88 m MD (log depth). In the tadpole plot the Opalinus Clay interval is indicated by a red bar.

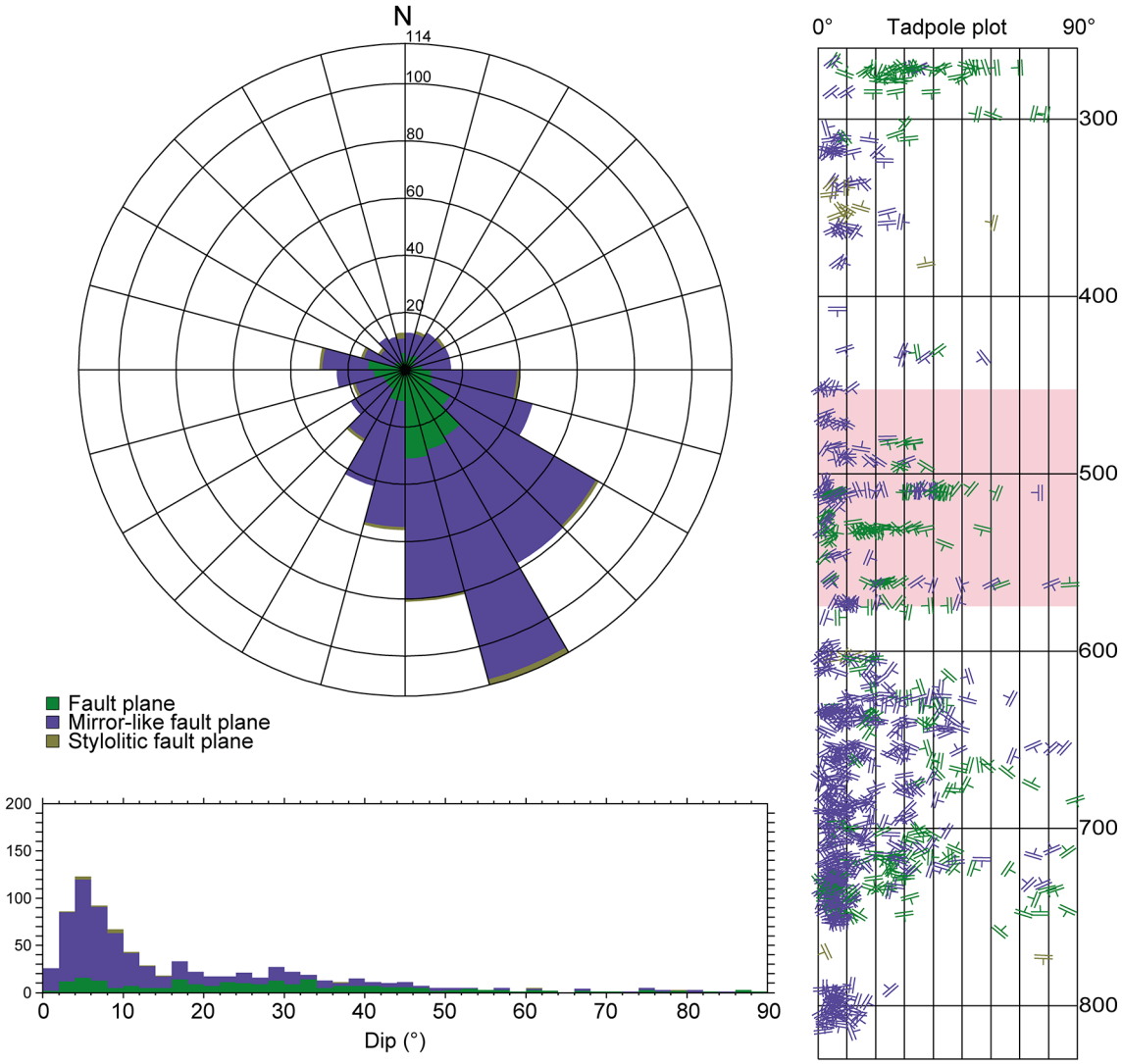

Fig. 4-6: Dip azimuth rose diagram, dip histogram and depth plot for fault planes in the entire cored interval

A total of 815 fault planes in oriented cores are plotted: fault planes (n = 241), mirror-like fault planes (n = 559) and stylolitic fault planes (n = 15). Depth range is 260.00 m to 829.88 mMD (log depth). In the tadpole plot the Opalinus Clay interval is indicated by a red bar.

Tension gashes / veins, joints and unassigned fractures

This group represents extensional features without shear indicators and comprises tension gashes / veins (n = 529) and joints (n = 36). Fractures (n = 54) which could not be assigned to a specific class of structure are also included. With a total of 619 individual structures, they represent a smaller group of structural discontinuities than the fault planes. Out of these 619 structures, 562 (91%) were recorded in oriented cores.

The spatial distribution of tension gashes / veins, joints and unassigned fractures along the BOZ2-1 borehole is presented in Fig. 4-4 and discussed in Section 4.1.4. Compared to faults, they reveal a considerable orientation scatter as shown in Figs. 4-7 and 4-8. However, a week orientation cluster of dipping planes with a vector mean of 164/07 (n = 65) could be defined (see Tab. 4-1).

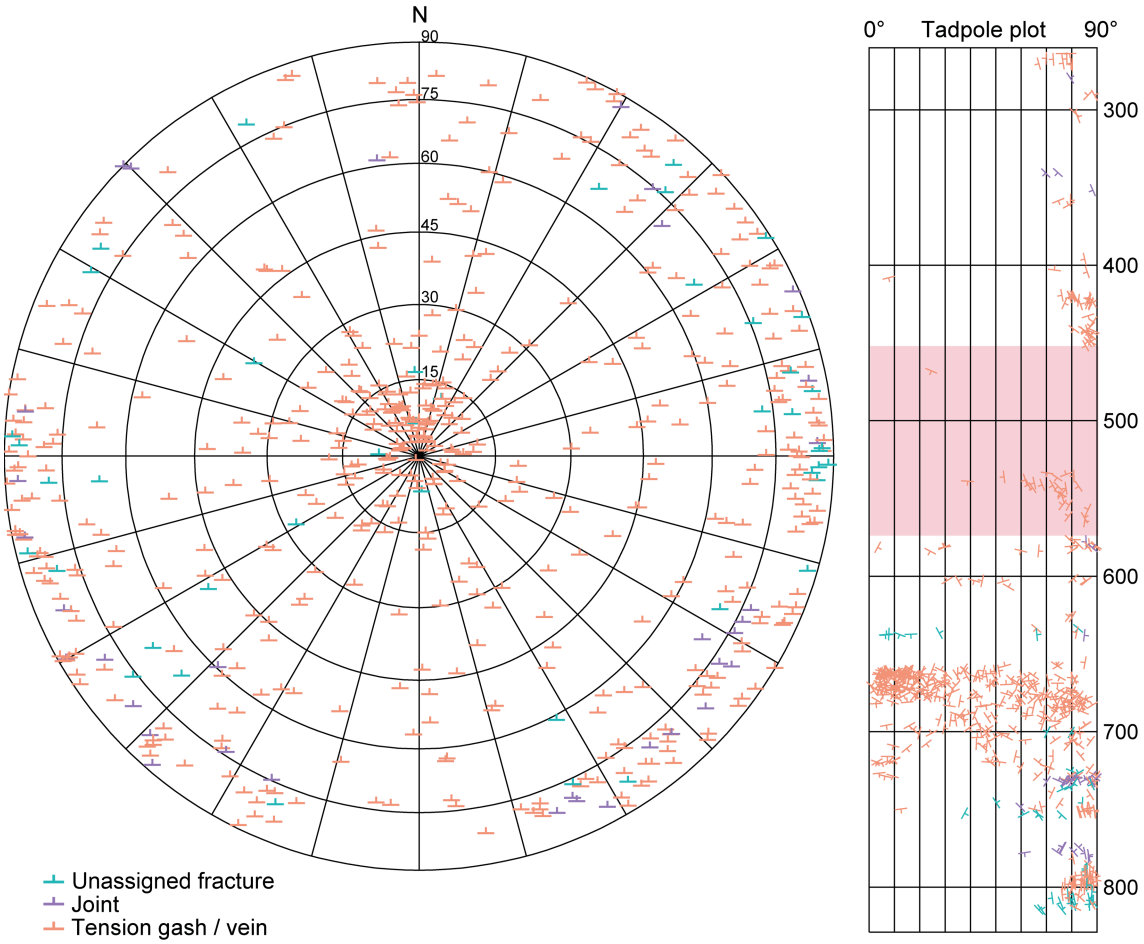

Fig. 4-7: Stereogram and depth plot for tension gashes / veins, unassigned fractures and joints in the entire cored interval

A total of 562 structures are displayed: tension gashes / veins (n = 485), joints (n = 34) and unassigned fractures (n = 43). Depth range is 260.00 m to 829.88 m MD (log depth). In the tadpole plot, the Opalinus Clay interval is indicated by a red bar.

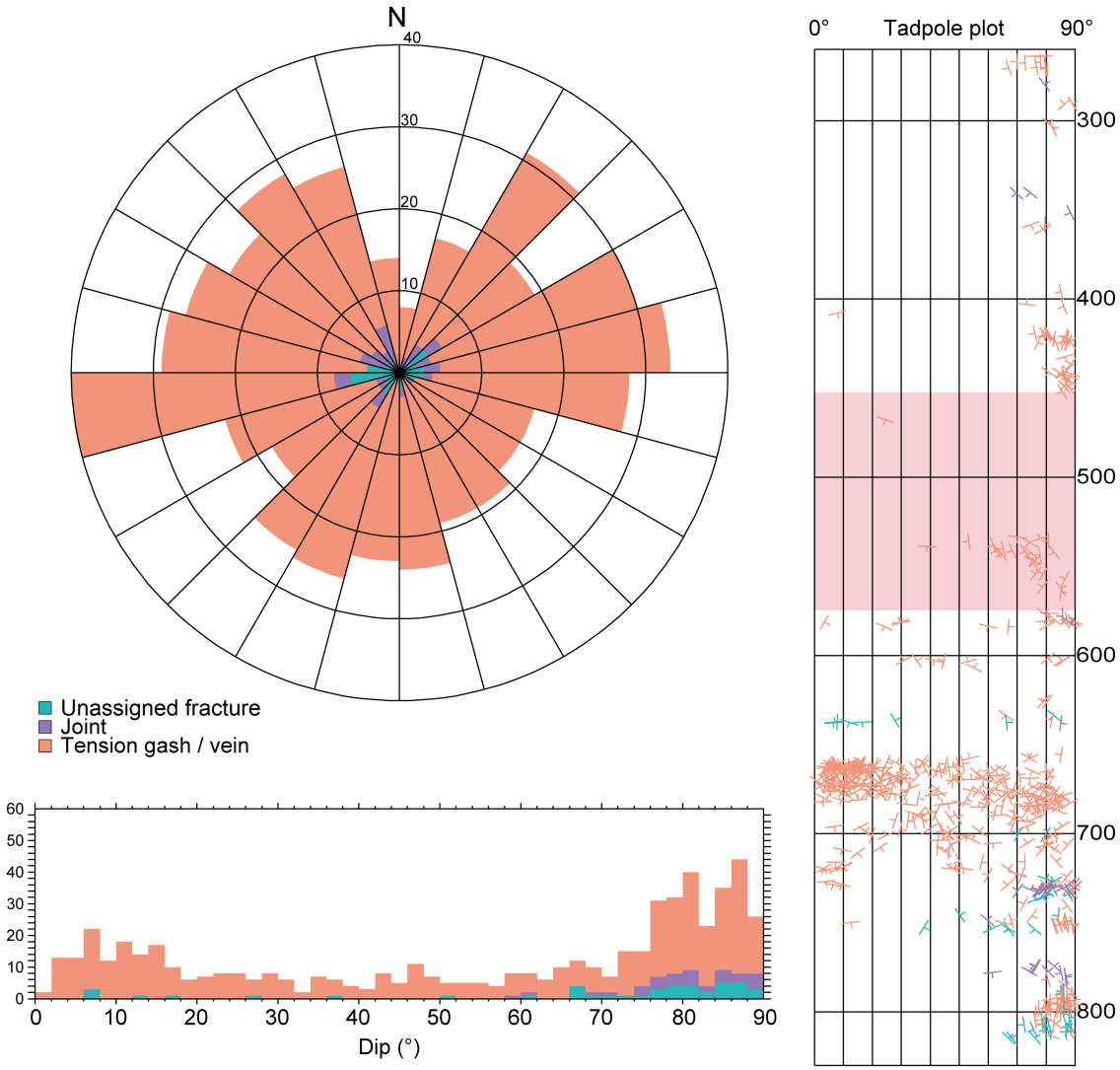

Fig. 4-8: Dip azimuth rose diagram of tension gashes / veins, unassigned fractures and joints in the entire cored interval

A total of 562 structures are displayed: tension gashes / veins (n = 485), joints (n = 34) and unassigned fractures (n = 43). Depth range is 260.00 m to 829.88 m MD (log depth). In the tadpole plot the Opalinus Clay interval is indicated by a red bar.

Stylolites

A total of 618 stylolites and 5 stylolite-rich zones were identified in BOZ2-1. Out of these, 580 (94%) were recorded in oriented cores. Particularly in stylolite-rich intervals such as the Malm and the Schinznach Formation (see Fig. 4-9), not all individual stylolites could be picked or documented and only dominant stylolites clearly observed in core photographs were recorded and categorised. Intervals with high densities of stylolites were defined as stylolitic.

Stylolites show one well developed orientation cluster (Figs. 4-9, 4-10 and Tab. 4-1) with sub-horizontal to shallow (1° to 25°) SE- to S-dipping features (overall mean: 158/04; n = 336).

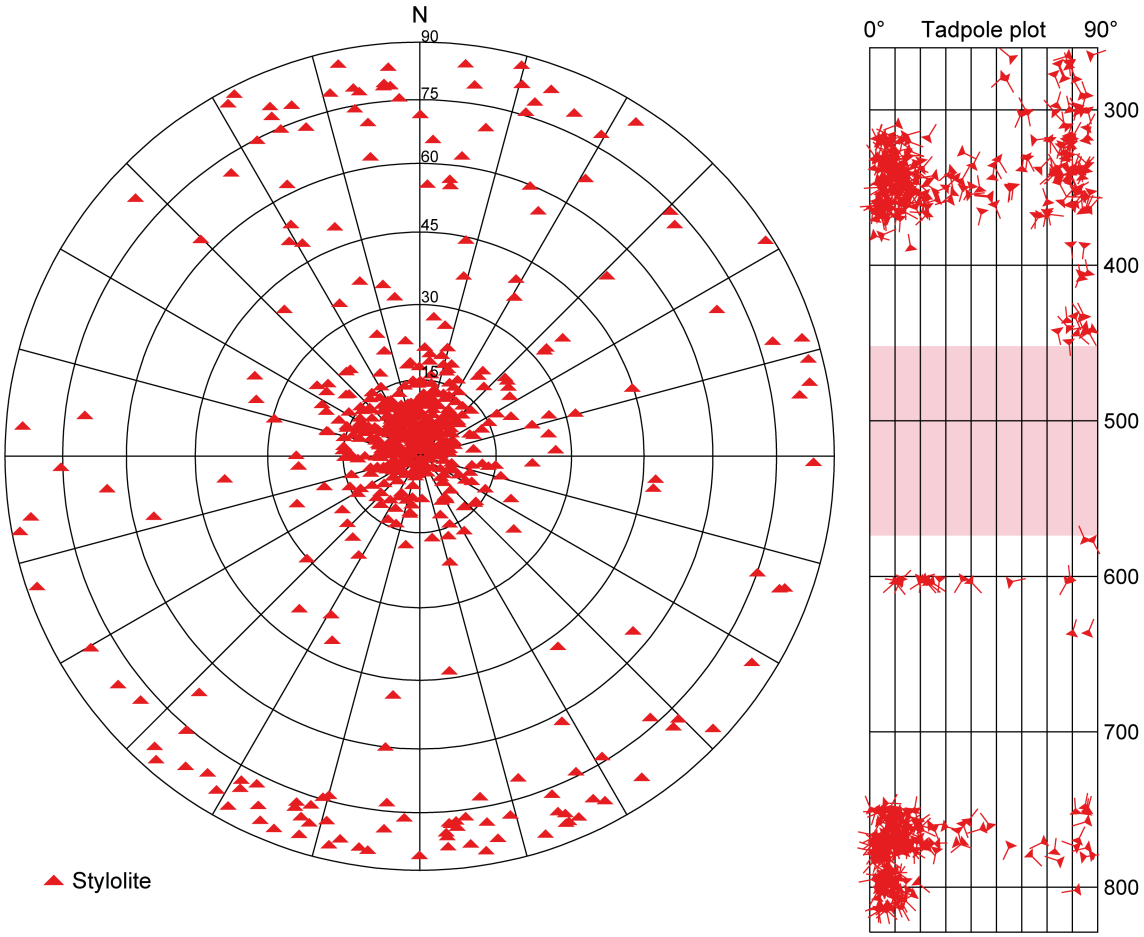

Fig. 4-9: Stereogram and depth plot for stylolites (n = 580) along the cored BOZ2-1 borehole

Depth range is 260.00 m to 829.88 m MD (log depth). In the tadpole plot, the Opalinus Clay interval is indicated by a red bar.

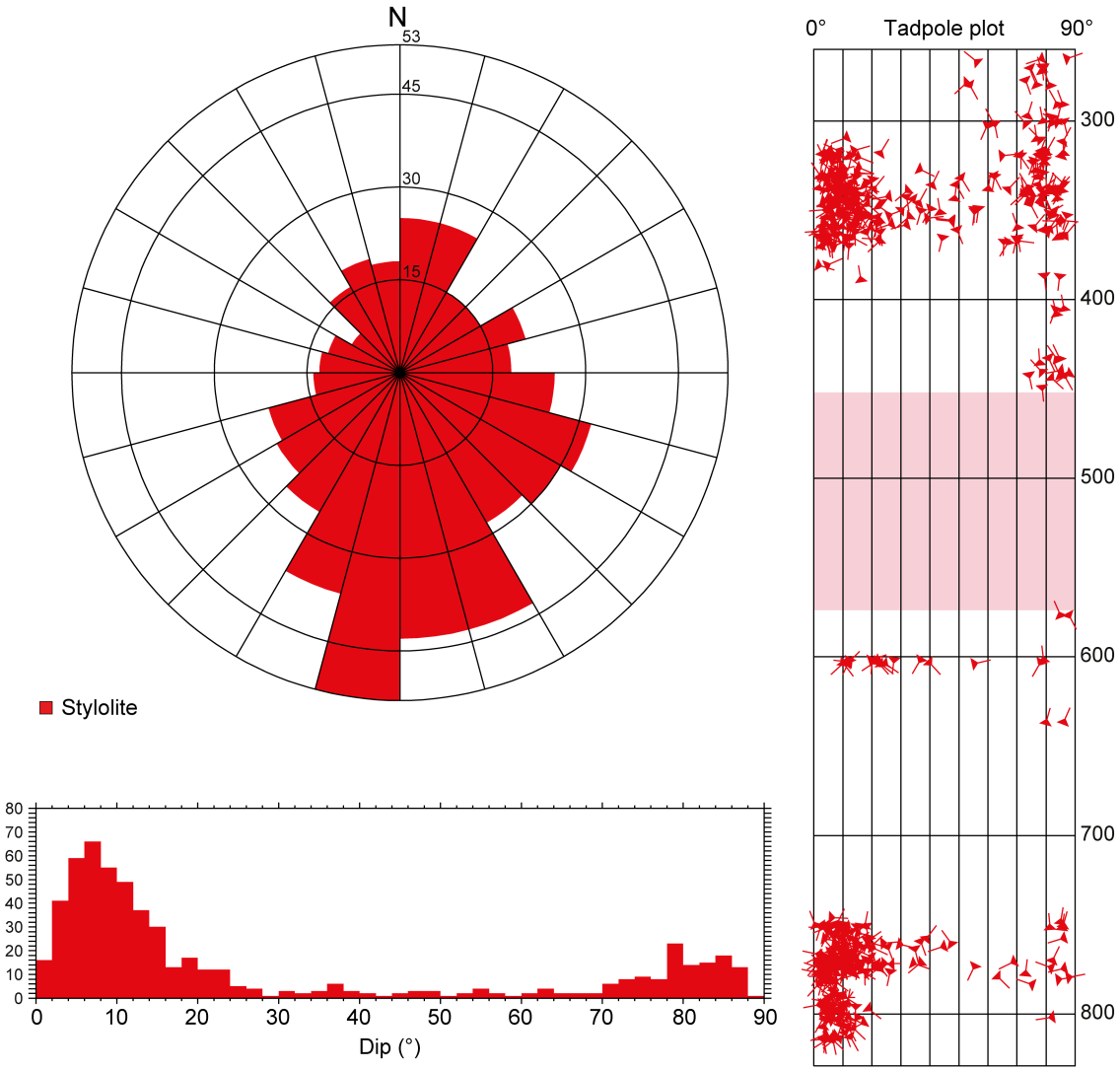

Fig. 4-10: Dip azimuth rose diagram and depth plot for stylolites in the entire cored interval

Depth range is 260.00 m to 829.88 m MD (log depth), n = 580. In the tadpole plot, the Opalinus Clay interval is indicated by a red bar.

4.1.3 Fracture density (P32) and distribution

Density histograms were calculated in order to evaluate the spatial distribution of fractures (see Fig. 4-4). As mentioned above, structures recorded in non-oriented cores (n = 172) were considered in the fracture density calculations.

Fault planes were unevenly distributed along the cored interval. High fault counts with up to 14 faults per metre occurred within the lower borehole interval from 603 m to 753 m MD (log depth) covering the lowermost Staffelegg Formation, the entire Klettgau Formation, the Bänkerjoch Formation and the uppermost Schinznach Formation. The highest densities of fault planes with up to 17 planes per metre were observed within the fault zones in the Opalinus Clay. Abundant faults commonly form prominent fault zones associated with intensely fractured and partly disintegrated drill cores (FDC 2 - 3; see Tab. 4-2 and Fig. 4-4). The average density of fault planes for the entire cored borehole section was 1.6 planes per metre.

Tension gashes / veins, joints and unassigned fractures are particularly abundant from approximately 657.00 m to 829.88 m MD (log depth) within the Bänkerjoch Formation, the Schinznach Formation and the Zeglingen Formation (see Fig. 4-4). The highest density (with up to 17 structures per metre) was encountered within the Bänkerjoch Formation from approximately 660 m to 685 m MD (log depth). However, the average density for the entire cored borehole section was about 1.1 planes per metre.

Stylolites revealed an uneven distribution along the borehole and occurred almost exclusively within the carbonate-rich lithologies of the Hauptrogenstein from approximately 316 m to 380 m MD (log depth) and in the Schinznach Formation from approximately 749 m to 821 m MD (log depth). The highest density with up to 14 stylolites per metre occurred within the Schinznach Formation at 750 m MD (log depth). However, the average density for the entire borehole section was about 1.1 stylolites per metre.

4.1.4 Kinematic indicators

Striations could be measured on 615 fault planes; some fault planes included more than one kinematic indicator resulting in a total of 628 measured lineations. In total, 93% of the striations (n = 586) were observed in oriented cores. The orientations of the striations in oriented cores are given in Figs. 4-11 to 4-16. There is a clear predominance of S-dipping striations. The plunge of striations varies between subhorizontal to steep (1° to 50°). However, the vast majority does not exceed 10°.

Three different shear senses were distinguished on the analysed drill cores:

- up = thrusting / reverse faulting
- down = normal faulting
- dextral / sinistral = strike-slip faulting

A total of 155 shear indicators were identified as thrusts / reverse faults (Tab. 4-3). In contrast, the number of faults classified as normal faults (n = 49) or strike-slip faults (n = 7) is much lower (Tab. 4-3). However, the shear sense of most fault planes (n = 417) was uncertain (Tab. 4-3).

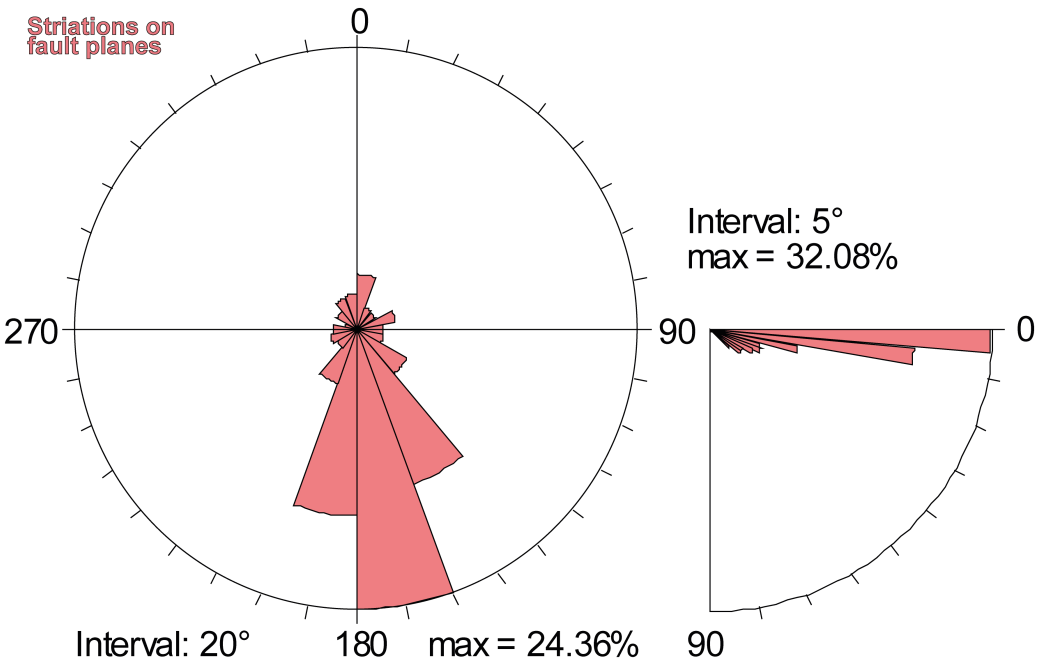

Fig. 4-11: Plunge azimuth of striations along fault planes in the entire cored interval

The striations (n = 586) from oriented cores of the entire cored interval from the Malm to the Muschelkalk are presented. Left: plunge azimuth rose diagram, right: plunge histogram. Depth range is 260.00 m to 829.88 m MD (log depth).

Tab. 4-3: List of all kinematic indicators in oriented and non-oriented cores

Shear sense	**Number**
Up	155
Down	49
Sinistral	4
Dextral	3
Unknown	417
In oriented cores	586
In non-oriented cores	42
Total measured lineations	628

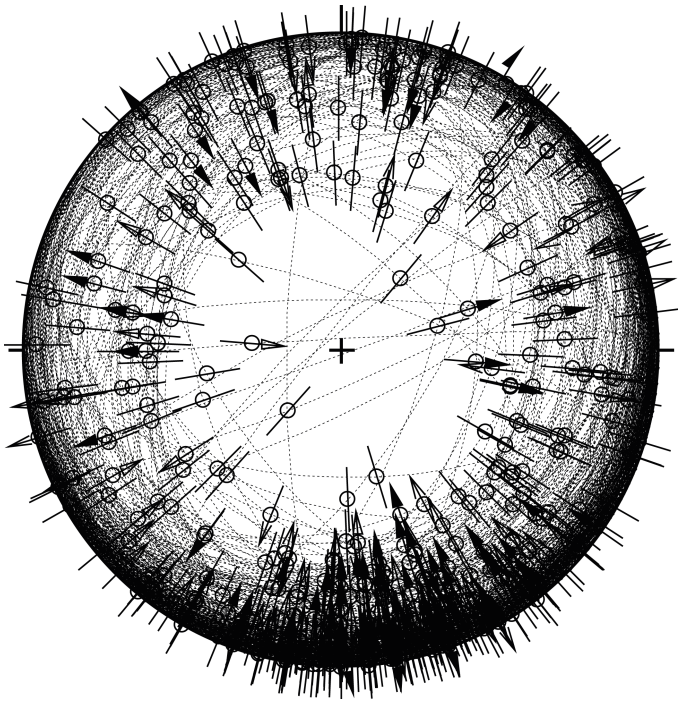

Fig. 4-12: Stereogram of striations on all oriented fault planes (including multiple lineations on a single fault plane) and associated kinematic data

Shear sense up (n = 150), down (n = 47), dextral (n = 3), sinistral (n = 2) and unknown (n = 384). Depth range is 260.00 m to 829.88 m MD (log depth).

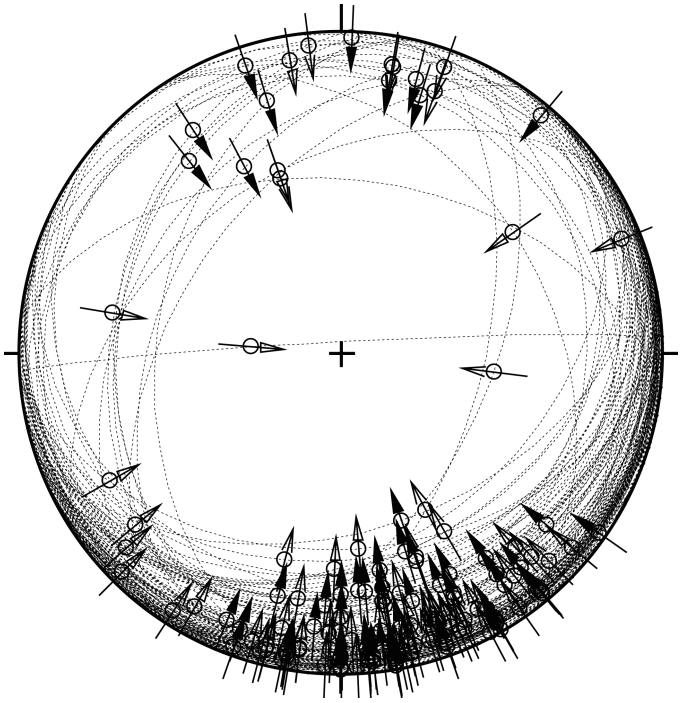

Fig. 4-13: Stereogram with striations of oriented thrust / reverse fault planes (including multiple lineations on a single fault plane)

Shear sense up (n = 150). Depth range is 260.00 m to 829.88 m MD (log depth).

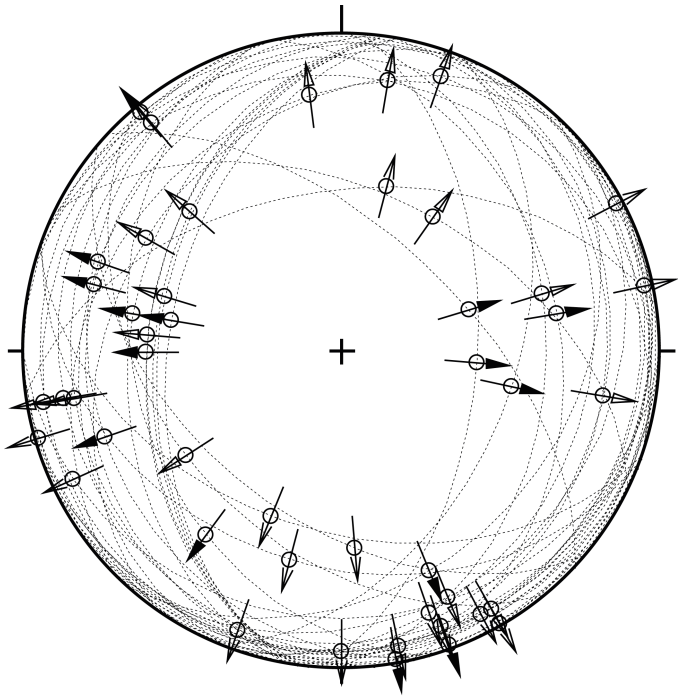

Fig. 4-14: Stereogram of striations on all oriented normal fault planes (including multiple lineations on a single fault plane)

Shear sense down (n = 47). Depth range is 260.00 m to 829.88 m MD (log depth).

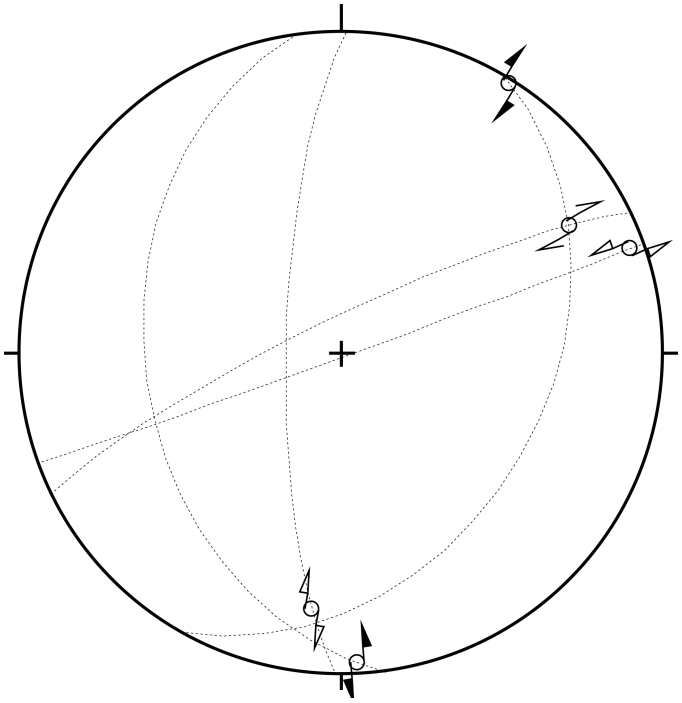

Fig. 4-15: Stereogram of striations on all oriented strike-slip fault planes

Shear sense dextral (n = 3), sinistral (n = 2). Depth range is 260.00 m to 829.88 m MD (log depth).

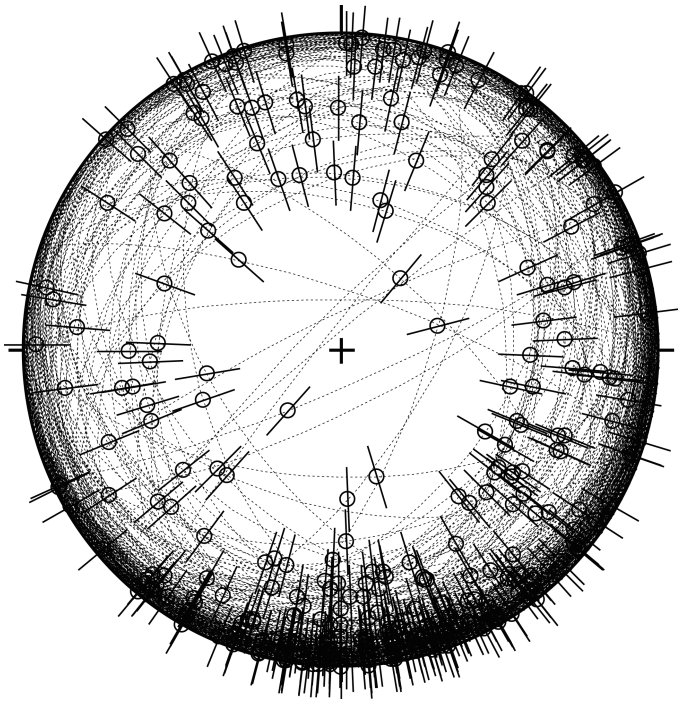

Fig. 4-16: Stereogram of striations on all fault planes with unknown shear sense (including multiple lineations on a single fault plane)

Shear sense unknown (n = 384). Depth range is 260.00 m to 829.88 m MD (log depth).

4.2 Malm

The cored Malm covers the interval from 260.00 m to 304.38 m MD (log depth). For the stereographic evaluation, only one lithostratigraphic unit (Wildegg Formation) was defined within the Malm interval. Only the data from oriented cores are presented.

4.2.1 Wildegg Formation

The orientation and spatial depth distribution of recorded structures in the Wildegg Formation (260.00 m to 304.38 m MD [log depth]) are shown in Figs. 4-17 to 4-23. The Wildegg Formation showed a small number of structures with a preferred orientation dipping towards the SE. The few steeply dipping joints and tension gashes observed have a preferred dip direction to the WSW. Stylolites are generally steeply dipping and strike NNW-SSE.

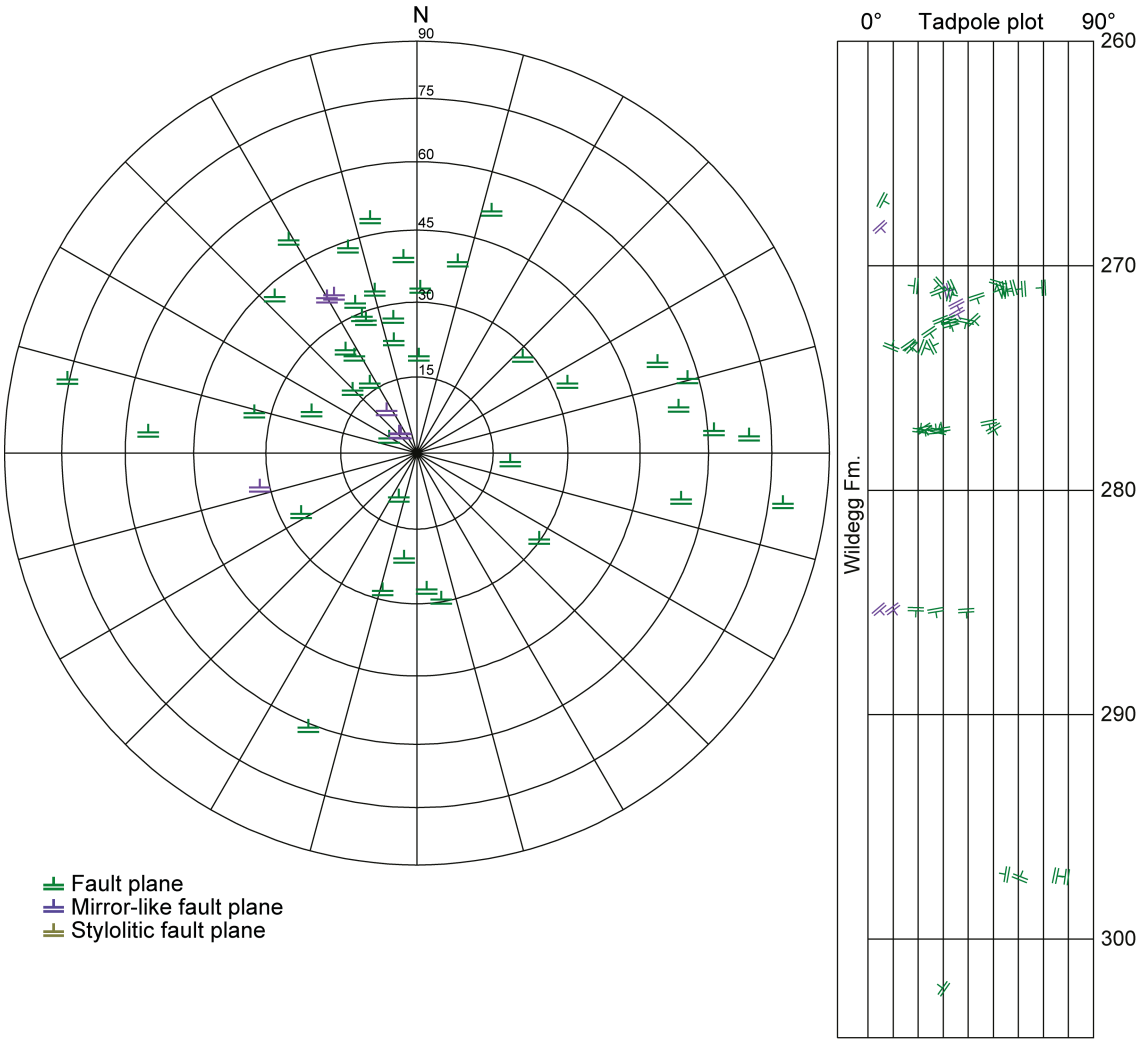

Fig. 4-17: Stereogram and depth plot of fault planes (Wildegg Formation)

Fault planes (n = 42) and mirror-like fault planes (n = 6); stylolitic fault planes were not observed (n = 0).

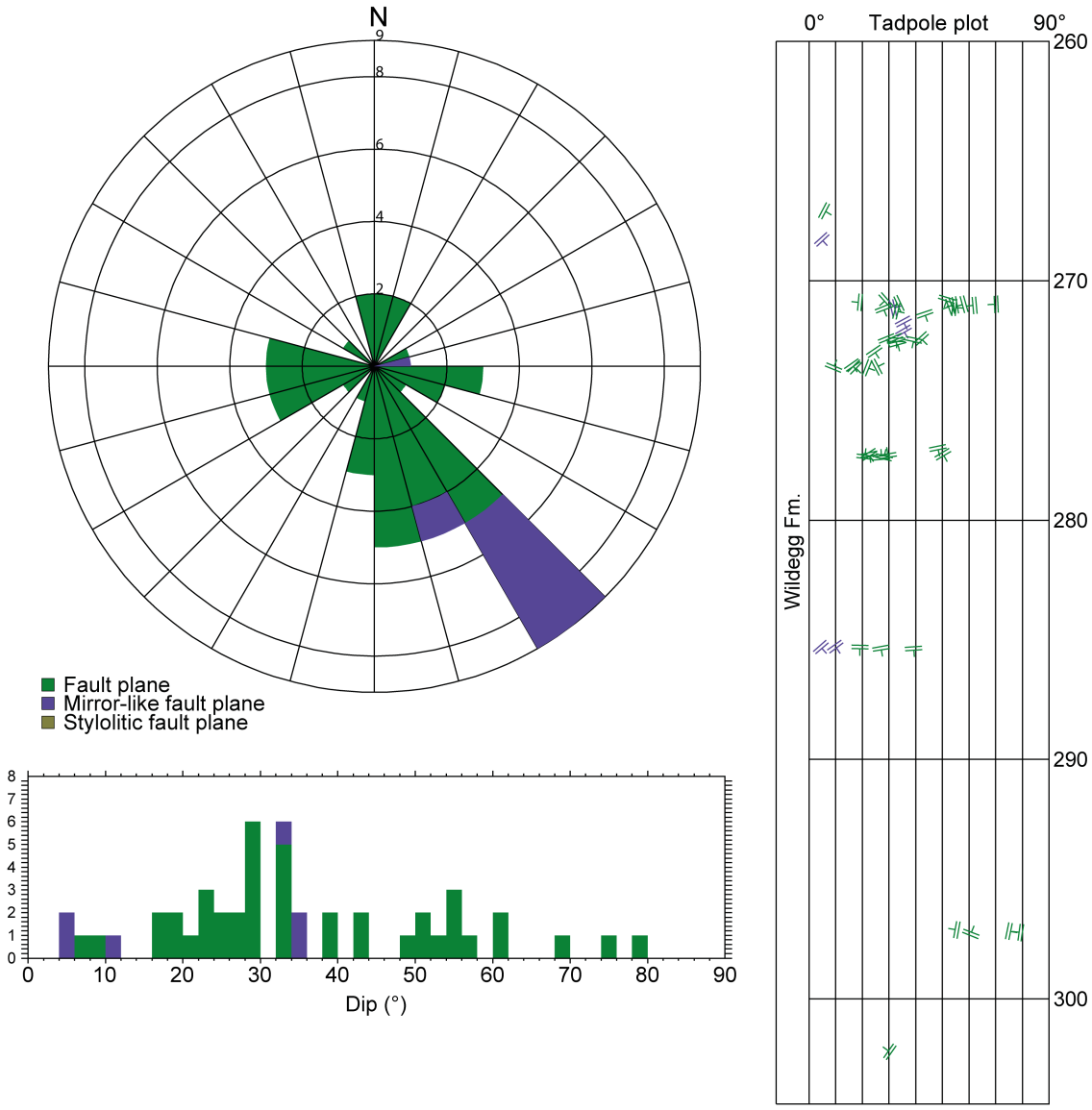

Fig. 4-18: Dip azimuth rose diagram, dip histogram and depth plot of fault planes (Wildegg Formation)

Fault planes (n = 42) and mirror-like fault planes (n = 6); stylolitic fault planes were not observed (n = 0).

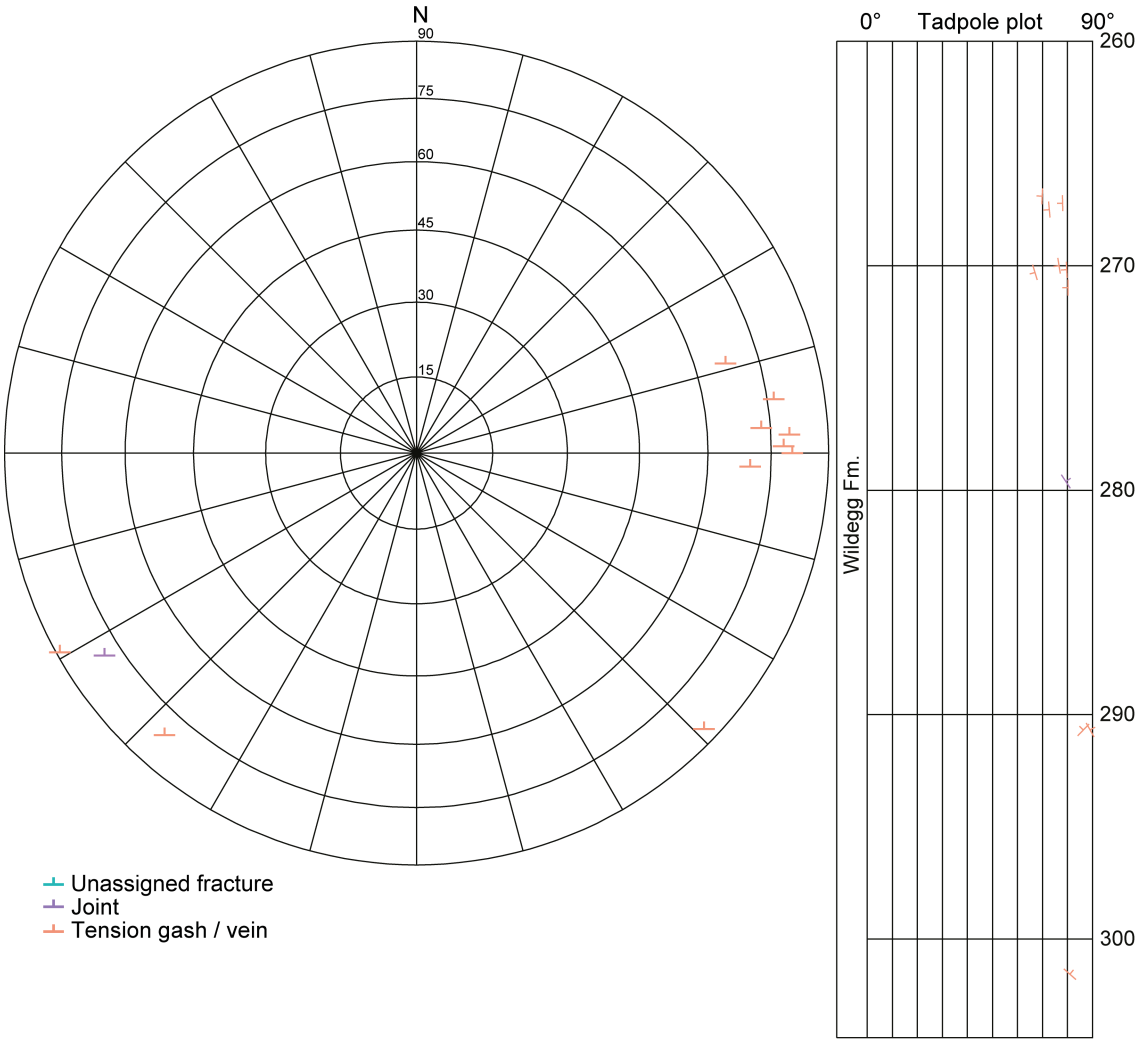

Fig. 4-19: Stereogram and depth plot of tension gashes / veins and unassigned fractures (Wildegg Formation)

Joints (n = 1) and tension gashes / veins (n = 10); no unassigned fractures were observed (n = 0).

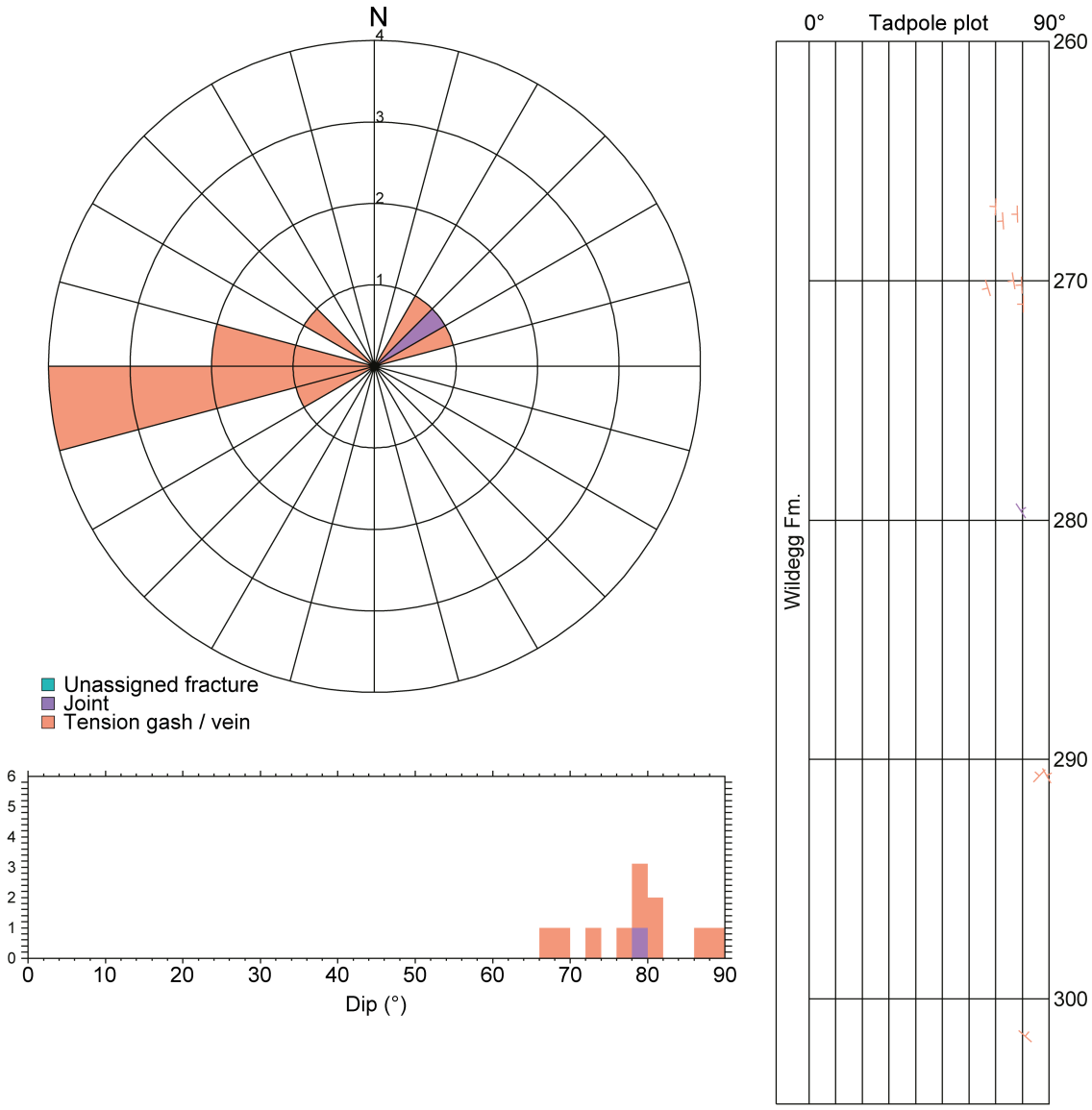

Fig. 4-20: Dip azimuth rose diagram, dip histogram and depth plot of tension gashes / veins, joints and unassigned fractures (Wildegg Formation)

Joints (n = 1) and tension gashes / veins (n = 10); no unassigned fractures were observed (n = 0).

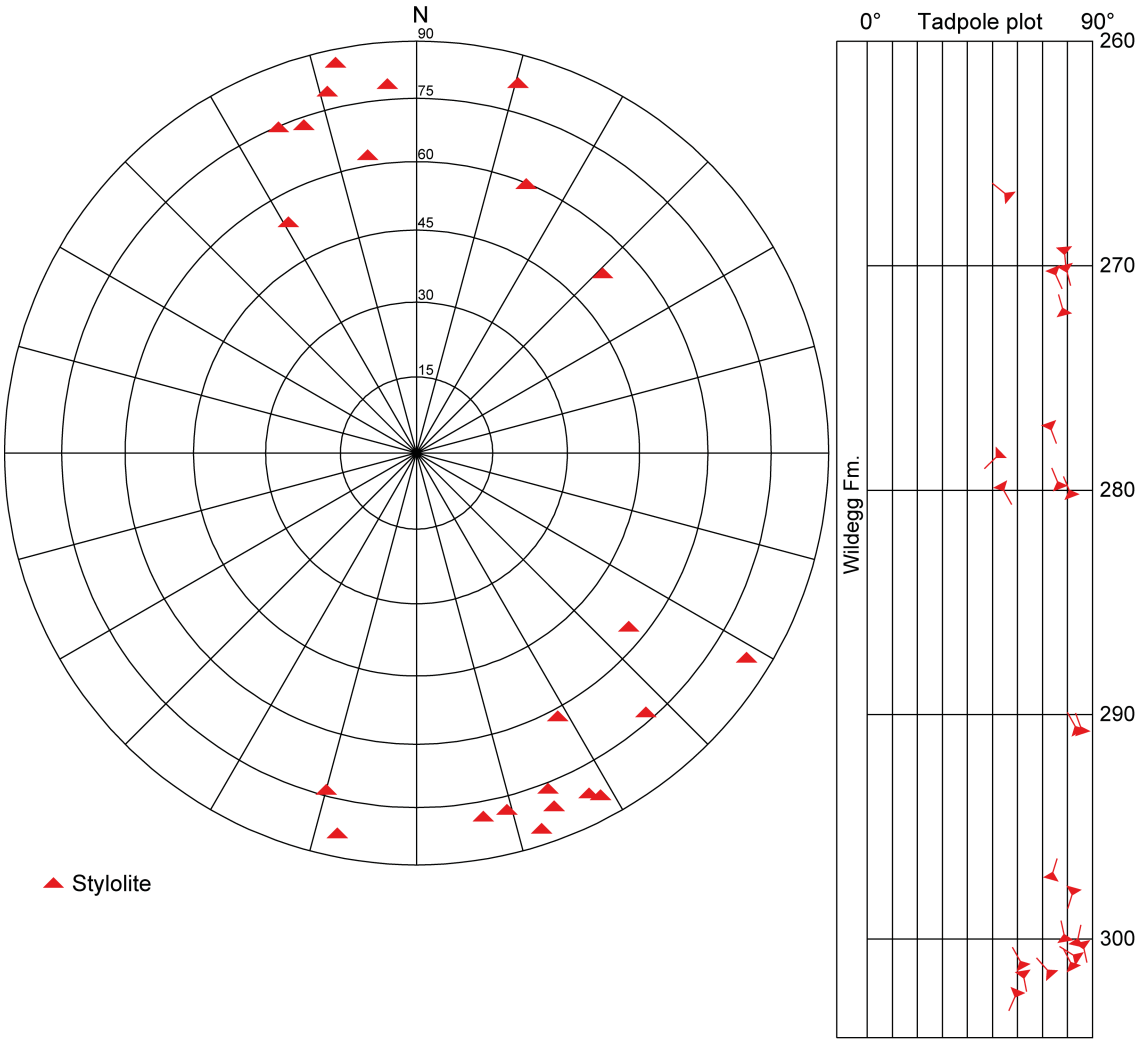

Fig. 4-21: Stereogram and depth plot of stylolites (Wildegg Formation; n = 23)

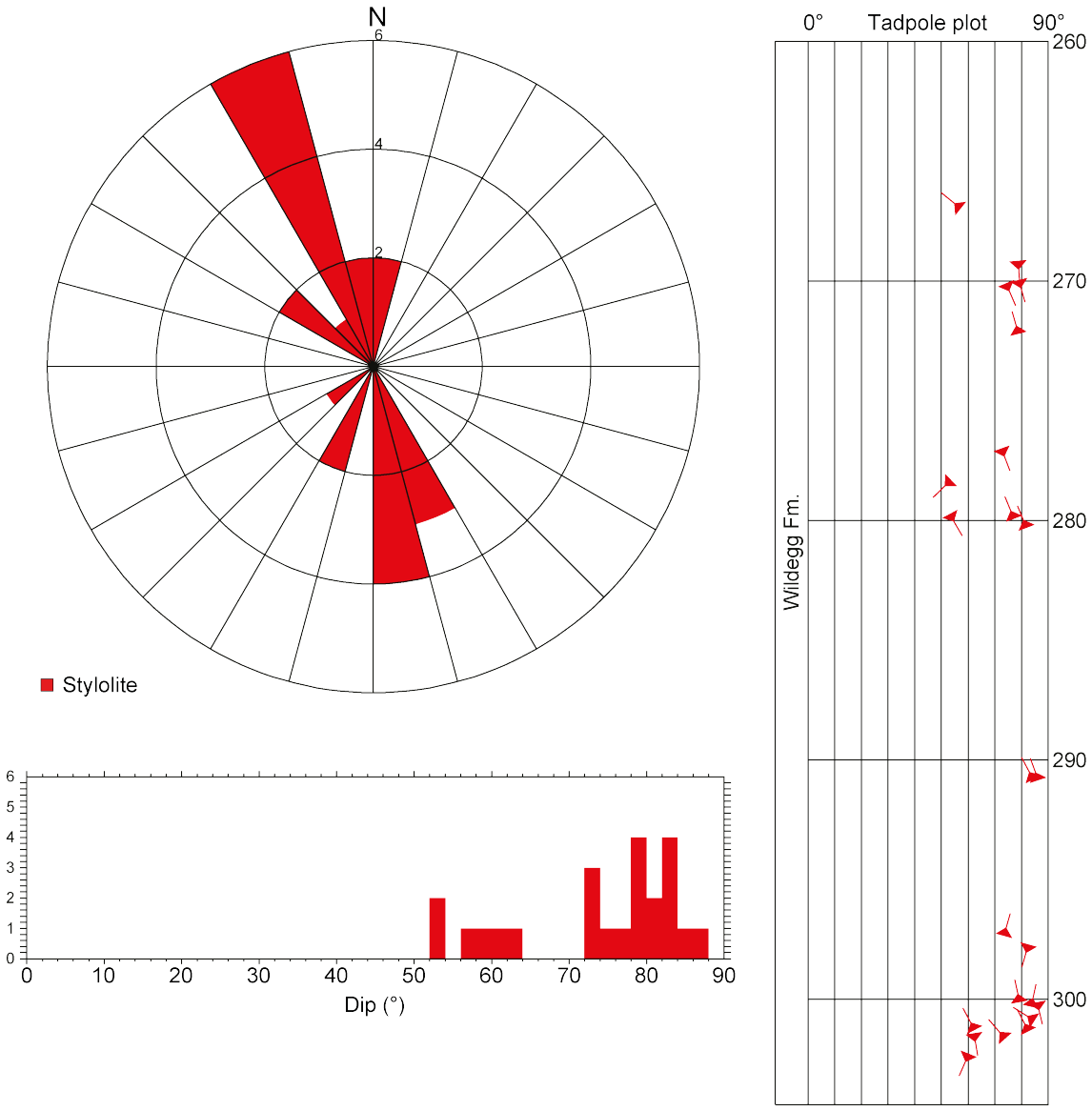

Fig. 4-22: Dip azimuth rose diagram, dip histogram and depth plot of stylolites (Wildegg Formation; n = 23)

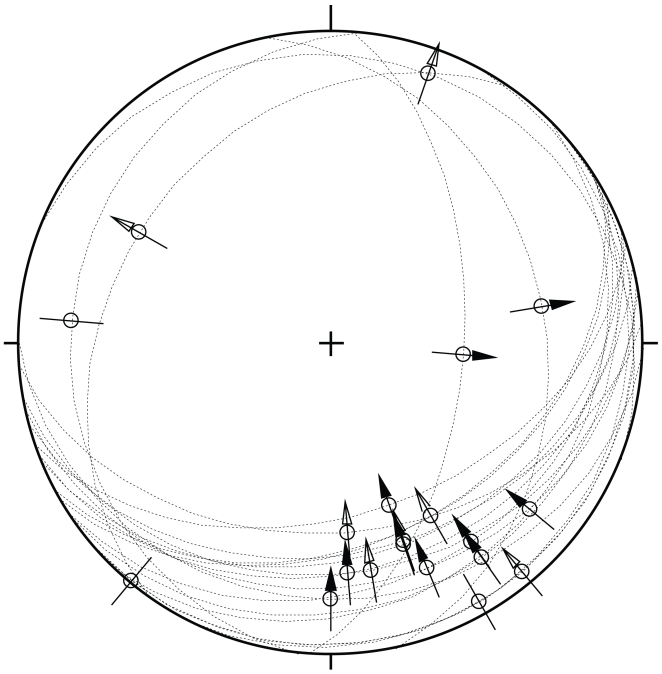

Fig. 4-23: Stereogram of striations on fault planes, including multiple lineations on a single fault plane (Wildegg Formation; n = 21)

4.3 Dogger

For the detailed stereographic evaluation, the Dogger was subdivided into three units: the Hauptrogenstein and the Ifenthal Formation, the Passwang Formation and the Opalinus Clay. The orientations and spatial distribution of structural discontinuities within the Dogger are visualised Figs. 4-24 to 4-40. Only the data from oriented cores are presented.

4.3.1 Hauptrogenstein to Ifenthal Formation

The Hauptrogenstein to Ifenthal Formation (304.38 m to 388.97 m MD [log depth]) show a moderate density of fault planes and stylolites. Fault planes generally have a flat to moderate dip and show a preferred dip towards the S to SE. Stylolites are either steep or subhorizontal. They generally show two strike directions: SE to SW and ESE-WNW. Tension gashes and joints are rare.

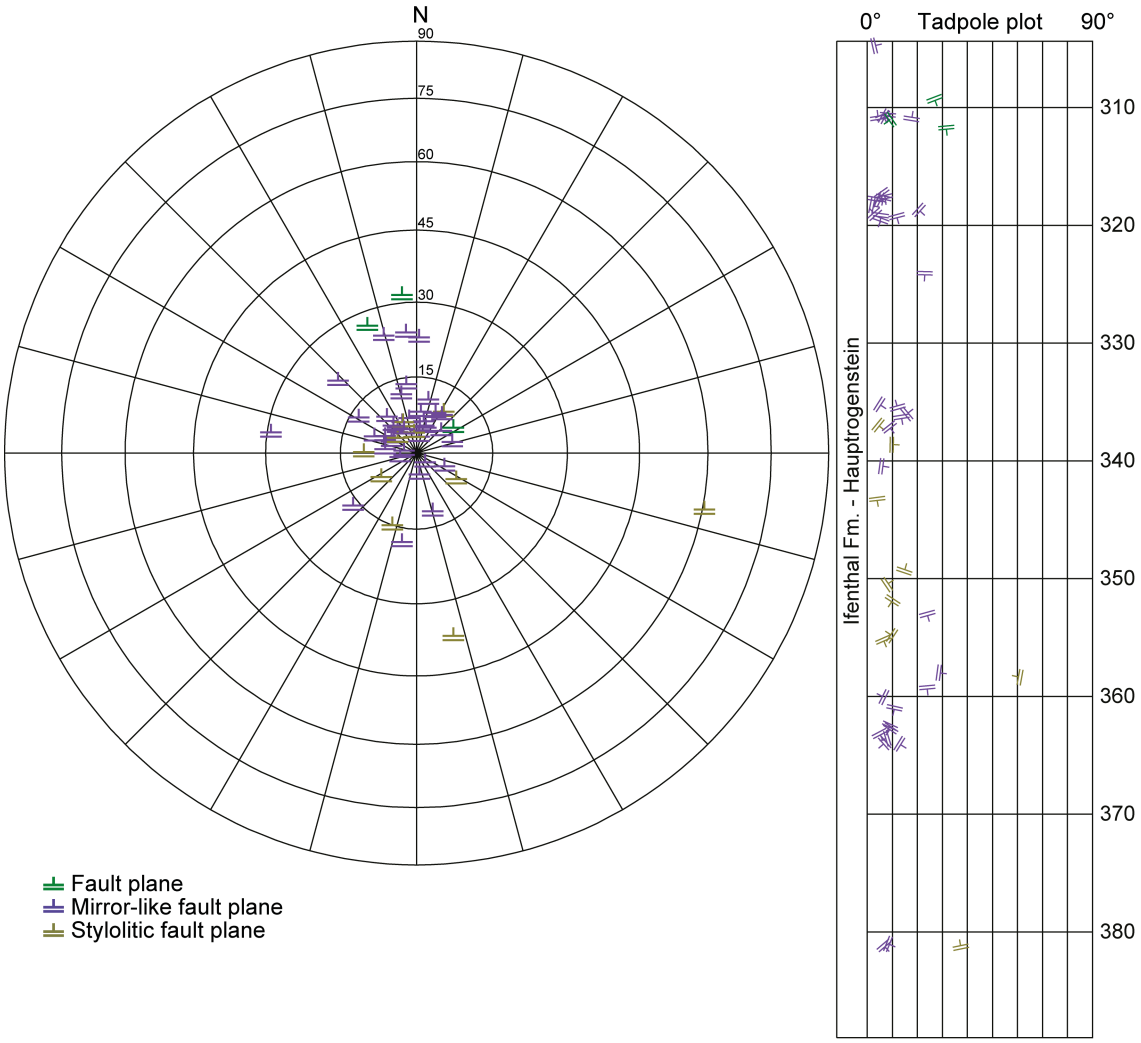

Fig. 4-24: Stereogram and depth plot of fault planes (Hauptrogenstein to Ifenthal Formation)
Fault planes (n = 3), mirror-like fault planes (n = 37) and stylolitic fault planes (n = 10).

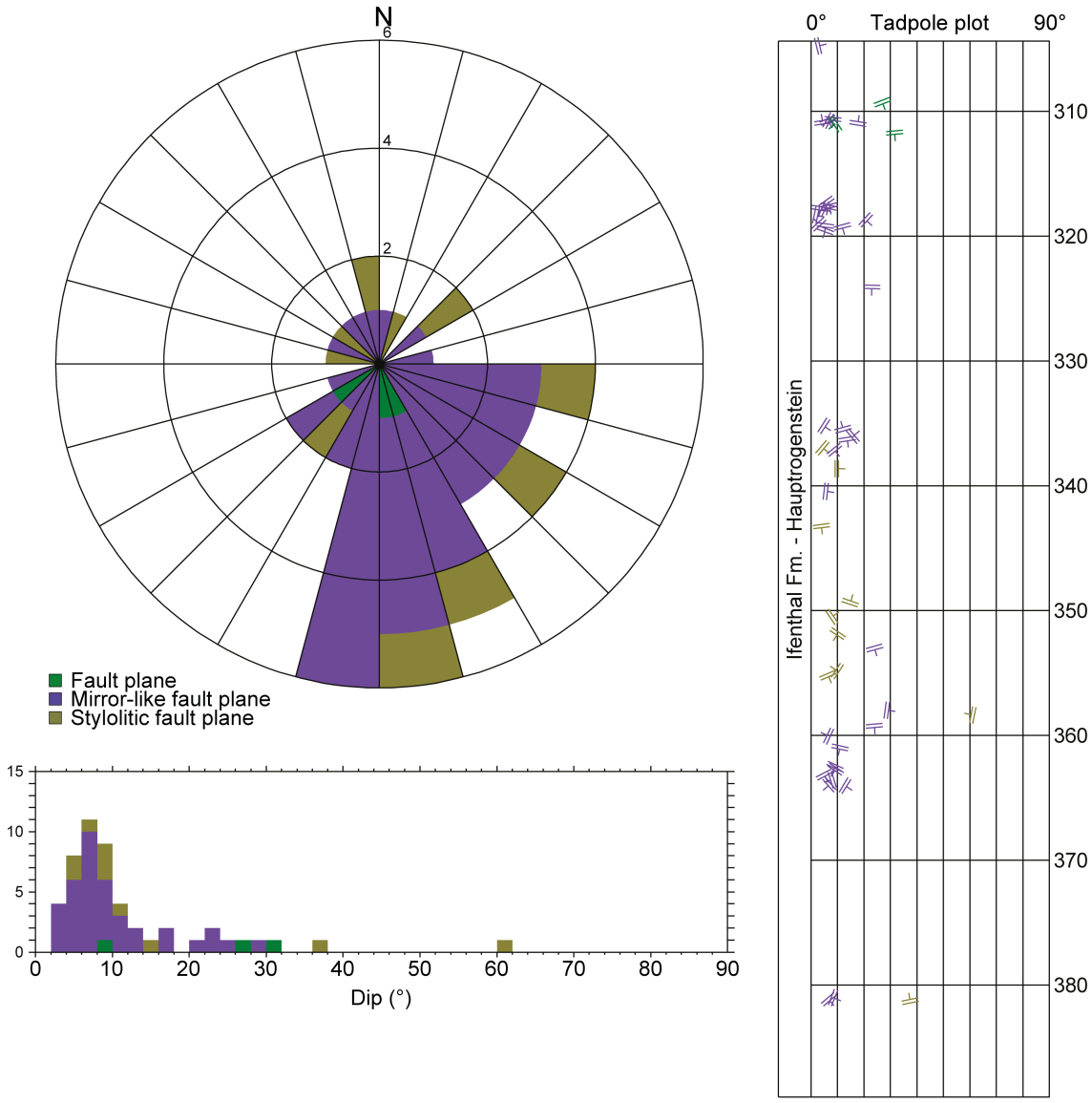

Fig. 4-25: Dip azimuth rose diagram, dip histogram and depth plot of fault planes (Hauptrogenstein to Ifenthal Formation)

Fault planes (n = 3), mirror-like fault planes (n = 37) and stylolitic fault planes (n = 10).

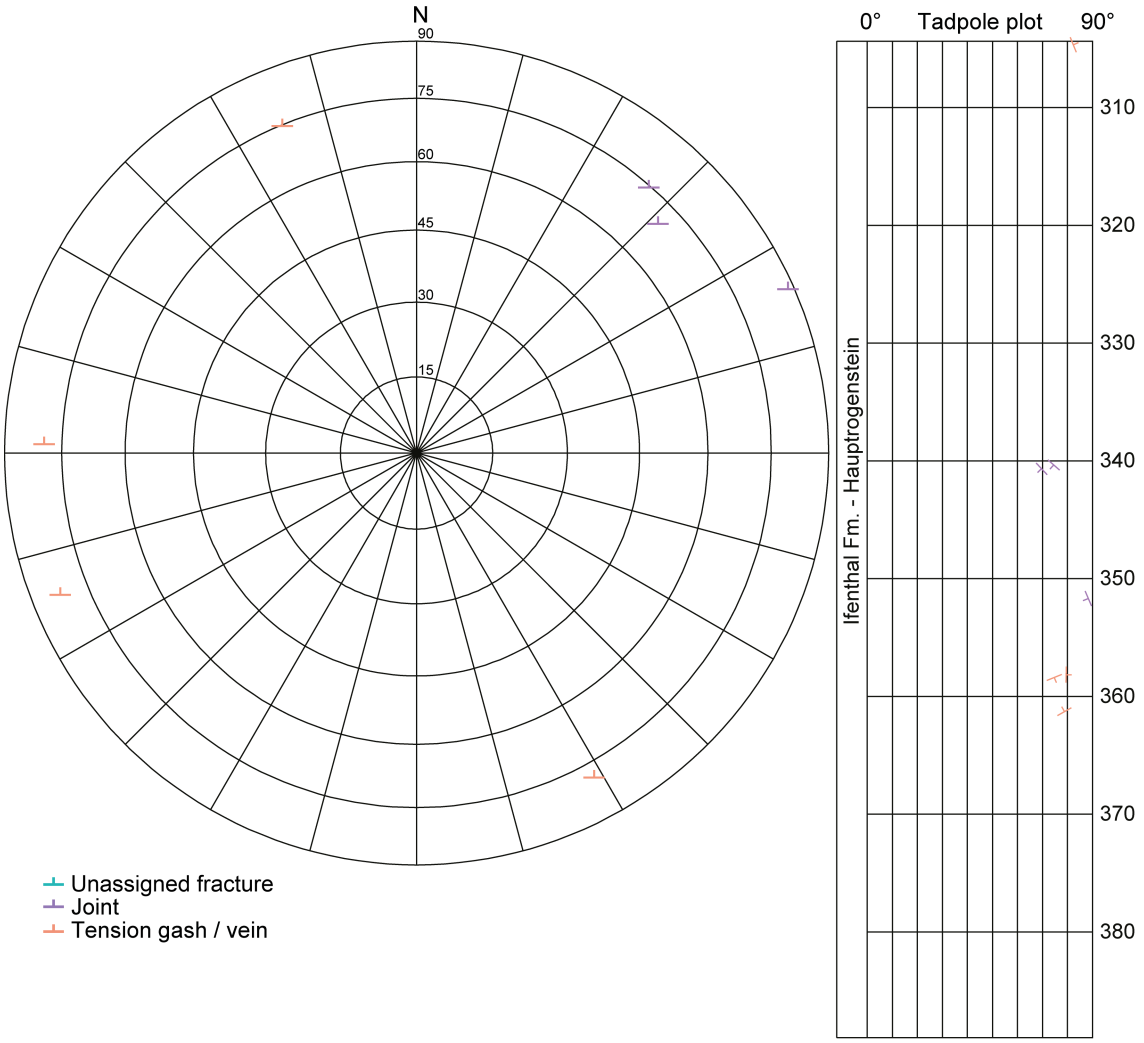

Fig. 4-26: Stereogram and depth plot of tension gashes / veins, joints and unassigned fractures (Hauptrogenstein to Ifenthal Formation)

Joints (n = 3) and tension gashes / veins (n = 4); no unassigned fractures were observed (n = 0).

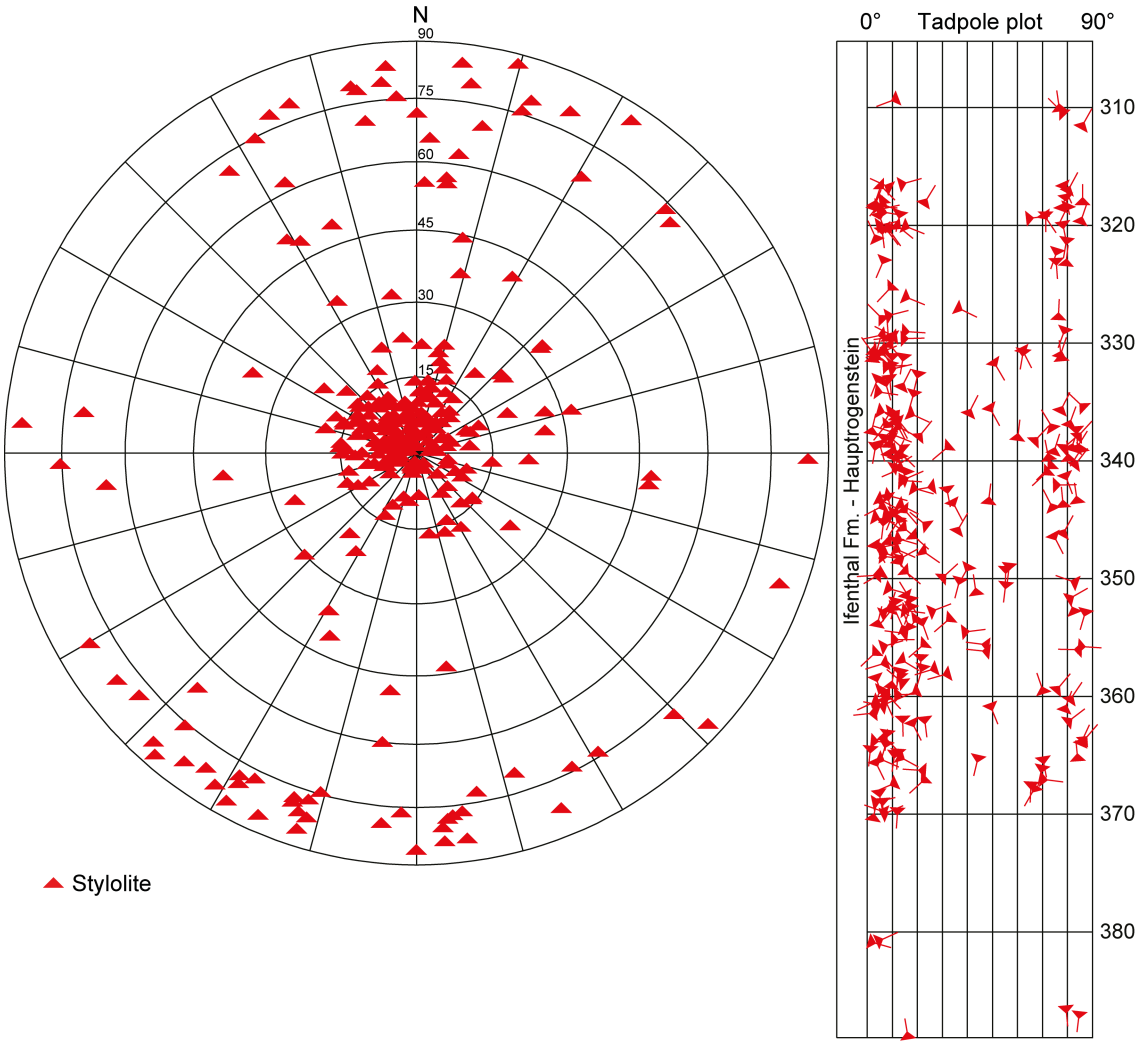

Fig. 4-27: Stereogram and depth plot of stylolites (Hauptrogenstein to Ifenthal Formation; n = 274)

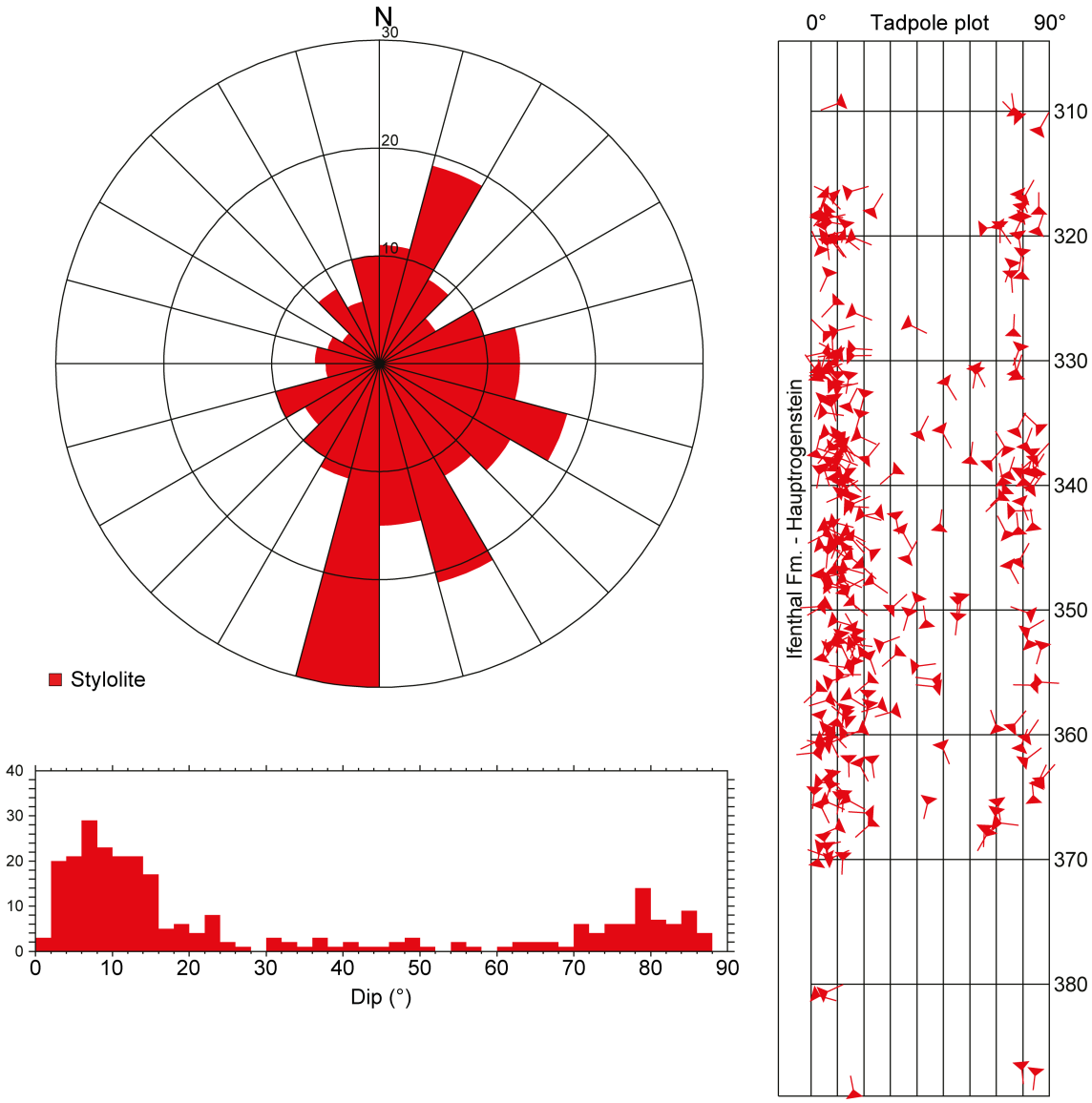

Fig. 4-28: Dip azimuth rose diagram, dip histogram and depth plot of stylolites (Hauptrogenstein to Ifenthal Formation; n = 274)

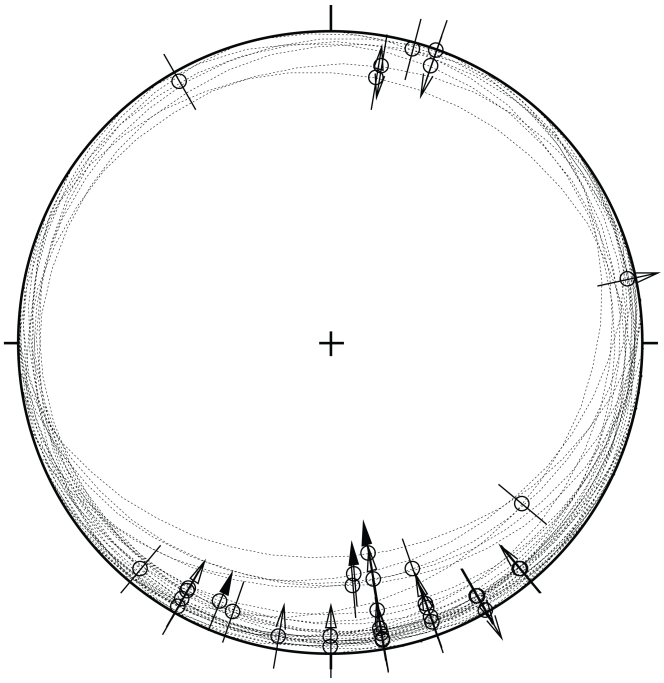

Fig. 4-29: Stereogram of striations on fault planes, including multiple lineations on a single fault plane (Hauptrogenstein to Ifenthal Formation; n = 38)

4.3.2 Passwang Formation

The Passwang Formation (388.97 m to 451.90 m MD [log depth]) is characterised by a low number of faults, tension gashes and stylolites. Tension gashes are steeply inclined with a general dip towards the SW. Stylolites are also steeply inclined with a general ENE-WSW strike.

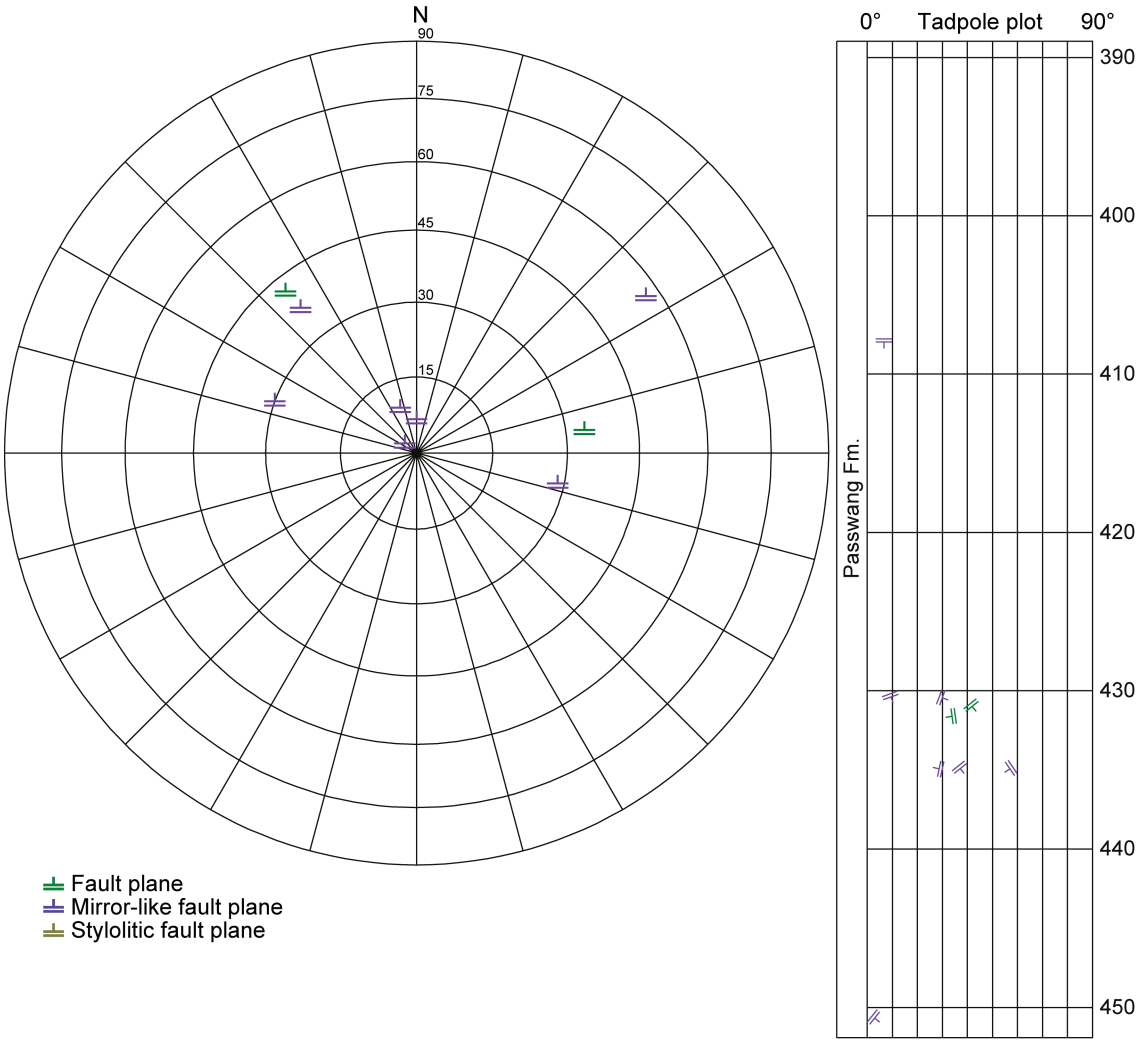

Fig. 4-30: Stereogram and depth plot of fault planes (Passwang Formation)

Fault planes (n = 2), mirror-like fault planes (n = 7); stylolitic fault planes were not observed (n = 0).

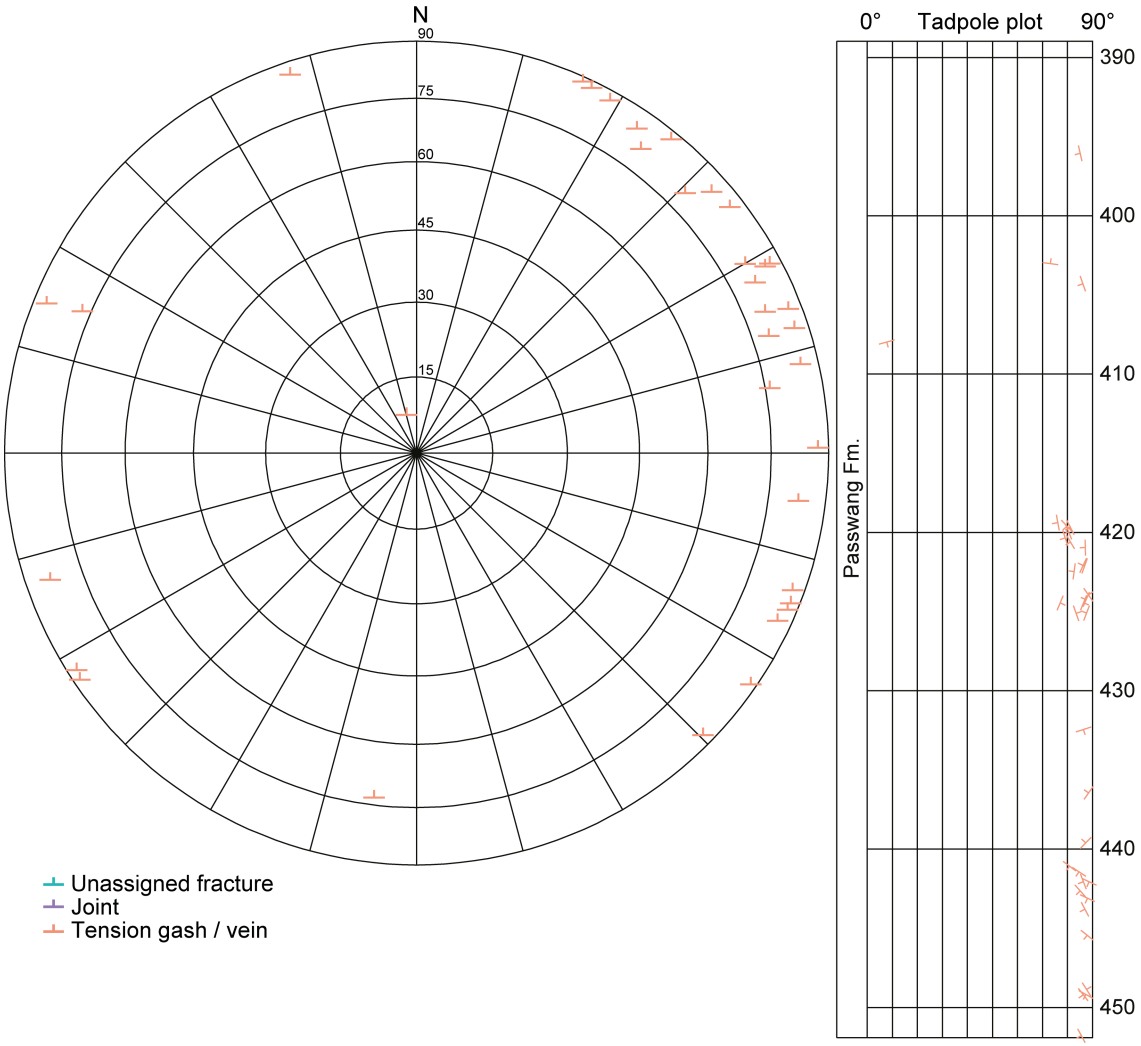

Fig. 4-31: Stereogram and depth plot of tension gashes / veins, joints and unassigned fractures (Passwang Formation)

Tension gashes / veins (n = 35); unassigned fractures and joints were not observed (n = 0).

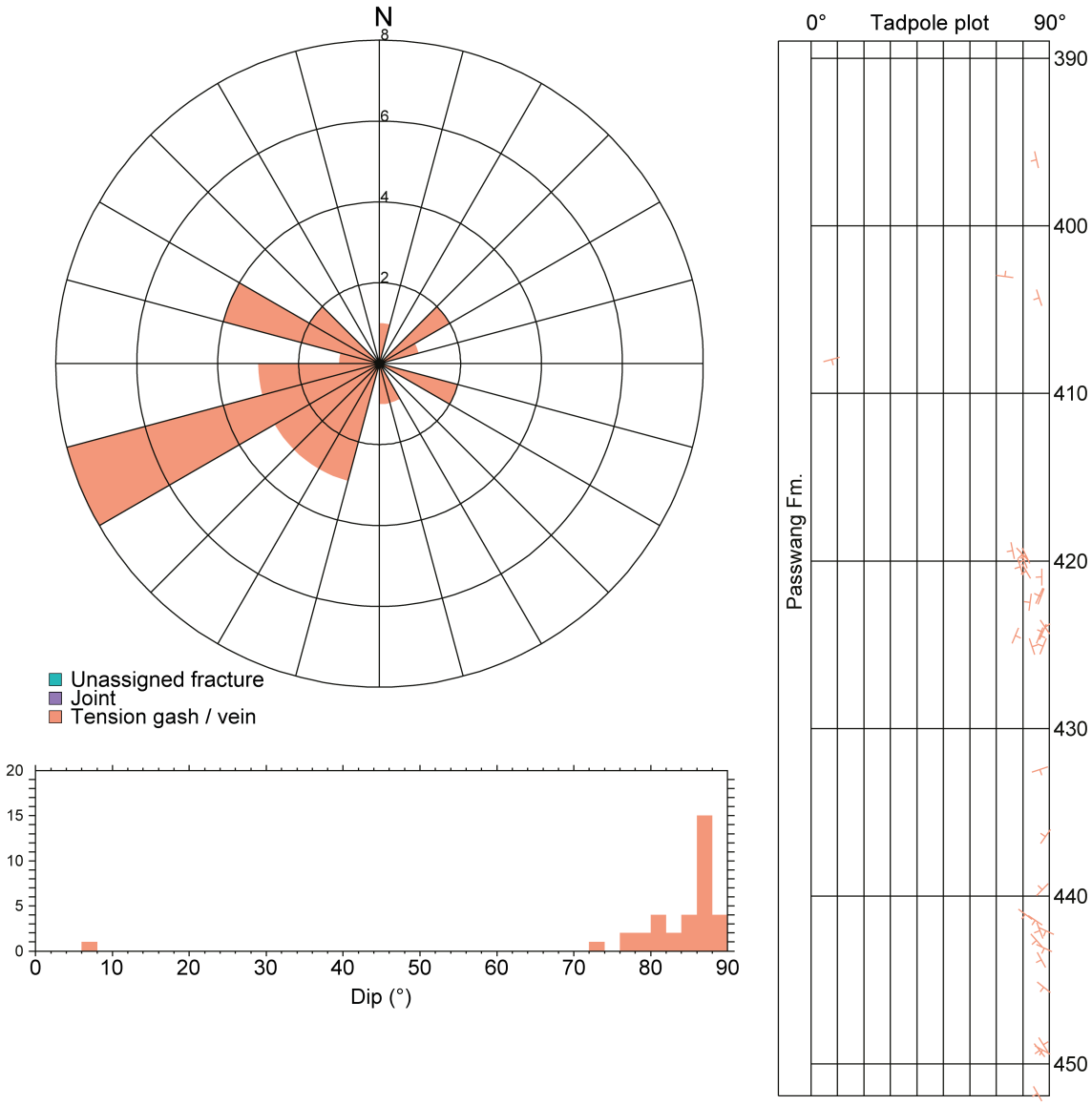

Fig. 4-32: Dip azimuth rose diagram, dip histogram and depth plot of tension gashes / veins, joints and unassigned fractures (Passwang Formation)

Tension gashes / veins (n = 35); unassigned fractures and joints were not observed (n = 0).

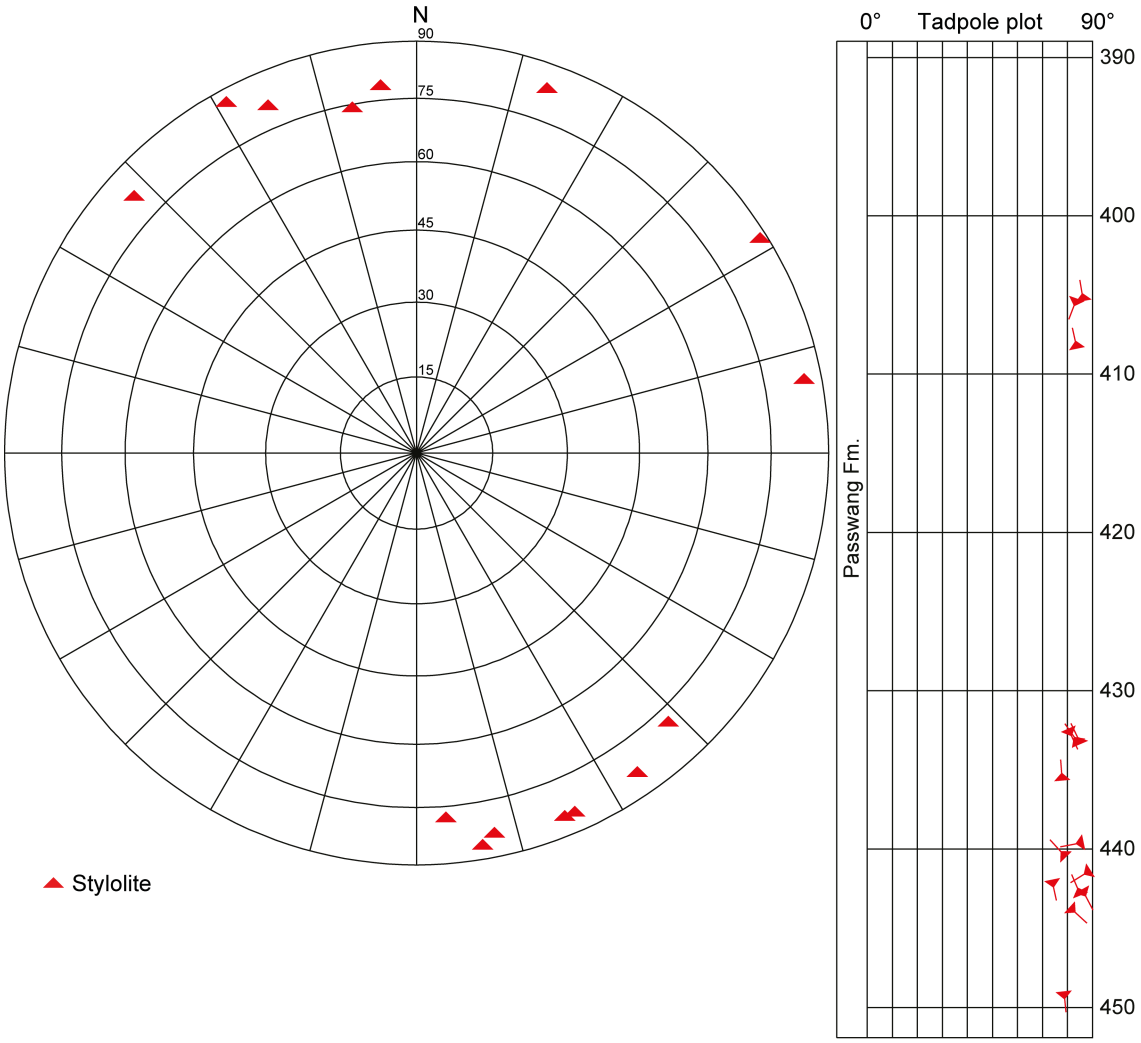

Fig. 4-33: Stereogram and depth plot of stylolites (Passwang Formation; n = 15)

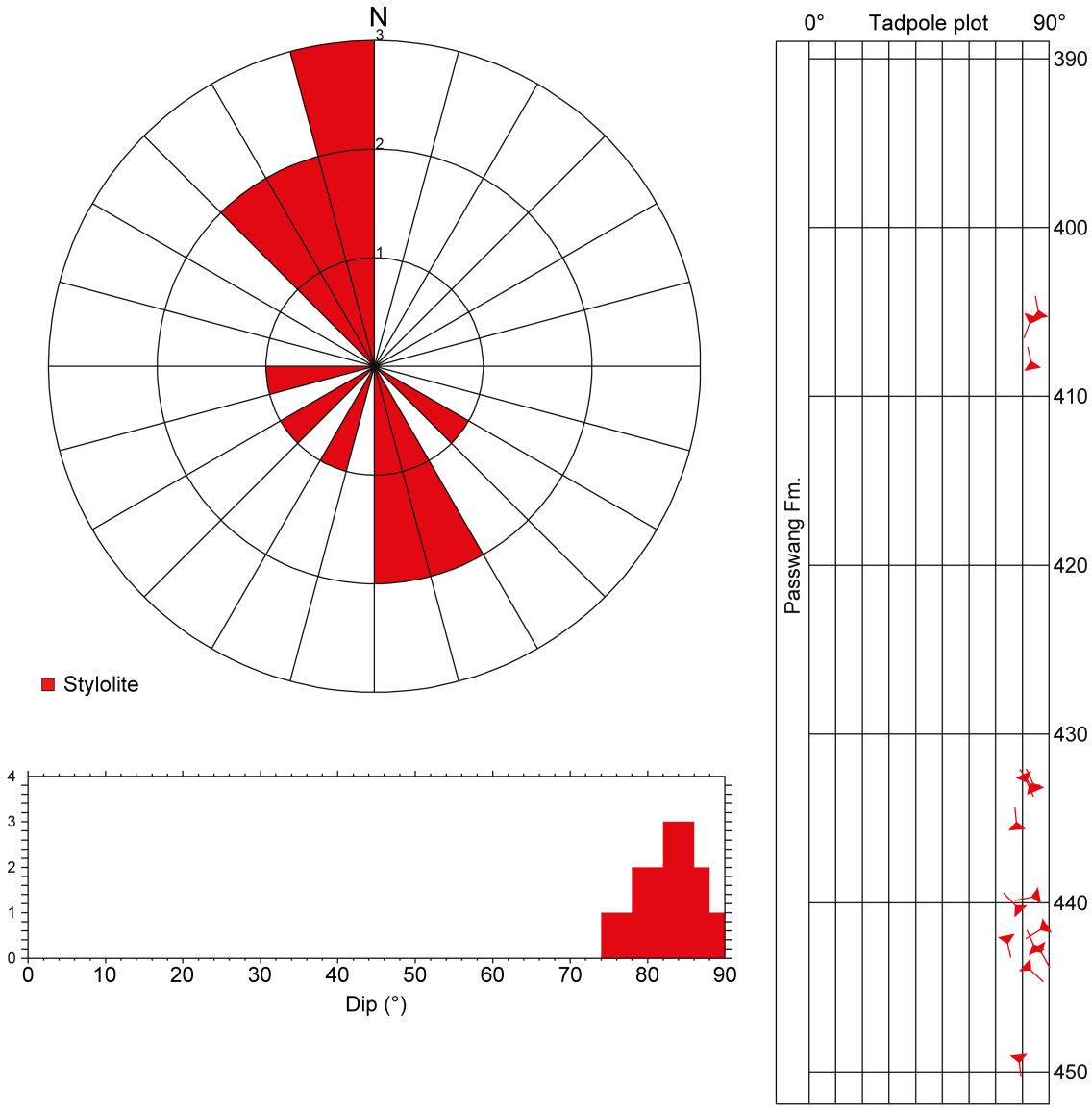

Fig. 4-34: Dip azimuth rose diagram, dip histogram and depth plot of stylolites (Passwang Formation; n = 15)

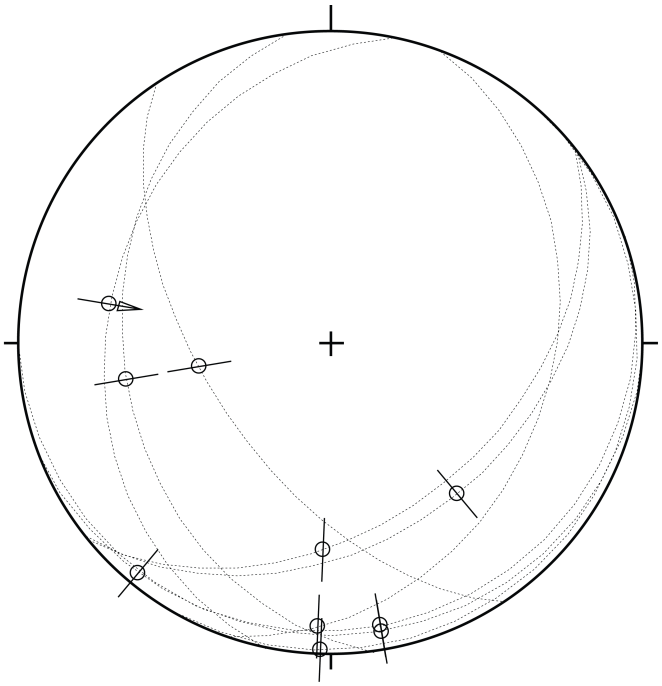

Fig. 4-35: Stereogram of striations on fault planes (including multiple lineations on a single fault plane) (Passwang Formation; n = 10)

4.3.3 Opalinus Clay

The Opalinus Clay (451.90 m to 573.89 m MD [log depth]) reveals a moderate density of fault planes and tension gashes. Fault planes are often concentrated within zones, e.g. from 509.03 m to 510.74 m MD (log depth) and from 530.51 m to 533.22 m MD (log depth). They are either related to fault zones or zones of soft-sediment deformation.

The fault planes have a shallow to moderate dip mainly towards the S or the W. The dominant shear sense is reverse, with the striations mainly dipping towards the S. Most of the tension gashes occur homogeneously in the lower third of the Opalinus Clay. They are generally steeply dipping towards the W. Both fault planes and tension gashes are often characterised by calcite fillings, which are commonly less than 1 mm thick. Stylolites were not observed in the Opalinus Clay.

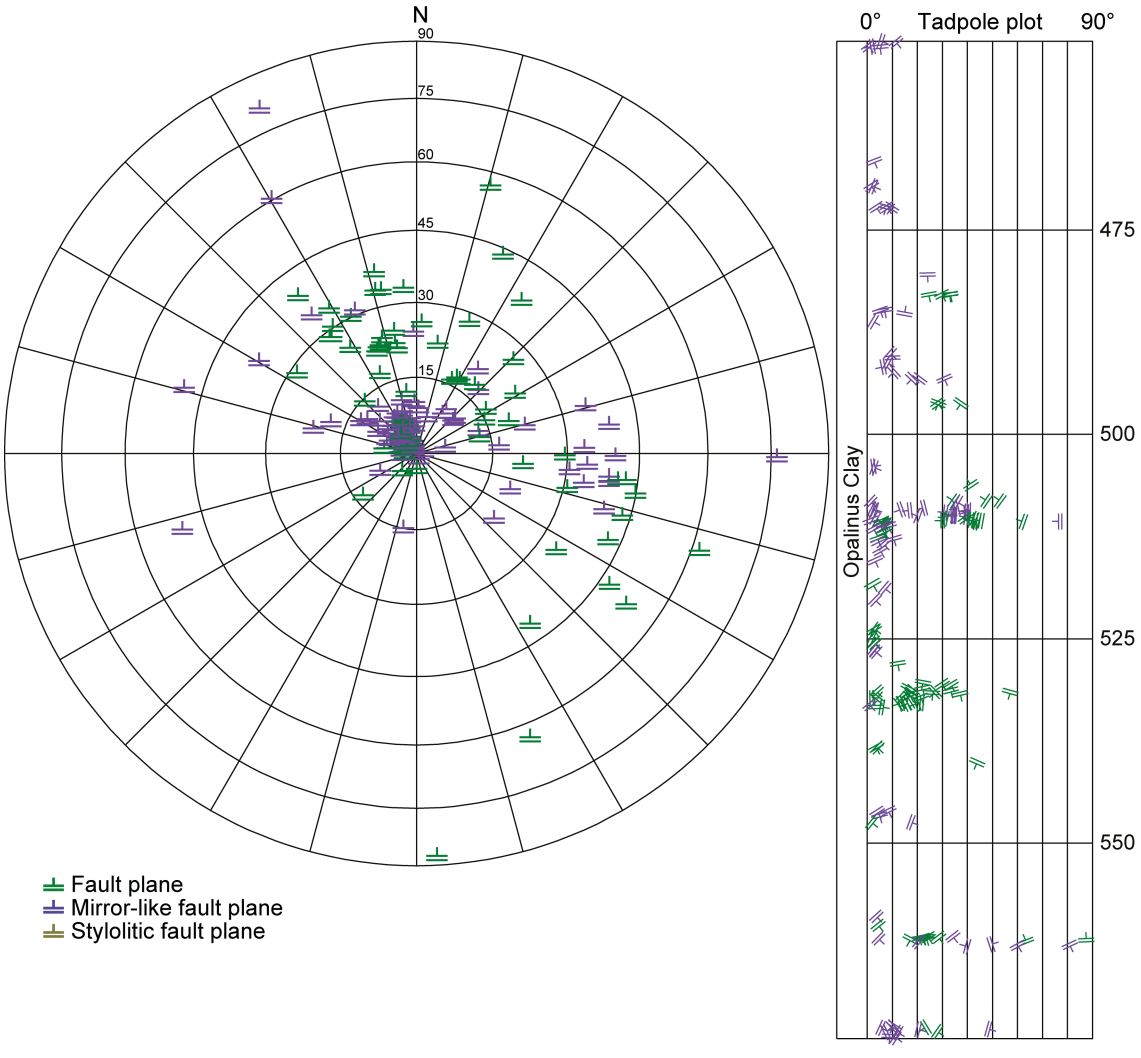

Fig. 4-36: Stereogram and depth plot of fault planes (Opalinus Clay)

Fault planes (n = 77), mirror-like fault planes (n = 82); stylolitic fault planes were not observed (n = 0).

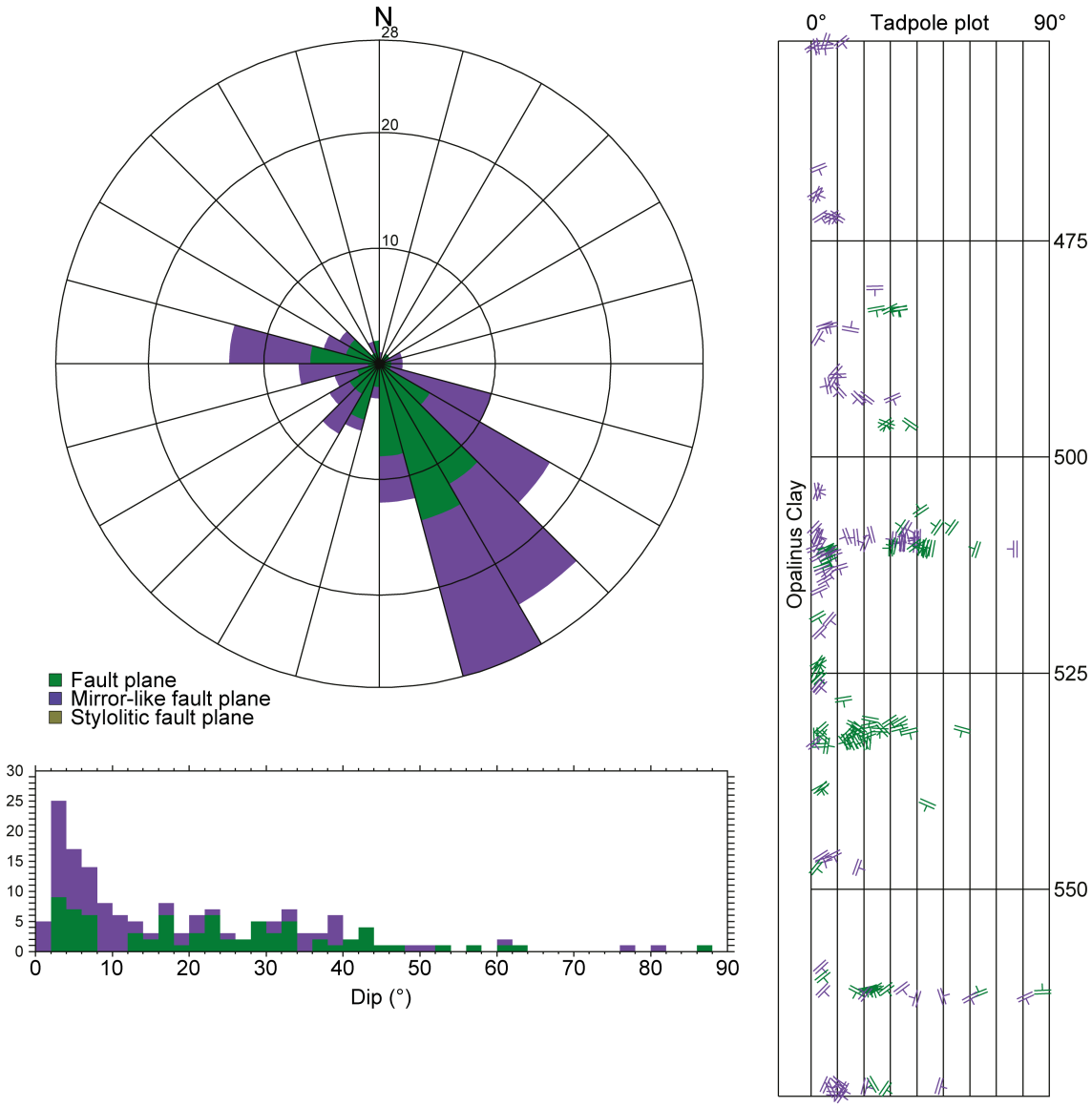

Fig. 4-37: Dip azimuth rose diagram, dip histogram and depth plot of fault planes (Opalinus Clay)

Fault planes (n = 77), mirror-like fault planes (n = 82); stylolitic fault planes were not observed (n = 0).

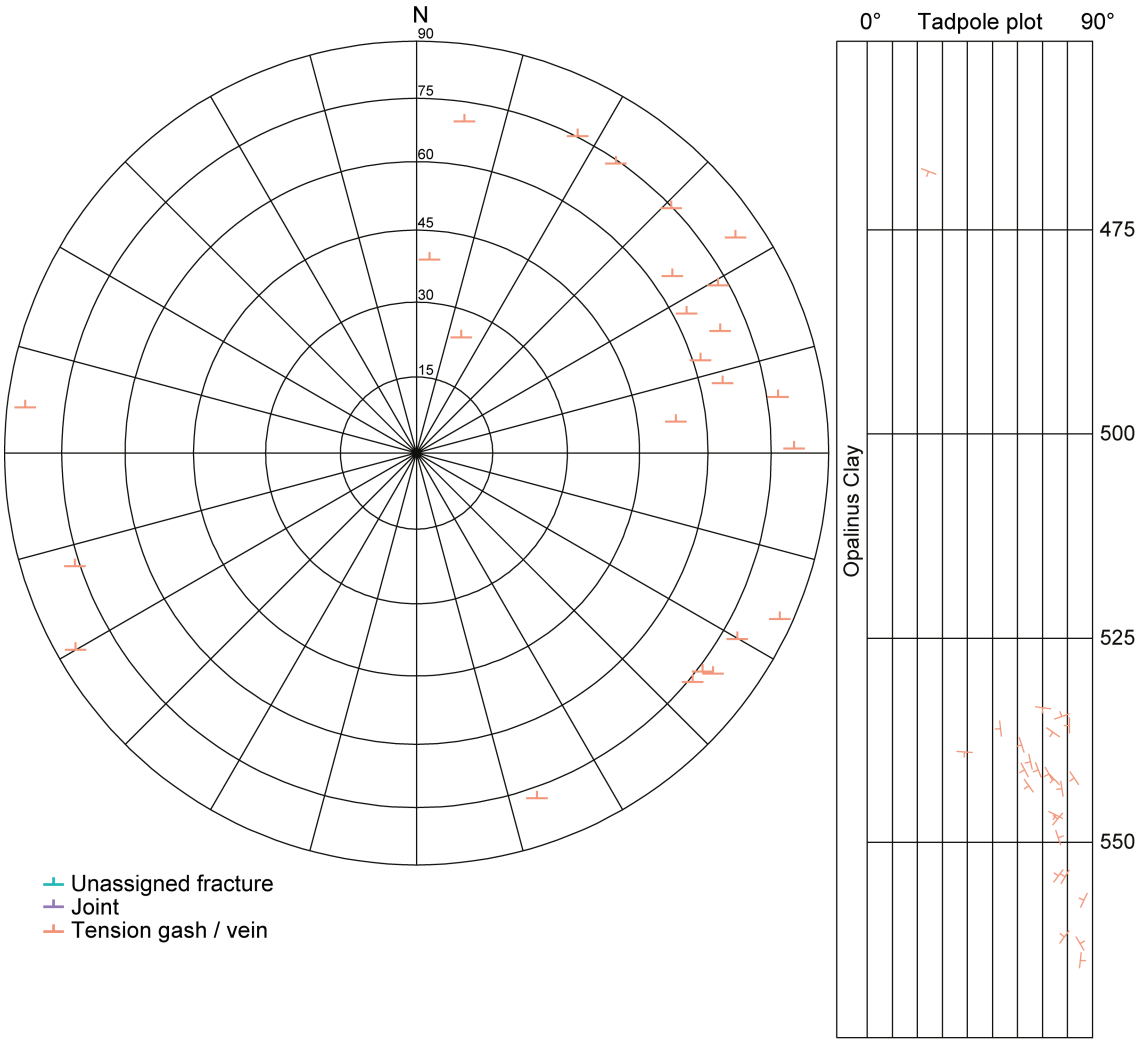

Fig. 4-38: Stereogram and depth plot of tension gashes / veins, joints and unassigned fractures (Opalinus Clay)

Tension gashes / veins (n = 25); unassigned fractures and joints were not observed (n = 0).

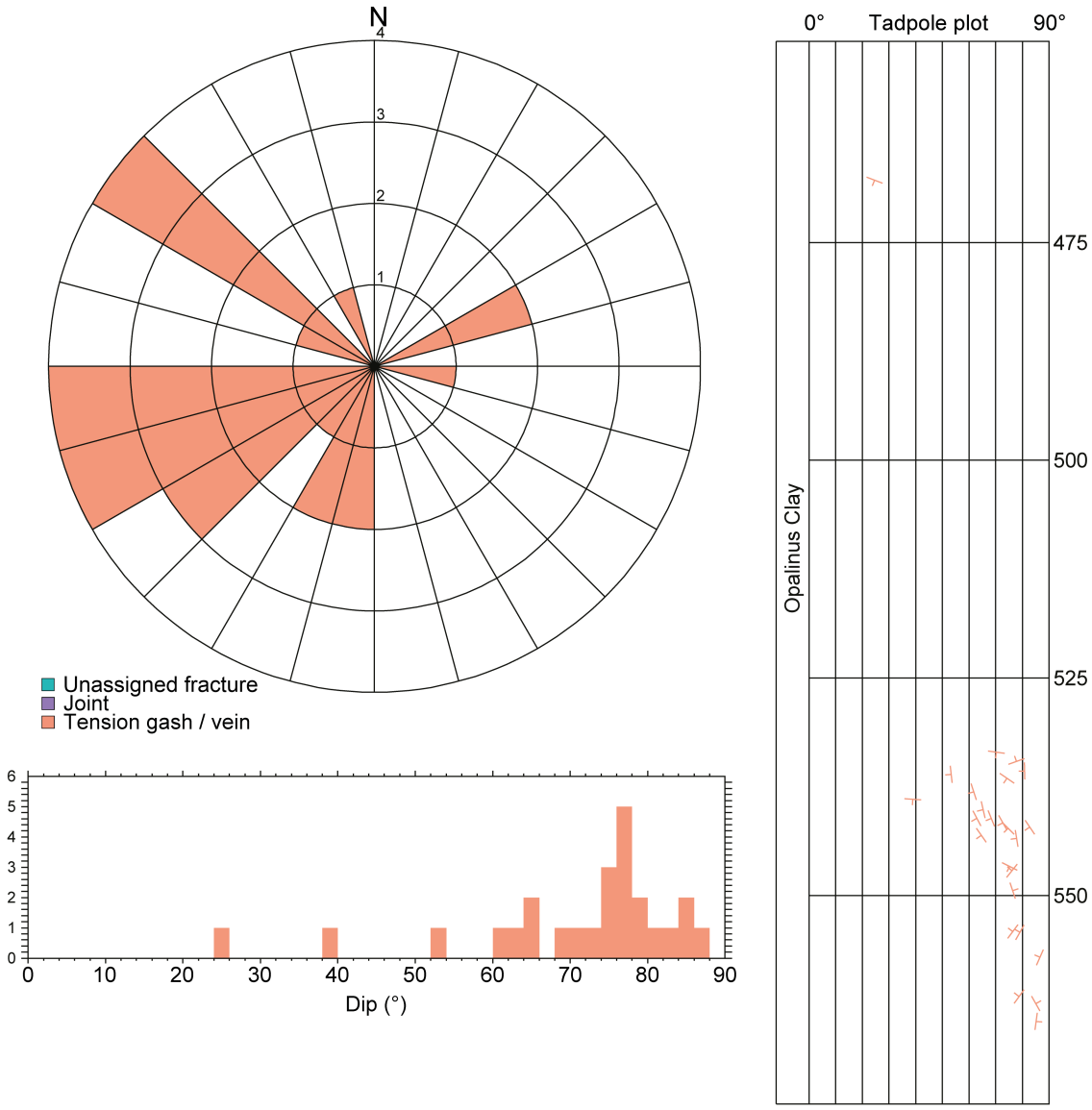

Fig. 4-39: Dip azimuth rose diagram, dip histogram and depth plot of tension gashes / veins, joints and unassigned fractures (Opalinus Clay)

Tension gashes / veins (n = 25); unassigned fractures and joints were not observed (n = 0).

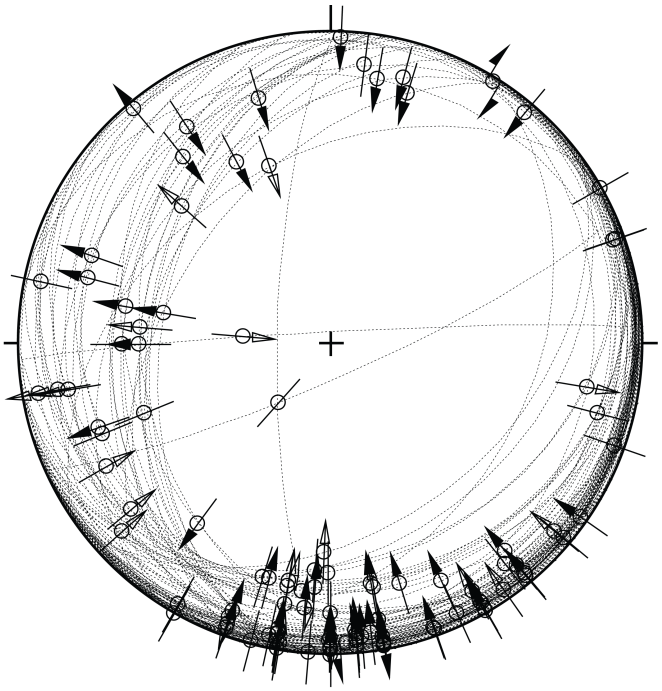

Fig. 4-40: Stereogram of striations on fault planes, including multiple lineations on a single fault plane (Opalinus Clay; n = 114)

4.4 Lias (Staffelegg Formation)

As presented in Figs. 4-41 to 4-47, the Lias (573.89 m to 612.76 m MD [log depth]) is characterised by a moderate number of structures, predominantly mirror-like fault planes, tension gashes and stylolites. Stylolites and tension gashes are concentrated in calcareous beds, while the mirror-like fault planes occur in clay-rich layers in the lower part of the Staffelegg Formation. Mirror-like fault planes are mostly subhorizontal and show a preferred dip towards the SE and the W. Stylolites and tension gashes tend to be more steeply dipping and are oriented more randomly. Only the data from oriented cores are presented.

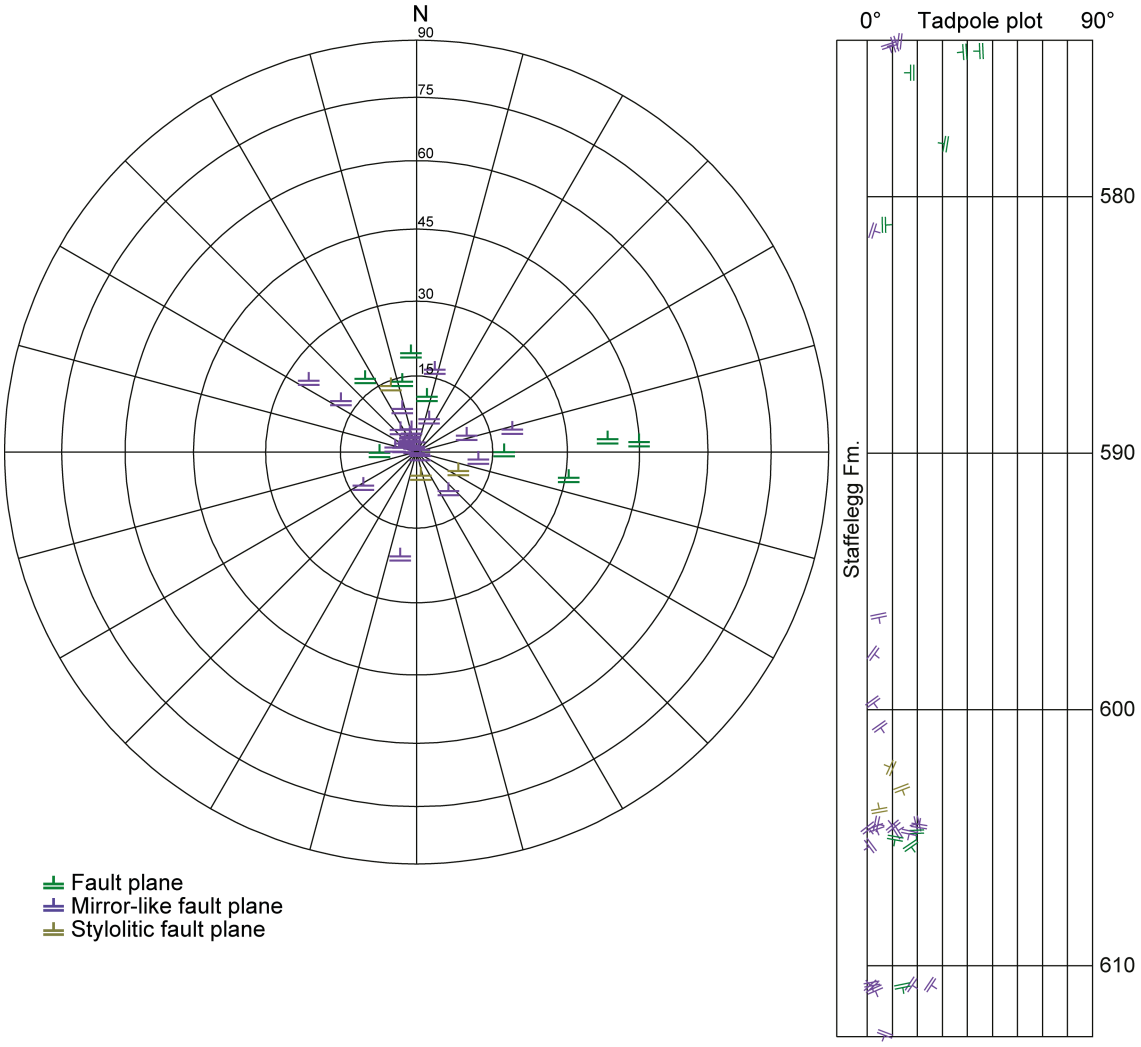

Fig. 4-41: Stereogram and depth plot of fault planes (Lias)

Fault planes (n = 9), mirror-like fault planes (n = 23) and stylolitic fault planes (n = 3).

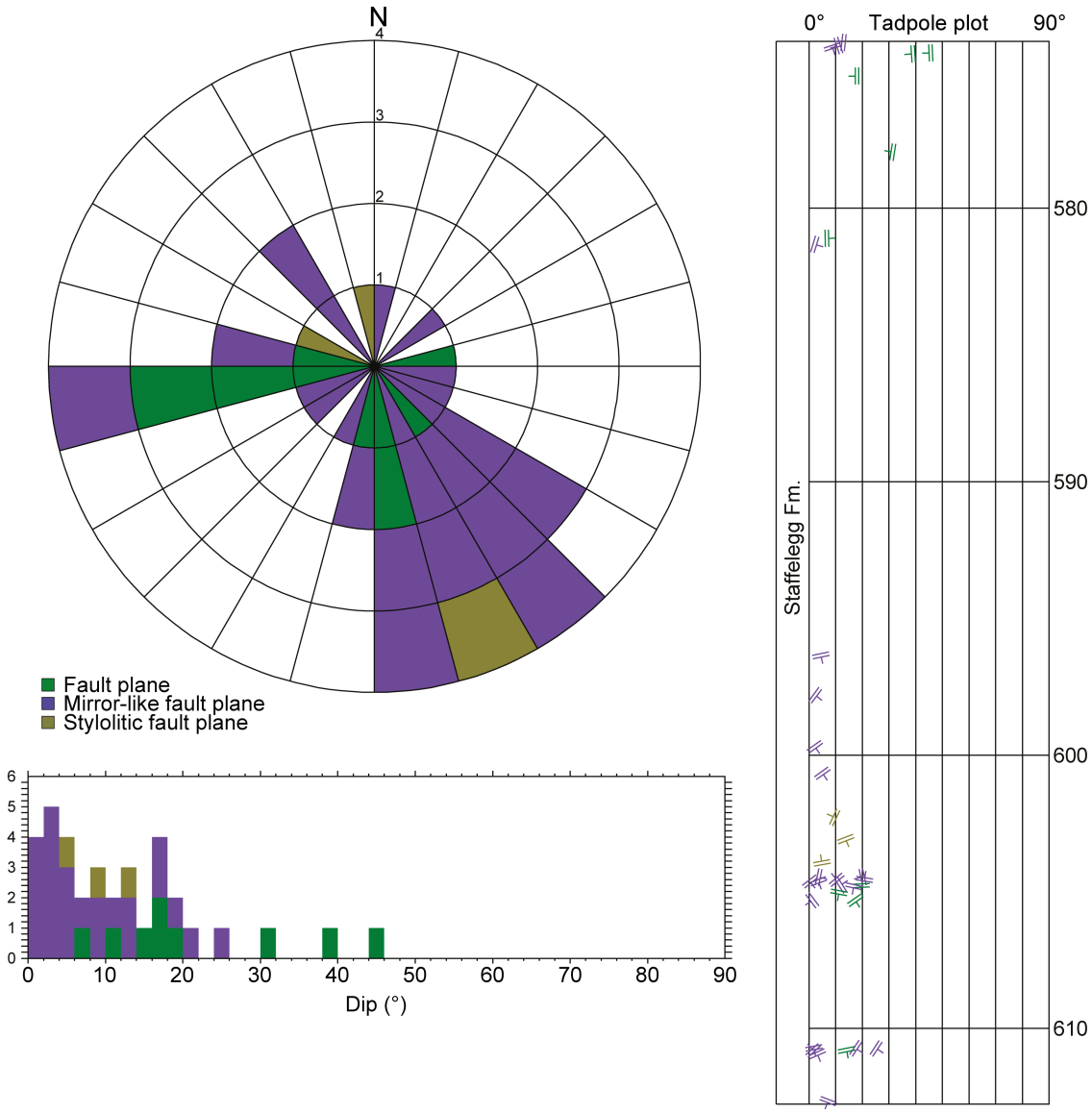

Fig. 4-42: Dip azimuth rose diagram, dip histogram and depth plot of fault planes (Lias)
Fault planes (n = 9), mirror-like fault planes (n = 23) and stylolitic fault planes (n = 3).

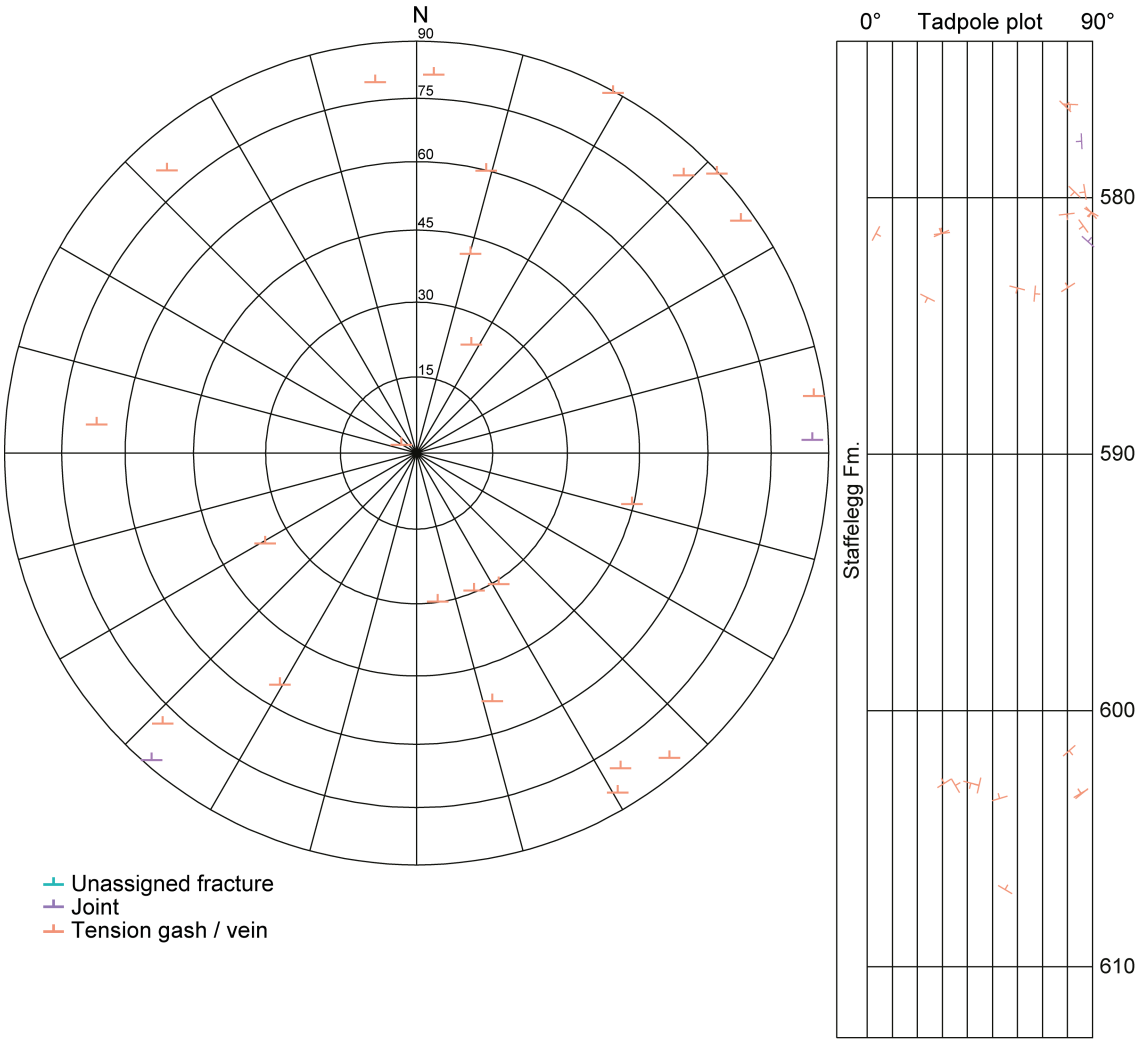

Fig. 4-43: Stereogram and depth plot of tension gashes / veins, joints and unassigned fractures (Lias)

Joints (n = 2) and tension gashes / veins (n = 24); unassigned fractures were not observed (n = 0).

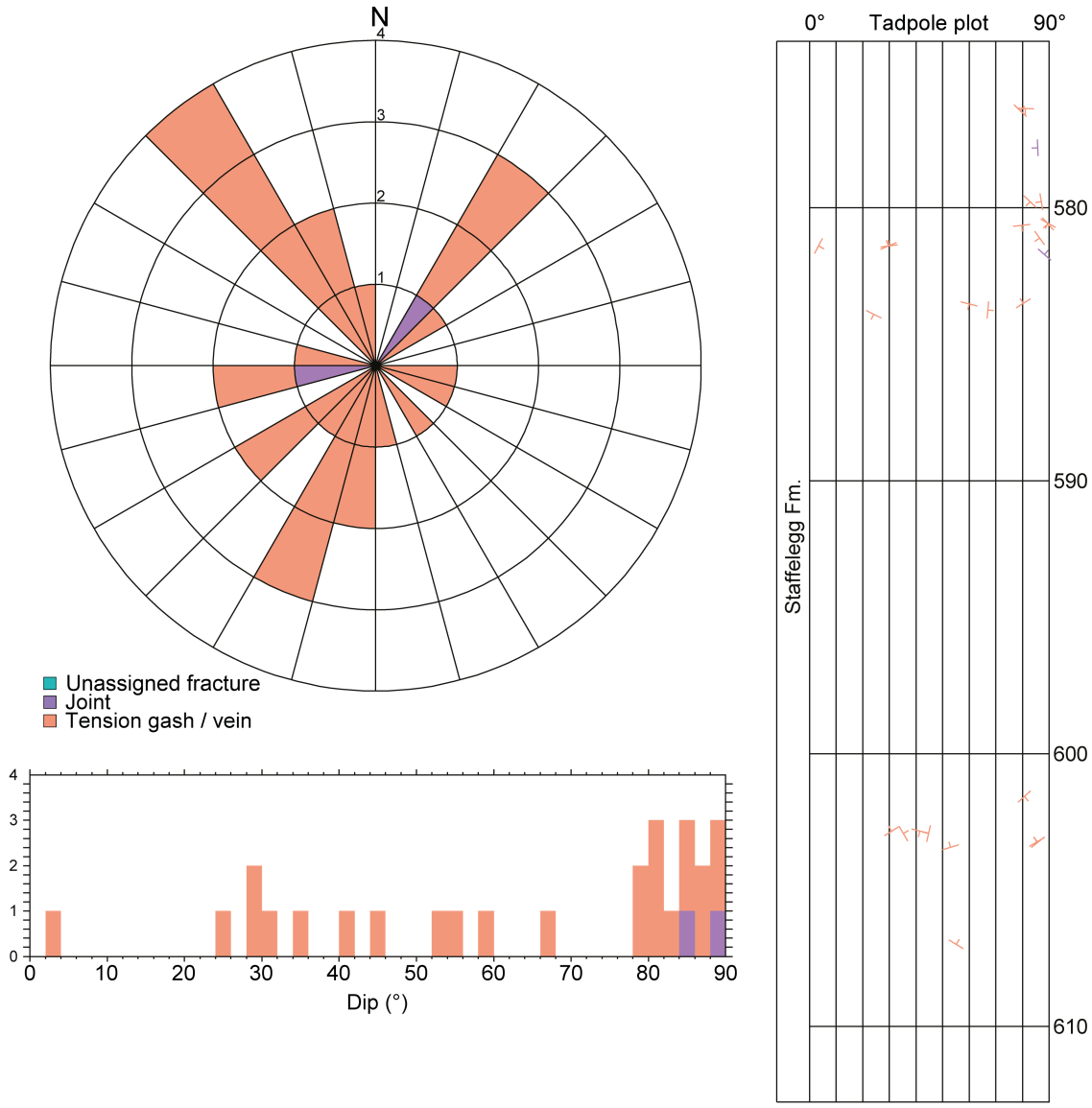

Fig. 4-44: Dip azimuth rose diagram, dip histogram and depth plot of tension gashes / veins, joints and unassigned fractures (Lias)

Joints (n = 2) and tension gashes / veins (n = 24); unassigned fractures were not observed (n = 0).

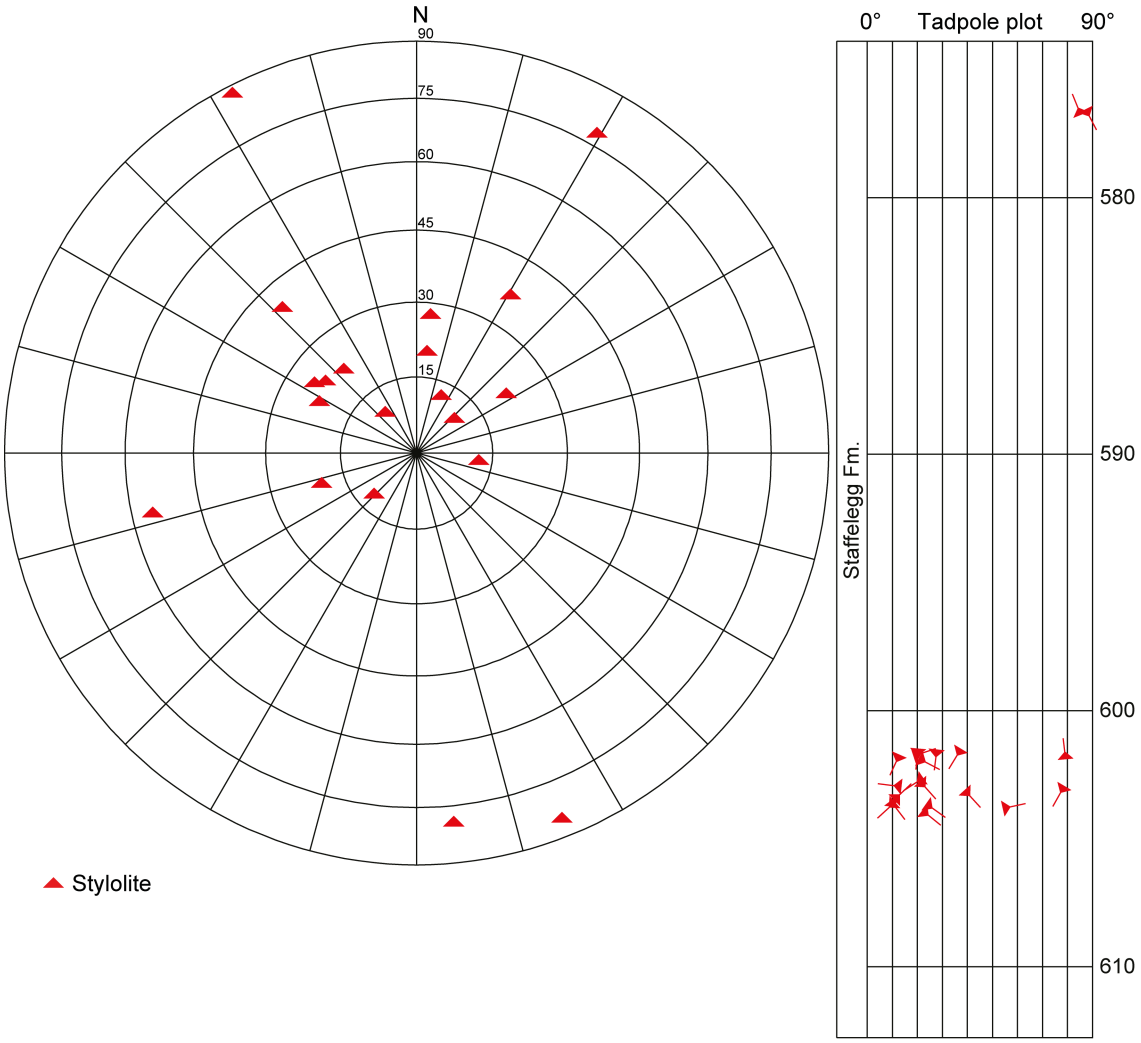

Fig. 4-45: Stereogram and depth plot of stylolites (Lias; n = 20)

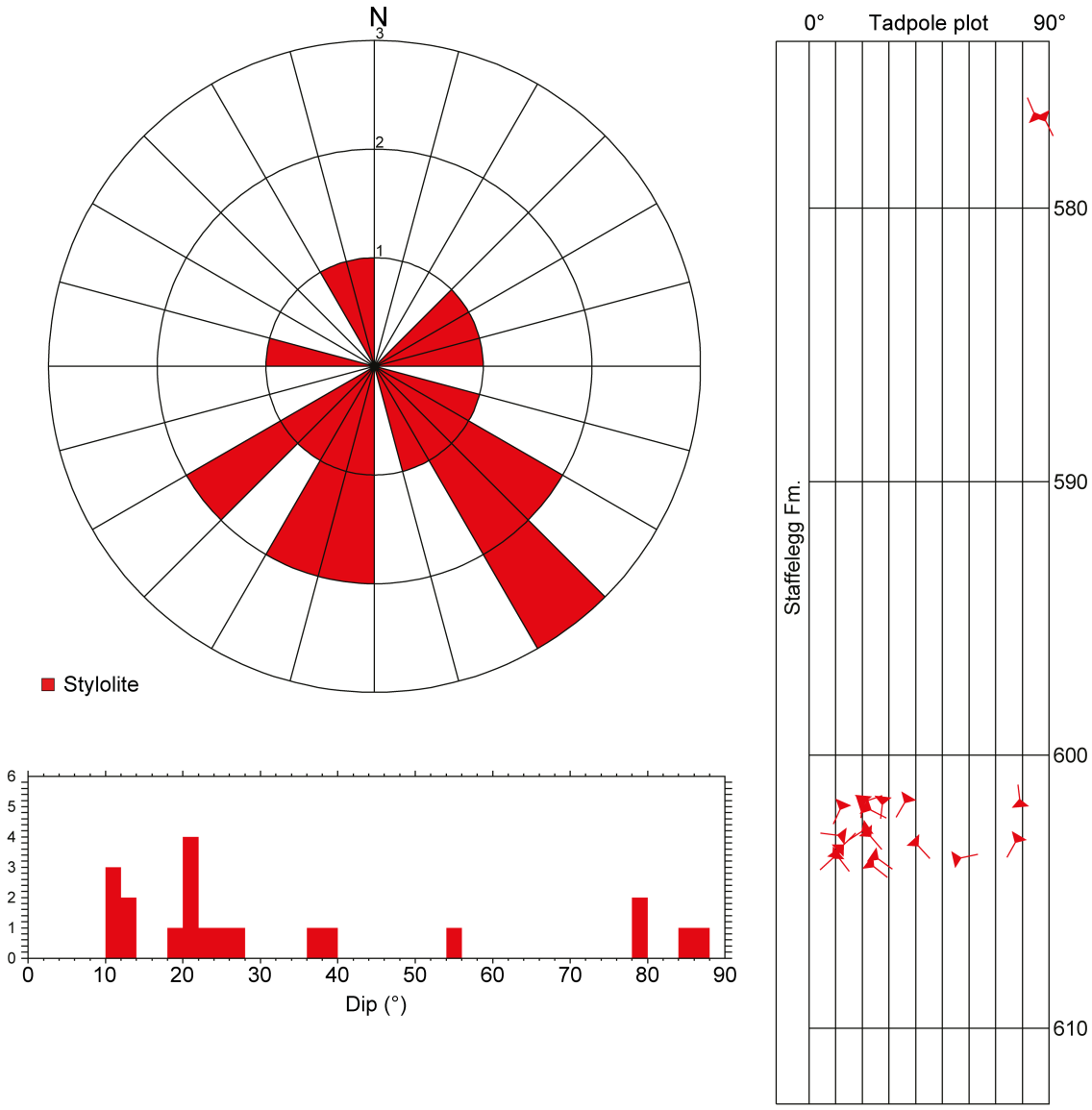

Fig. 4-46: Dip azimuth rose diagram, dip histogram and depth plot of stylolites (Lias; n = 20)

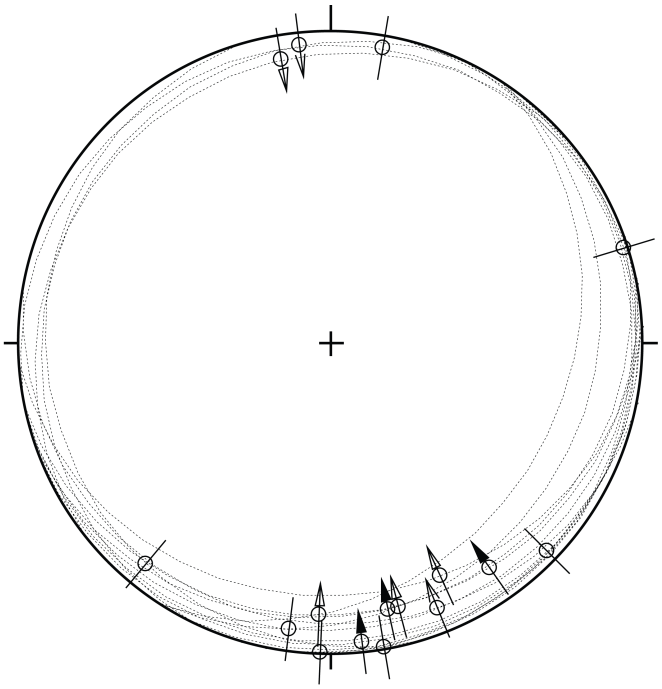

Fig. 4-47: Stereogram of striations on fault planes (Lias; n = 16)

4.5 Keuper

The Keuper (612.76 m to 749.52 m MD [log depth]) displays the highest average fracture density of 6.2 fractures per metre. Mirror-like fault planes and tension gashes / veins prevail. The latter are mainly found within the Bänkerjoch Formation and show random orientations. The fault planes display a preferred dip of less than 50° towards the SE. The dominant strike direction of striations is NNW-SSE. Only the data from oriented cores are presented.

4.5.1 Klettgau Formation

In the Klettgau Formation (612.76 m to 654.70 m MD [log depth]) mirror-like fault planes are the dominant fracture type (Figs. 4-48 to 4-53). They have oblique dip angles with a slight preference for a dip direction towards the SE. Tension gashes / veins, joints and stylolites were rare.

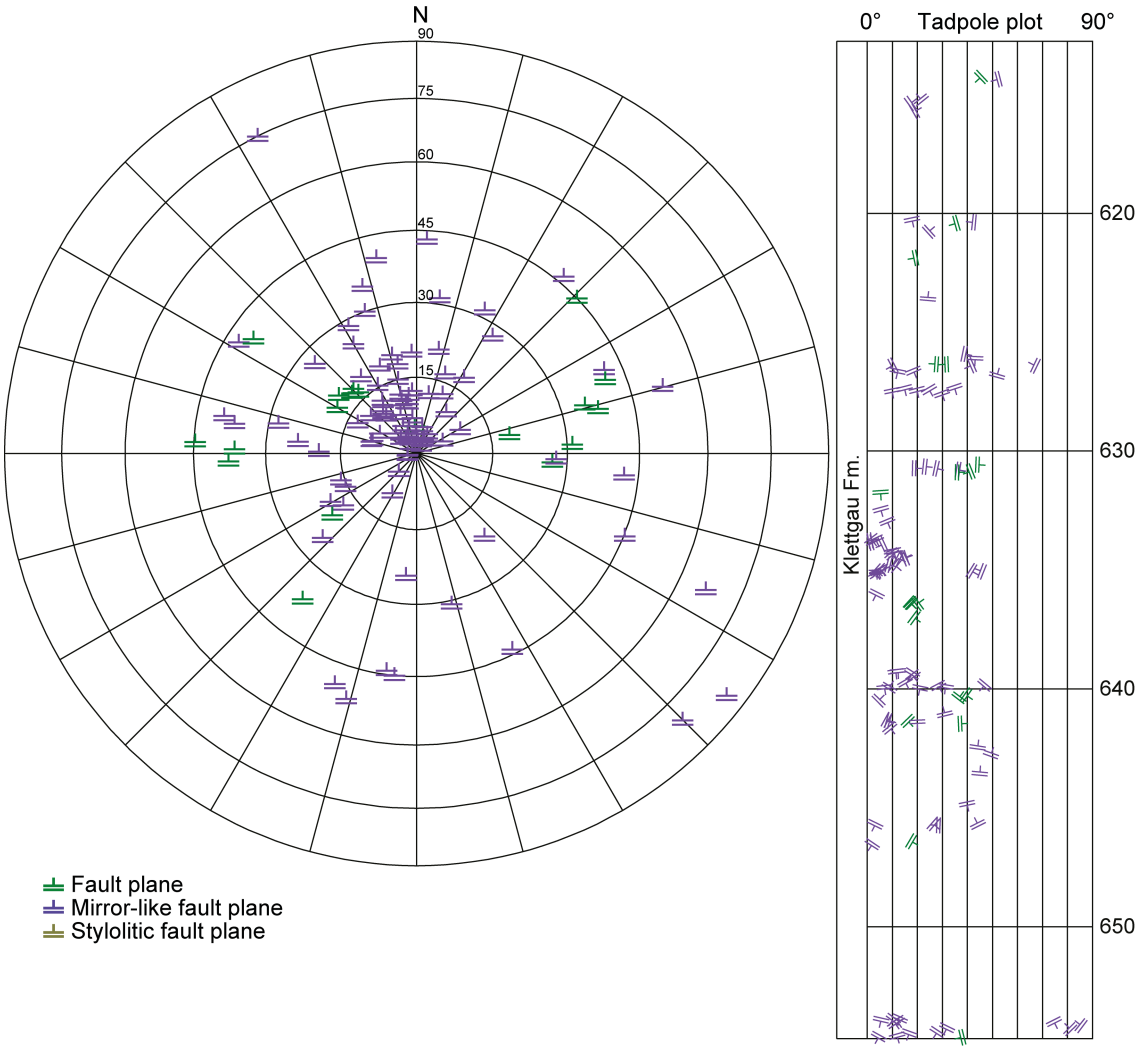

Fig. 4-48: Stereogram and depth plot of faults (Klettgau Formation)

Fault planes (n = 19) and mirror-like fault planes (n = 89); stylolitic fault planes were not observed (n = 0).

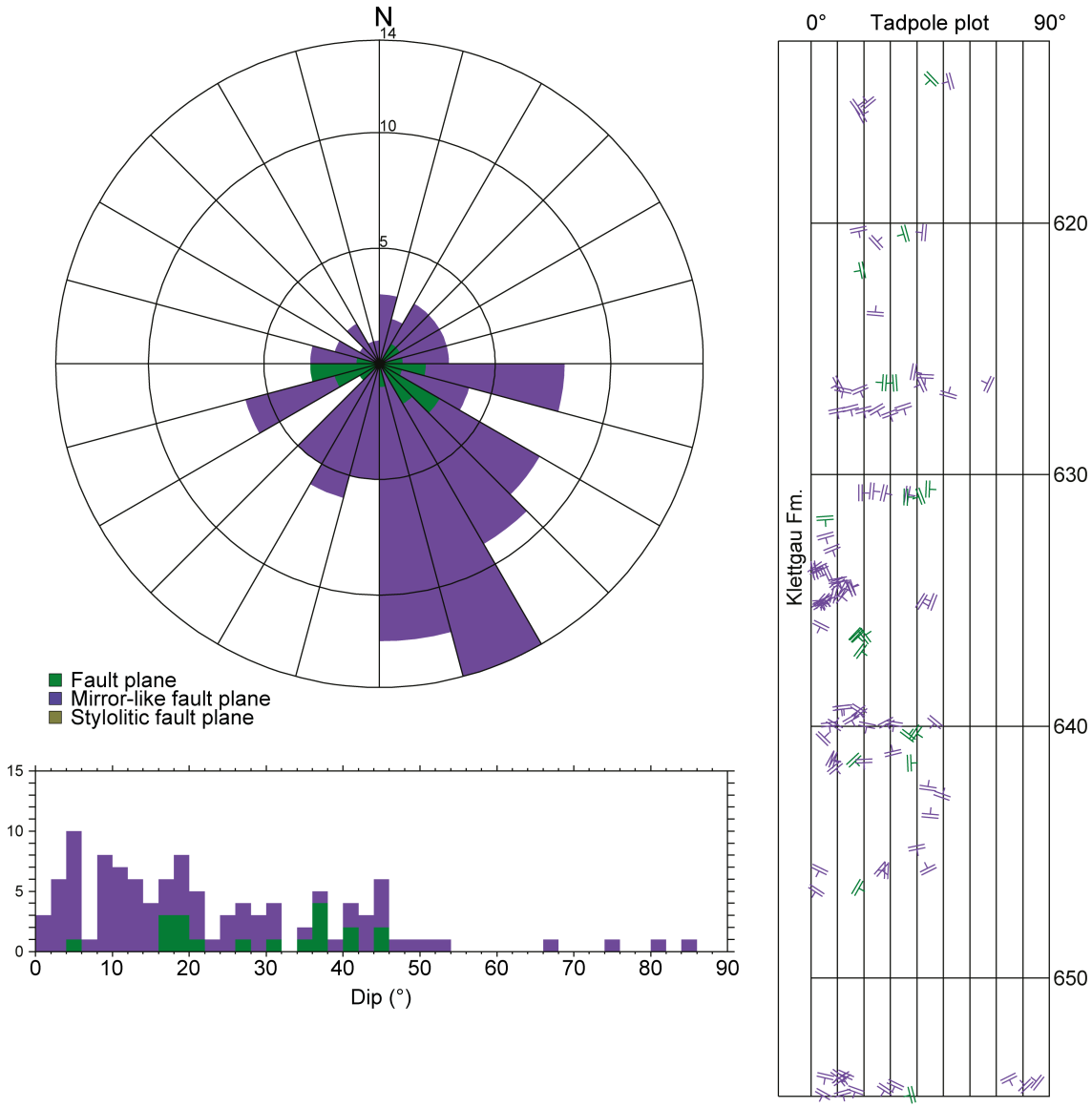

Fig. 4-49: Dip azimuth rose diagram, dip histogram and depth plot of faults (Klettgau Formation)

Fault planes (n = 19) and mirror-like fault planes (n = 89); stylolitic fault planes were not observed (n = 0).

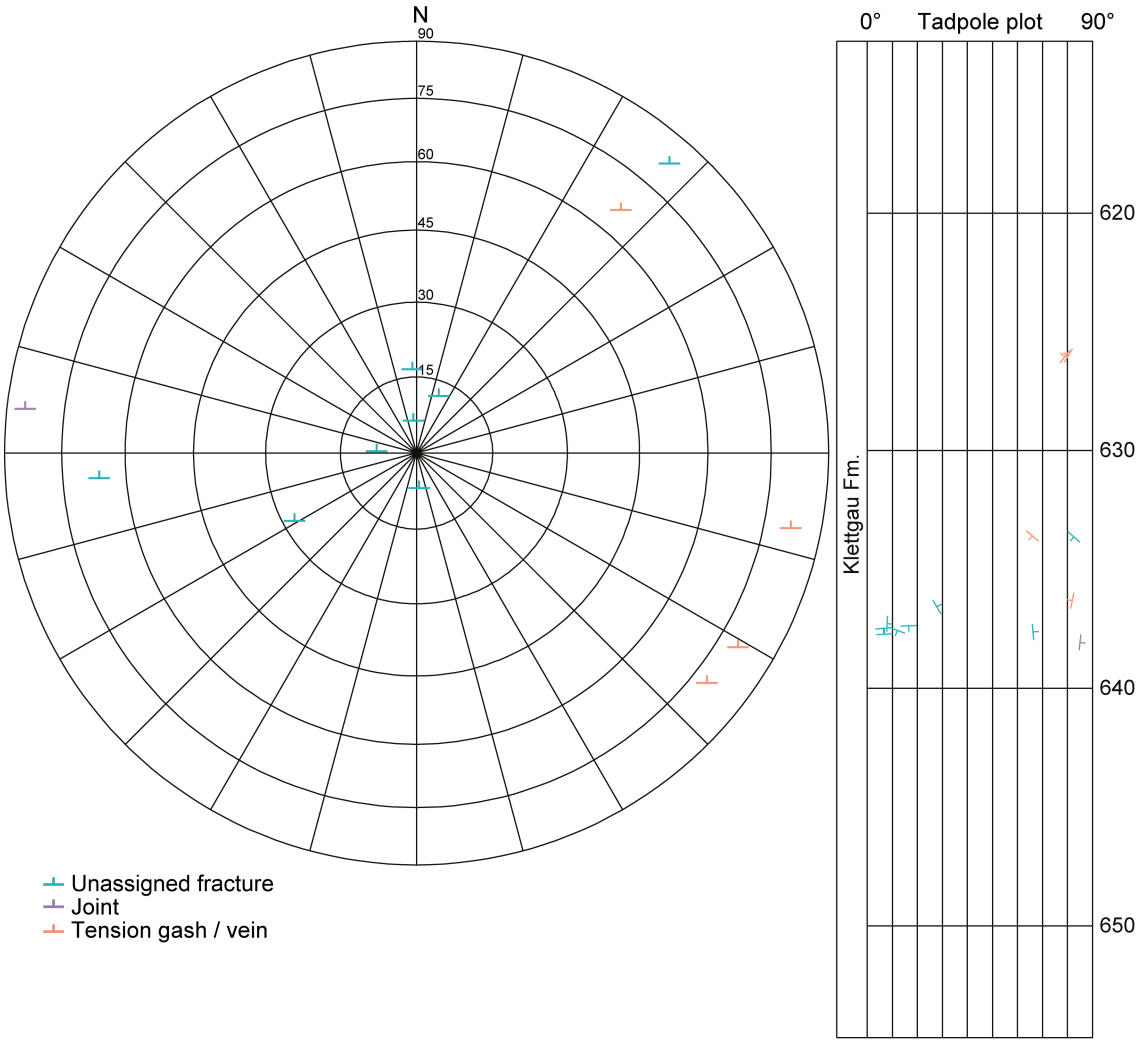

Fig. 4-50: Stereogram and depth plot of tension gashes / veins, joints and unassigned fractures (Klettgau Formation)

Unassigned fractures (n = 8), joints (n = 1) and tension gashes / veins (n = 4).

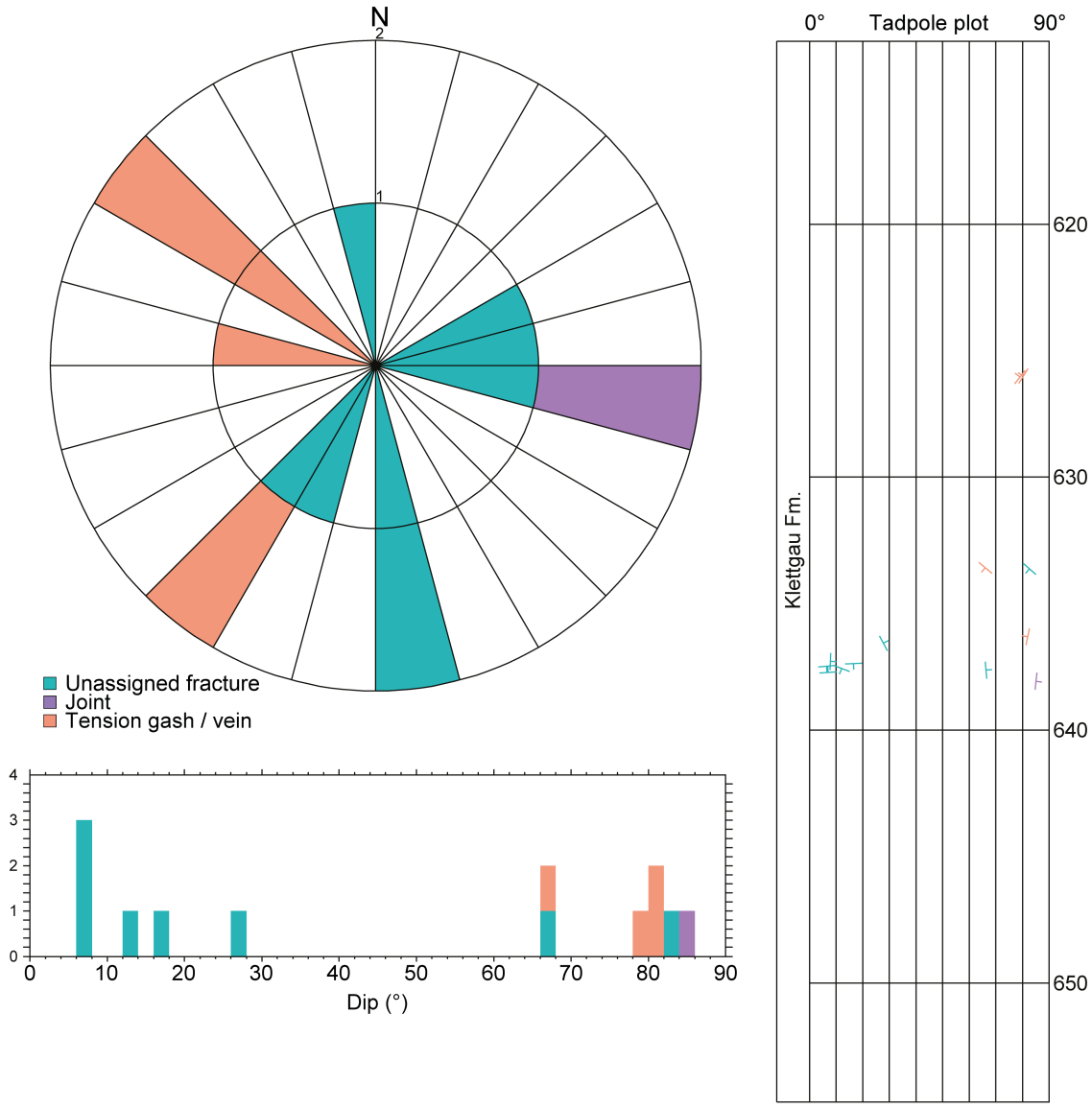

Fig. 4-51: Dip azimuth rose diagram, dip histogram and depth plot of tension gashes / veins, joints and unassigned fractures (Klettgau Formation)

Unassigned fractures (n = 8), joints (n = 1) and tension gashes / veins (n = 4).

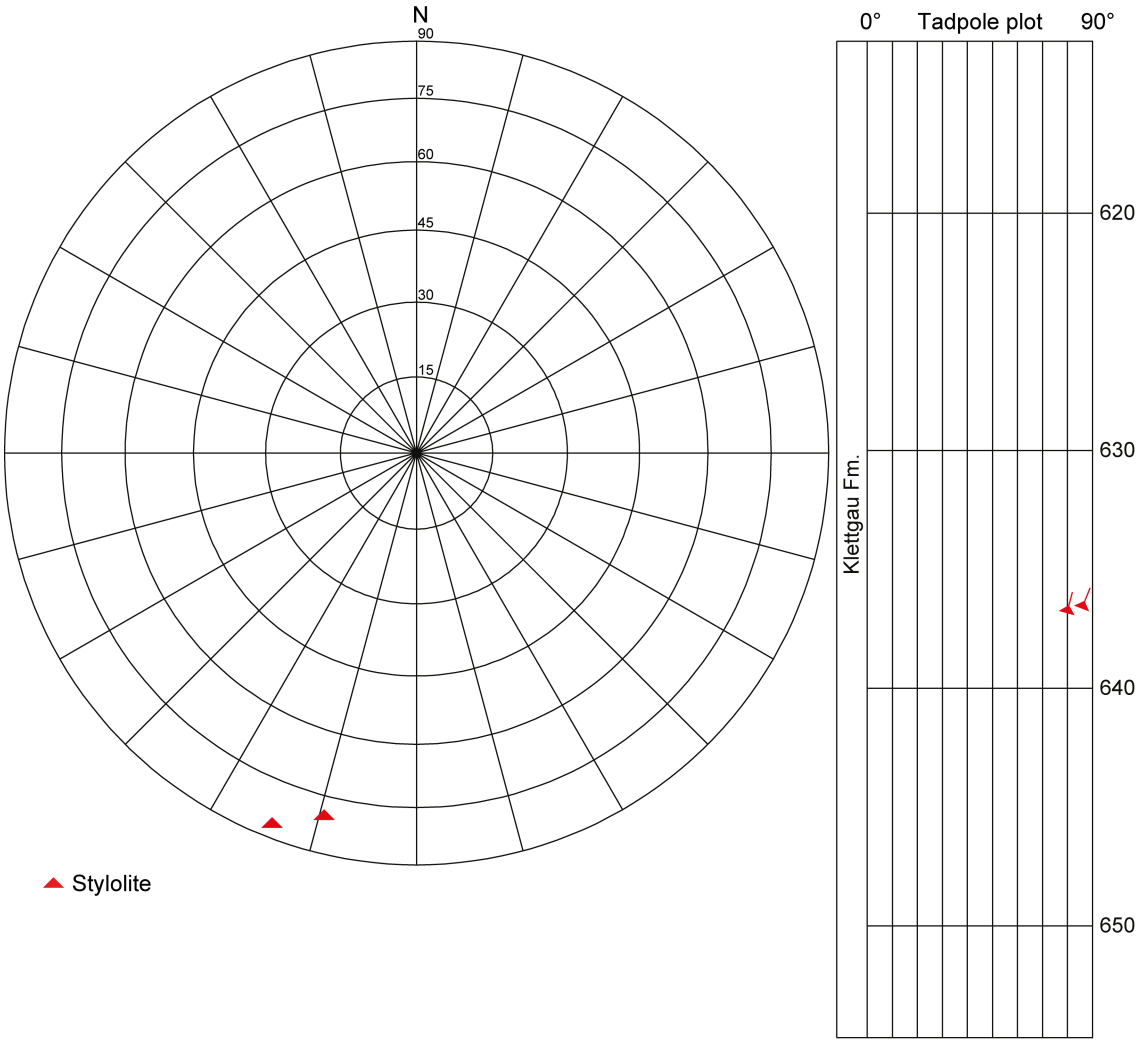

Fig. 4-52: Stereogram and depth plot of stylolites (Klettgau Formation; n = 2)

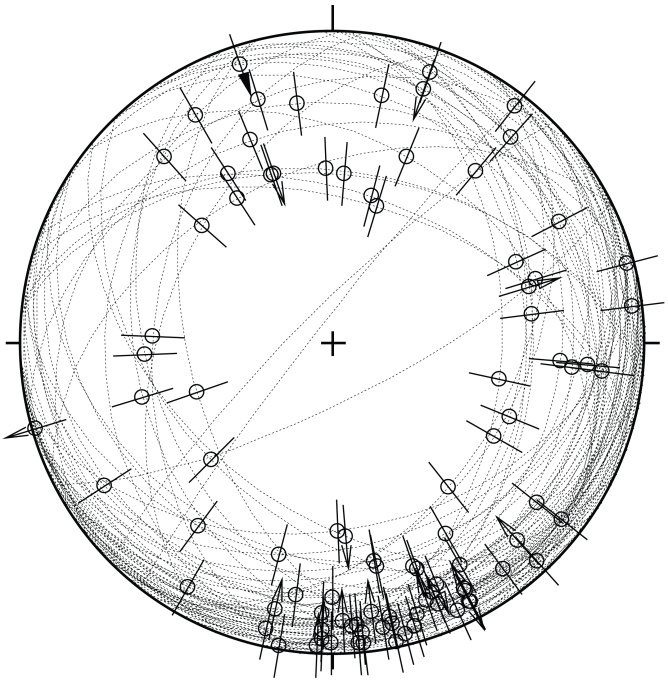

Fig. 4-53: Stereogram of striations on fault planes, including multiple lineations on a single fault plane (Klettgau Formation; n = 93)

4.5.2 Bänkerjoch Formation

The orientations and spatial distributions of the structural inventory of the Bänkerjoch Formation (654.70 m to 749.52 m MD [log depth]) are shown in Figs. 4-54 to 4-59. The abundant mirror-like fault planes and tension gashes are evenly distributed throughout the formation. The mirror-like fault planes generally have a subhorizontal to oblique dip and show a preferred dip orientation towards the SE. Most of the observed striations are N-S oriented. The tension gashes are oriented rather randomly. Structure types other than fault planes and tension gashes were rare within this formation.

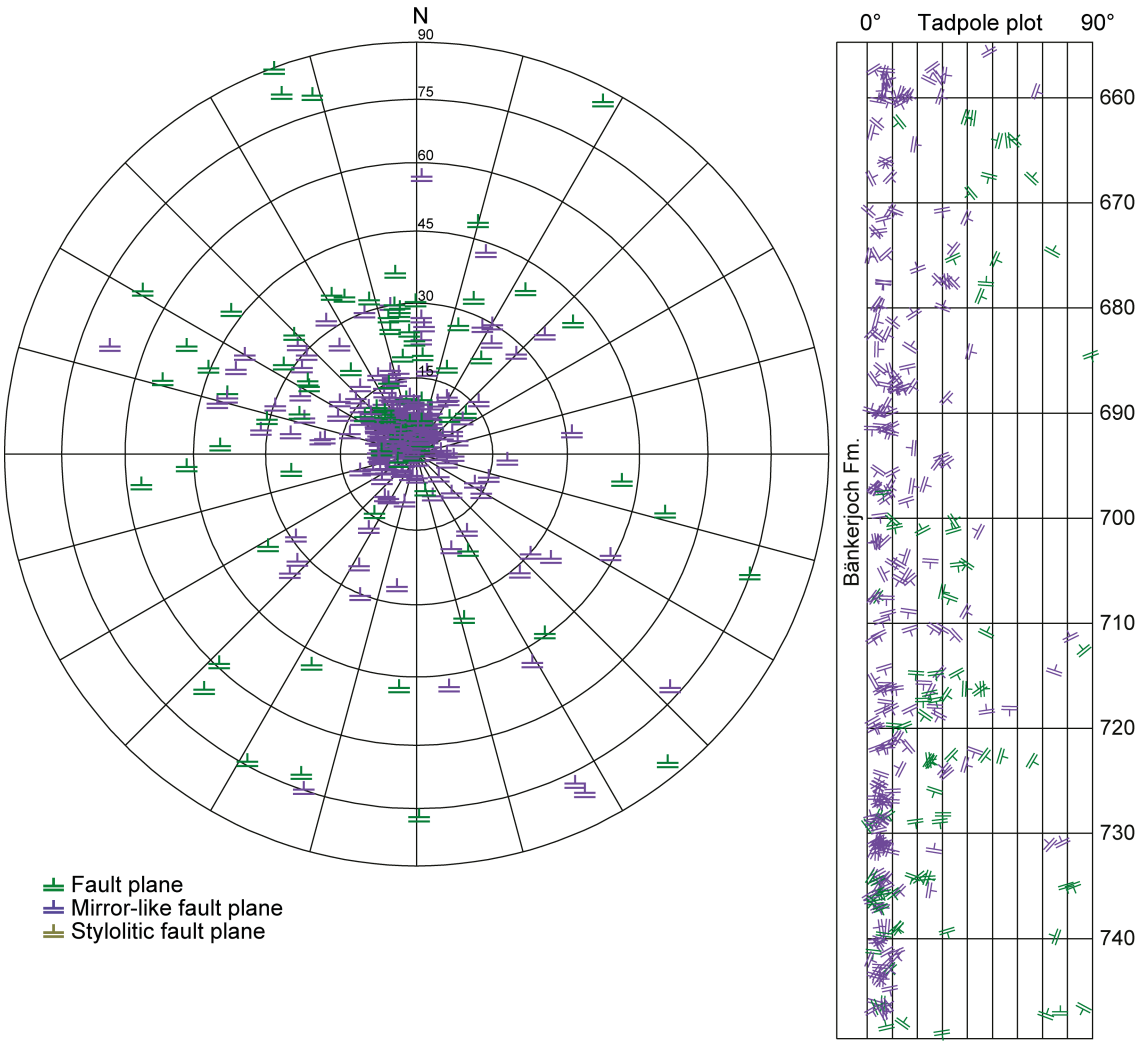

Fig. 4-54: Stereogram and depth plot of faults (Bänkerjoch Formation)

Fault planes (n = 86) and mirror-like fault planes (n = 250); stylolitic fault planes were not observed (n = 0).

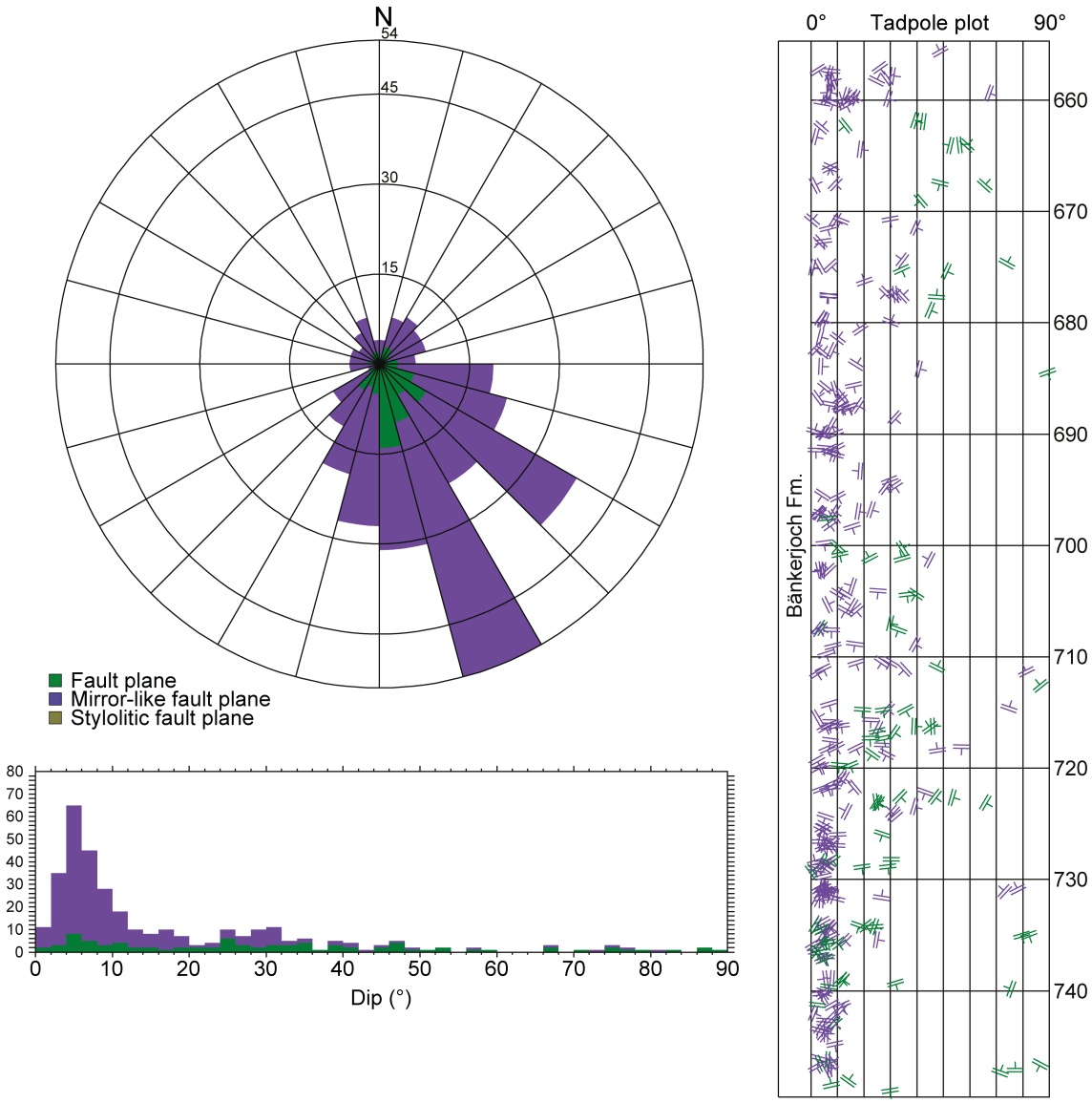

Fig. 4-55: Dip azimuth rose diagram, dip histogram and depth plot of faults (Bänkerjoch Formation)

Fault planes (n = 86) and mirror-like fault planes (n = 250); stylolitic fault planes were not observed (n = 0).

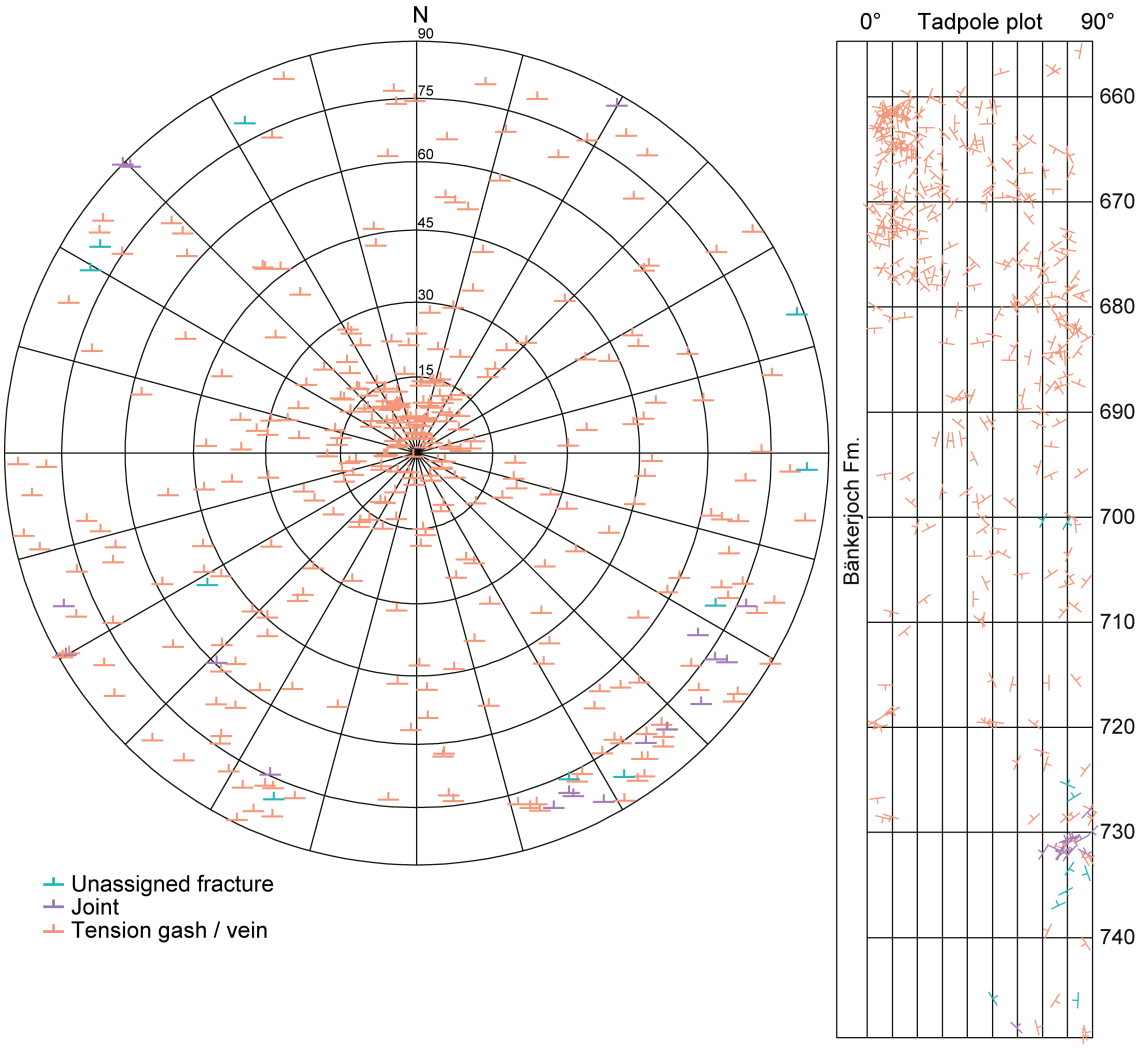

Fig. 4-56: Stereogram and depth plot of tension gashes / veins, joints and unassigned fractures (Bänkerjoch Formation)

Unassigned fractures (n = 10), joints (n = 18) and tension gashes / veins (n = 332).

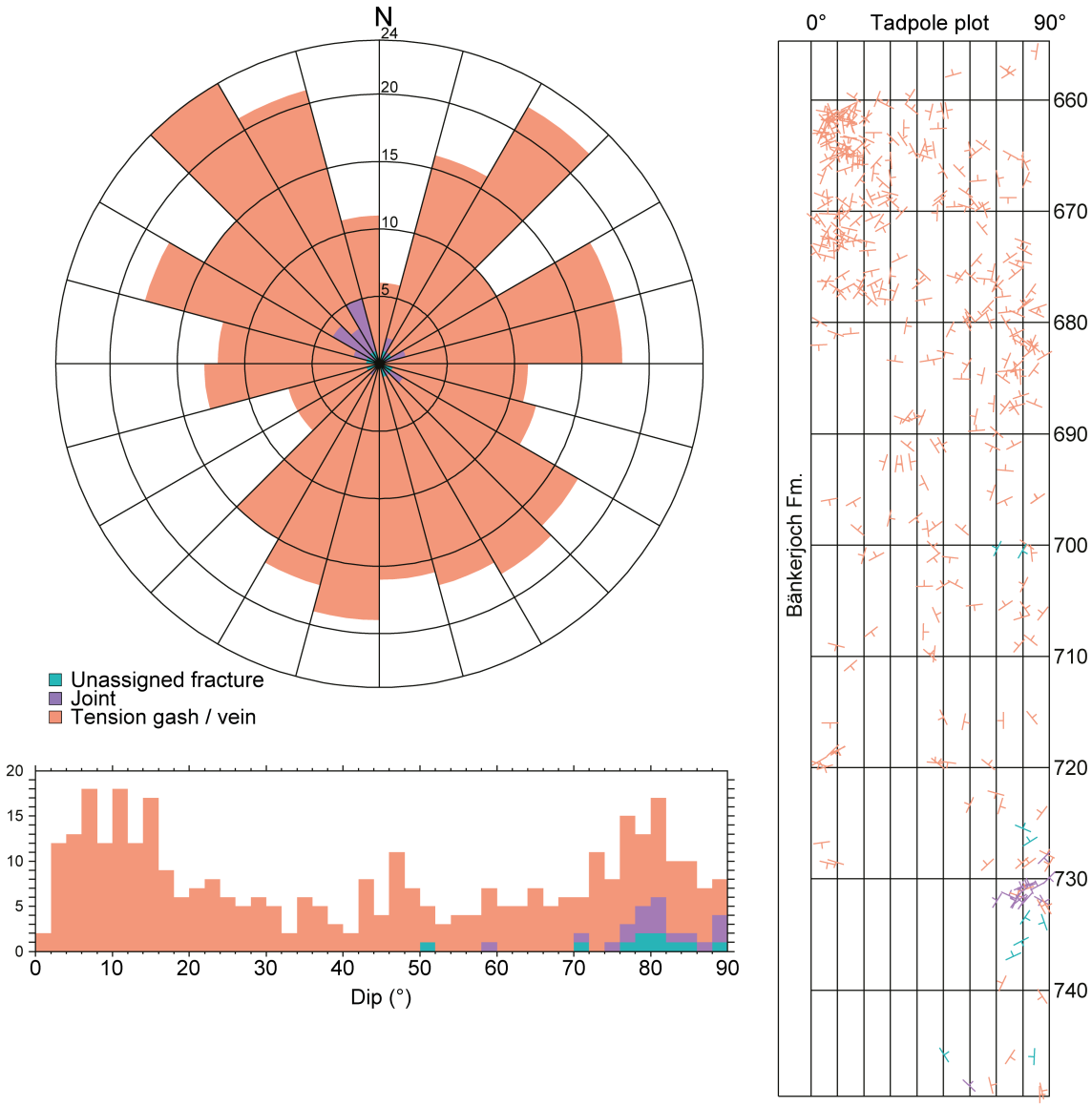

Fig. 4-57: Dip azimuth rose diagram, dip histogram and depth plot of tension gashes / veins, joints and unassigned fractures (Bänkerjoch Formation)

Unassigned fractures (n = 10), joints (n = 18) and tension gashes / veins (n = 332).

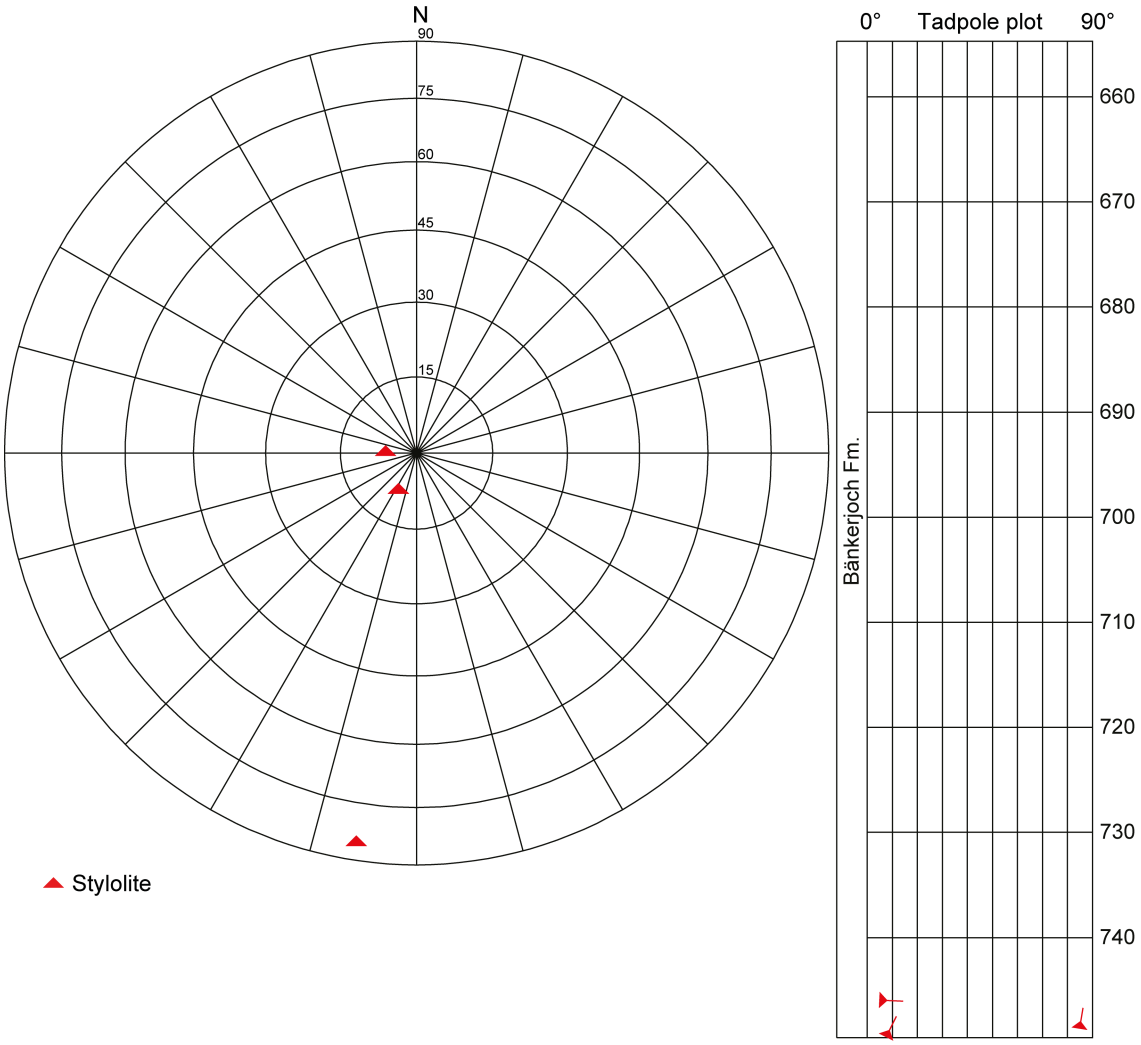

Fig. 4-58: Stereogram and depth plot of stylolites (Bänkerjoch Formation; n = 3)

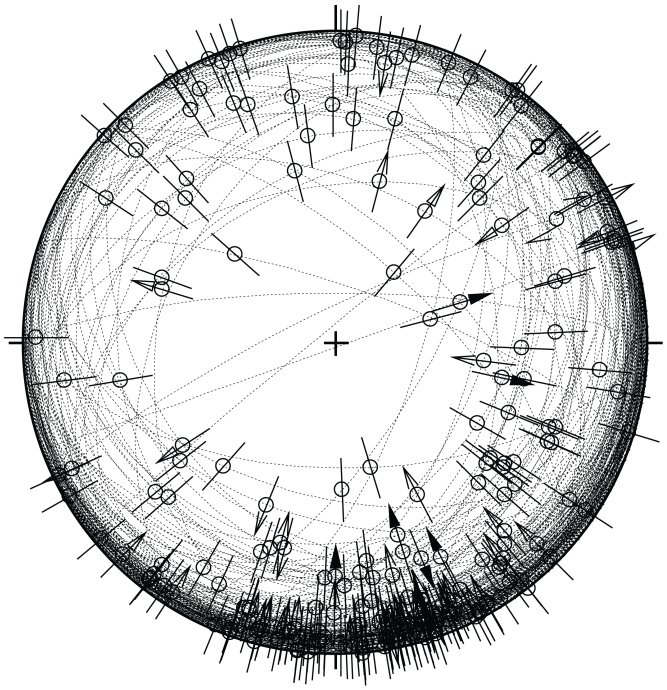

Fig. 4-59: Stereogram of striations on fault planes, including multiple lineations on a single fault plane (Bänkerjoch Formation; n = 250)

4.6 Muschelkalk

The Muschelkalk (749.52 m to final depth at 829.88 m MD [log depth]) shows a high density of all types of structures. The dominant structures are stylolites followed by mirror-like fault planes and tension gashes. In addition, an abundance of mm- to cm-sized open pores (vugs) was observed. Only the data for oriented cores are presented.

4.6.1 Schinznach Formation

The orientations and spatial distributions of structures observed in the Schinznach Formation (749.52 m to 821.09 m MD [log depth]) are shown in Figs. 4-60 to 4-66. The Schinznach Formation displays a high density of all structure types. Most fault planes and stylolites have shallow dip angles towards the SE to SW. In contrast, tension gashes and fractures show a predominant subvertical dip directed towards the E or W.

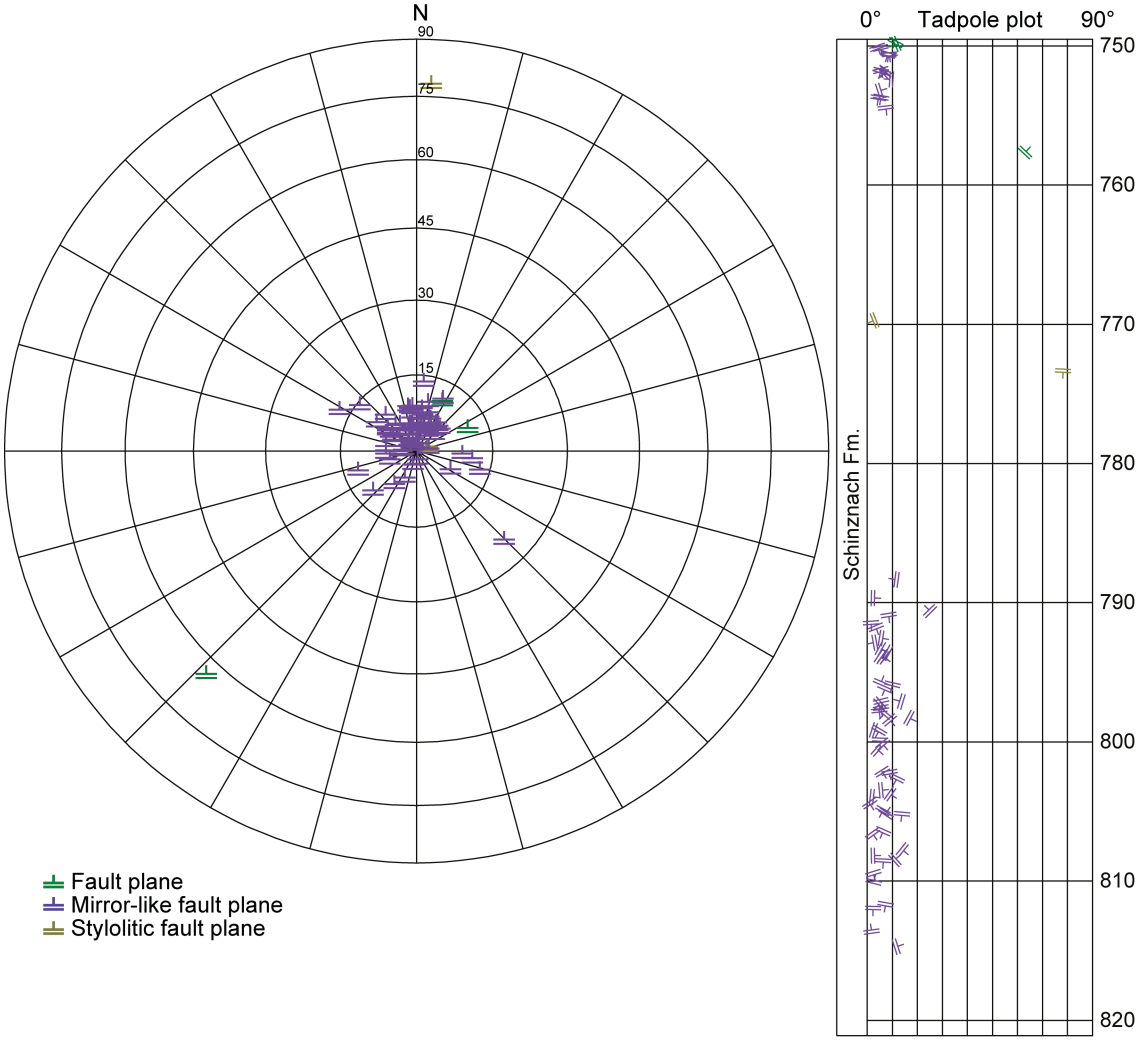

Fig. 4-60: Stereogram and depth plot of fault planes (Schinznach Formation)

Fault planes (n = 3), mirror-like fault planes (n = 65) and stylolitic fault planes (n = 2).

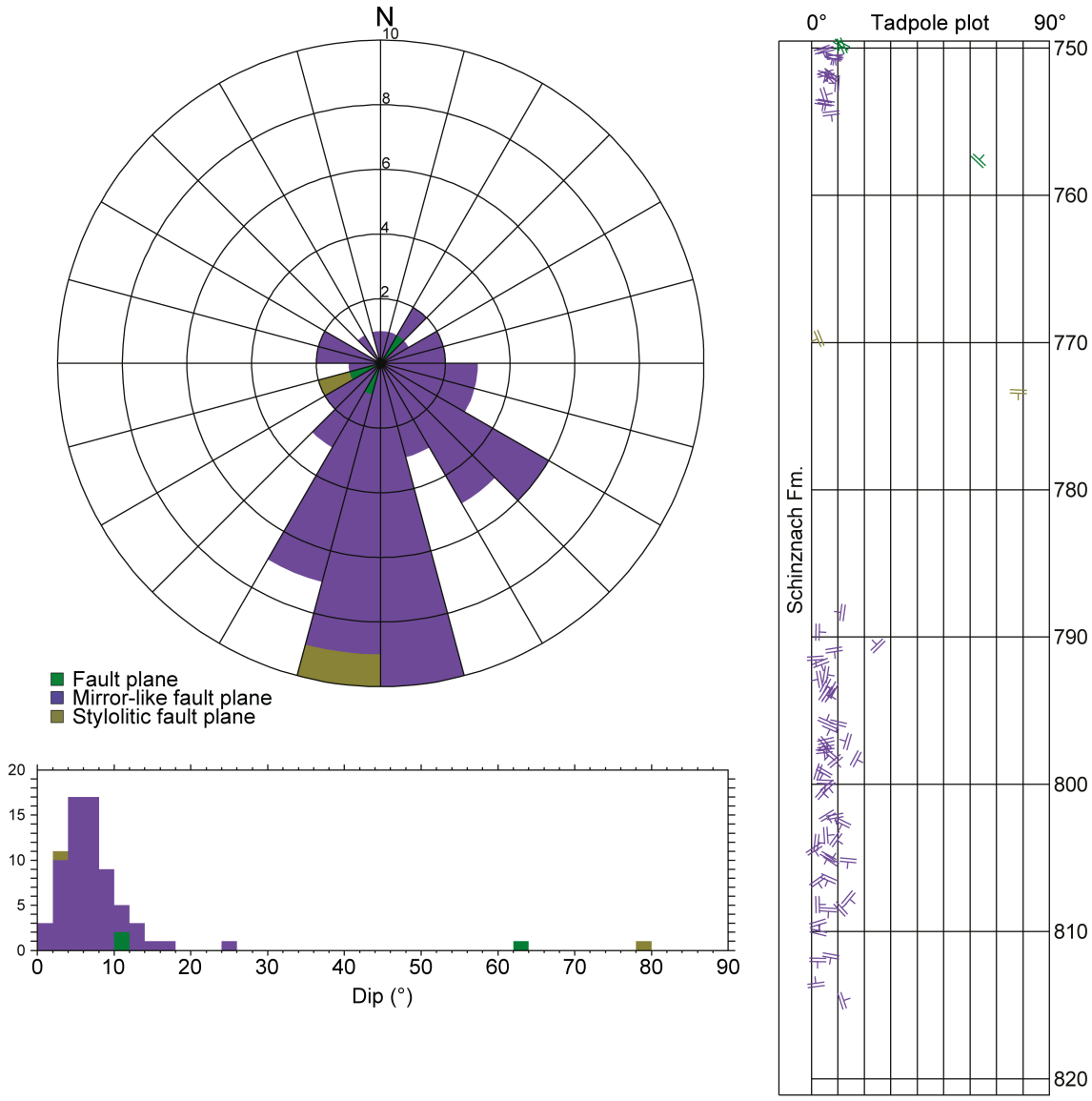

Fig. 4-61: Dip azimuth rose diagram, dip histogram and depth plot of fault planes (Schinznach Formation)

Fault planes (n = 3), mirror-like fault planes (n = 65) and stylolitic fault planes (n = 2).

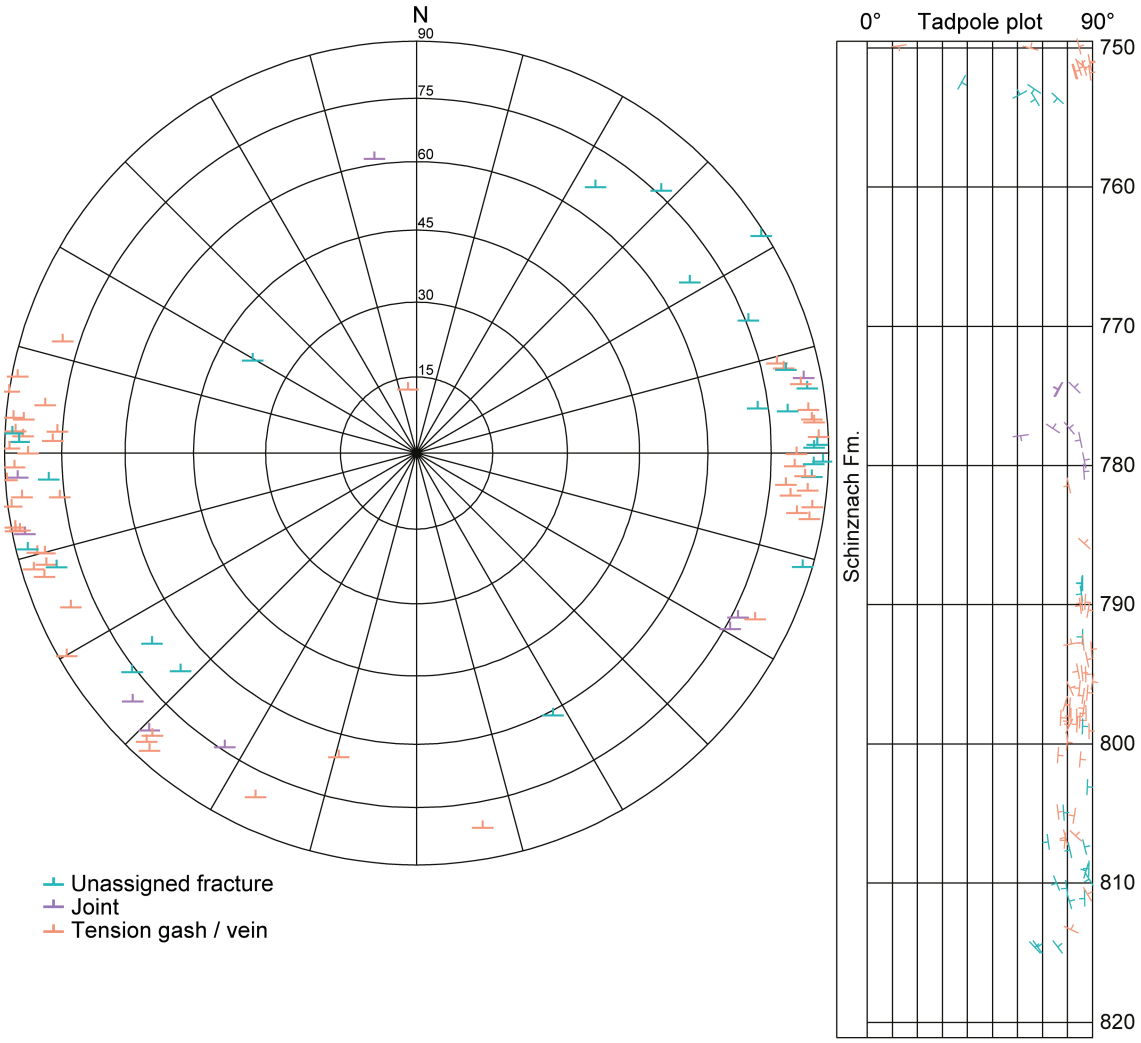

Fig. 4-62: Stereogram and depth plot of tension gashes / veins, joints and unassigned fractures (Schinznach Formation)

Unassigned fractures (n = 25), joints (n = 9) and tension gashes / veins (n = 51).

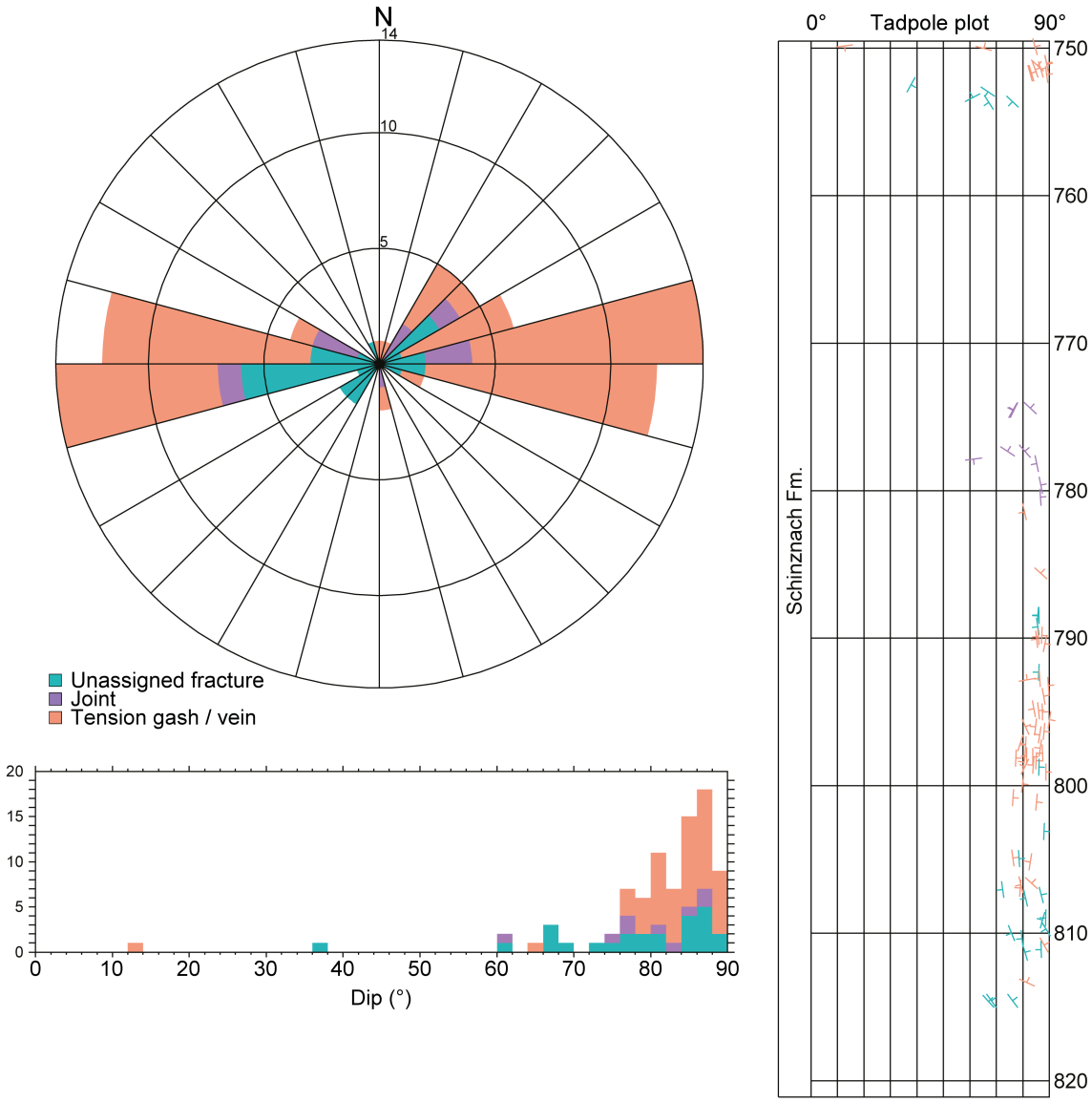

Fig. 4-63: Dip azimuth rose diagram, dip histogram and depth plot of tension gashes / veins, joints and unassigned fractures (Schinznach Formation)

Unassigned fractures (n = 25), joints (n = 9) and tension gashes / veins (n = 51).

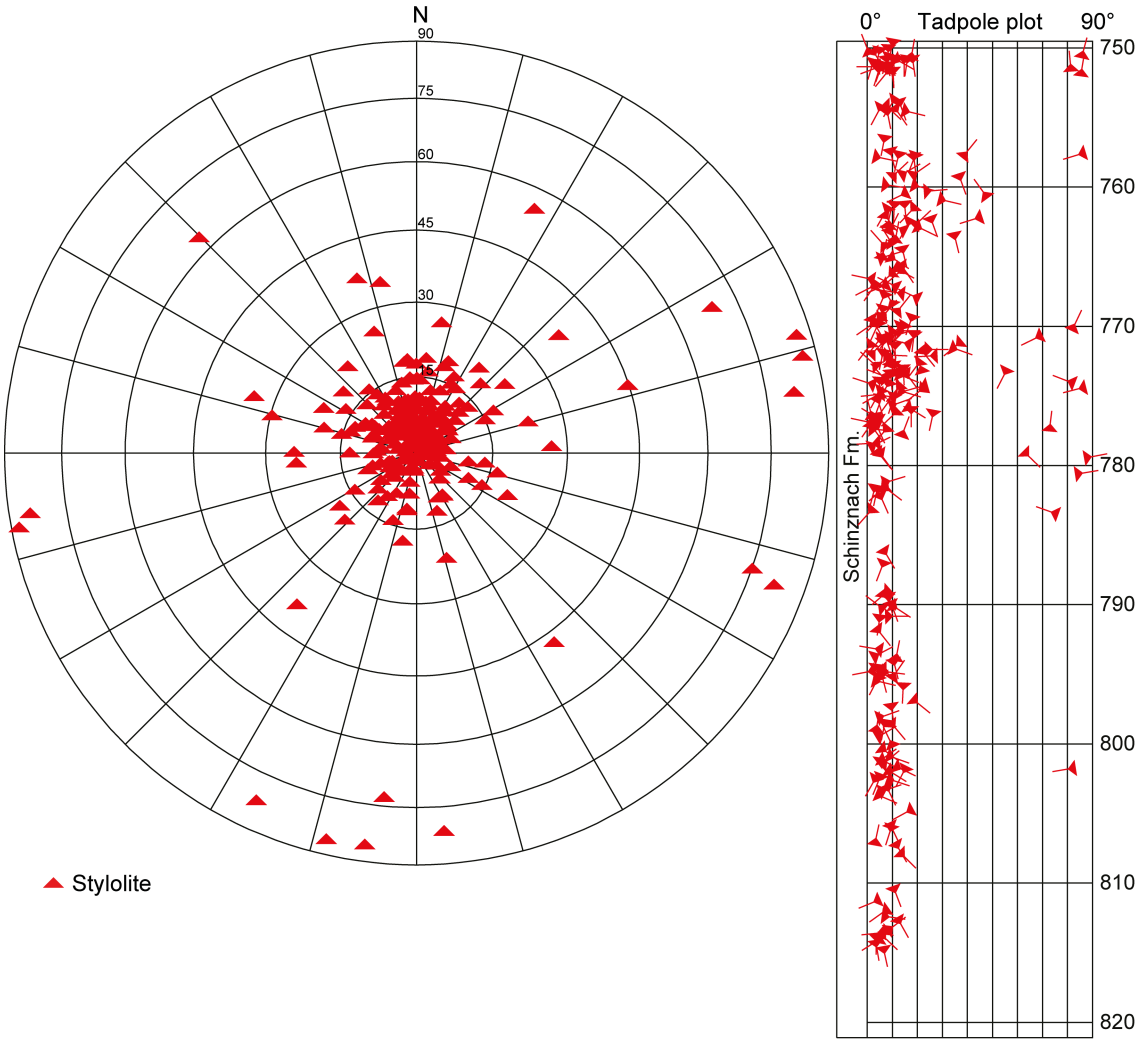

Fig. 4-64: Stereogram and depth plot of stylolites (Schinznach Formation; n = 243)

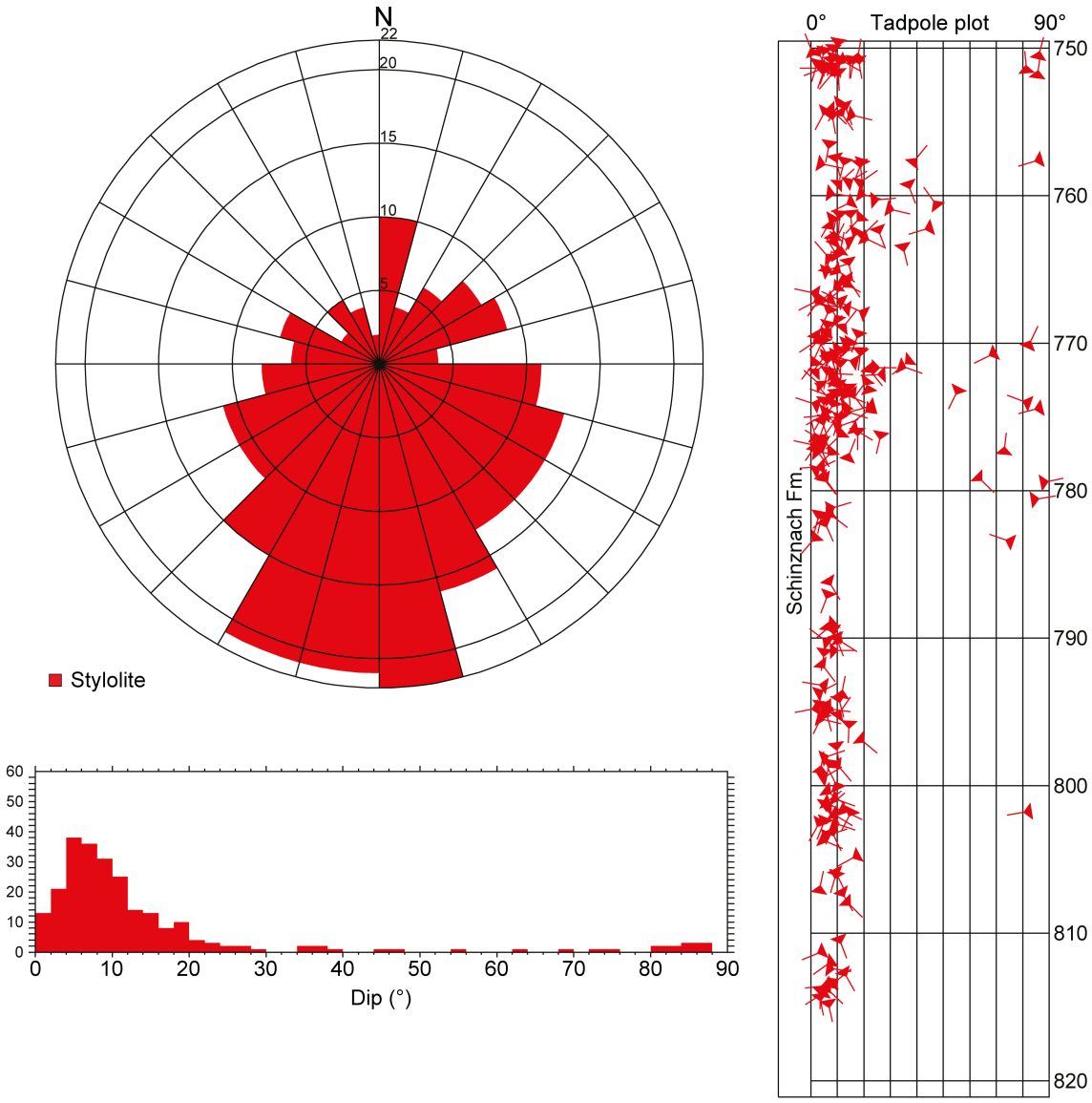

Fig. 4-65: Dip azimuth rose diagram, dip histogram and depth plot of stylolites (Schinznach Formation; n = 243)

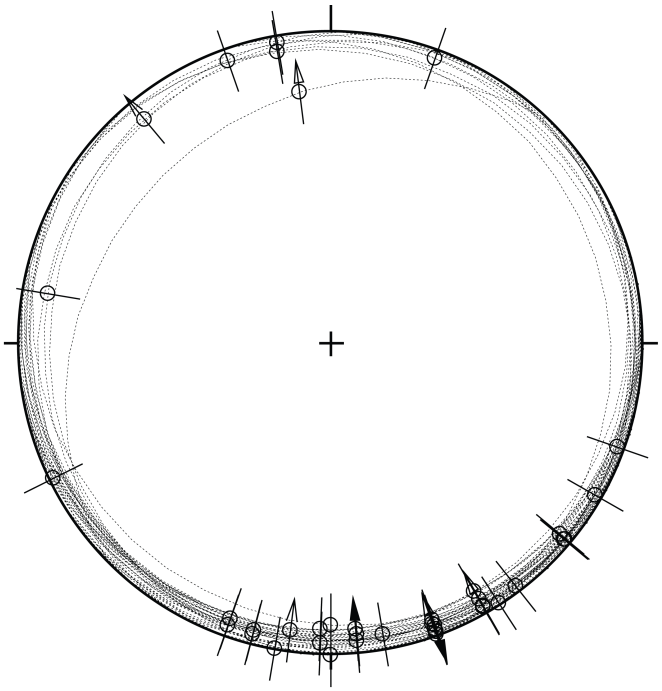

Fig. 4-66: Stereogram of striations of fault planes, including multiple lineations on a single fault plane (Schinznach Formation; n = 41)

4.6.2 Zeglingen Formation

Only the upper part of the Zeglingen Formation was cored (821.09 m to 829.88 m MD [log depth]). Due to poor FMI quality, this short, cored interval could not be oriented. Therefore, no diagrams for orientations and spatial distributions of the structures are presented. However, this interval showed a moderate density of subhorizontal mirror-like fault planes and steep tension gashes. An abundance of mm- to cm-sized vugs / open pores was also observed.

5 Main structural findings

Among the relevant geological features within the studied cored interval from 260.00 m to 829.88 m MD (log depth) presented in Chapters 3 and 4, a few particularly prominent structures and zones deserve a more detailed examination and are therefore described in the following sections.

5.1 Single fracture at 351.70 m MD

Drilling fluid / mud losses were detected during the drilling operations in BOZ2-1. A total of 83 m^3 mud loss (*cf.* Dossier I) occurred at a depth of 351.70 m MD (log depth) in the Hauptrogenstein and corresponds to a fracture that was observed in both the UBI / FMI logs and the drill core (see purple lines in Fig. 5-1). In the FMI and UBI images the subvertical fracture, categorised as a joint, has a conductive image response confirming its open character (Fig. 5-1). In the core, the joint is only 30 cm long and has a steep dip (88°) towards the WSW (246°). No striations or indications of shear were observed on the joint plane. The fact, that only a short section of the joint was captured in the core let conclude, that this steep feature has local irregularities. It further visualises, that especially with steep fractures, it is possible to detect them on the borehole image but not on the core.

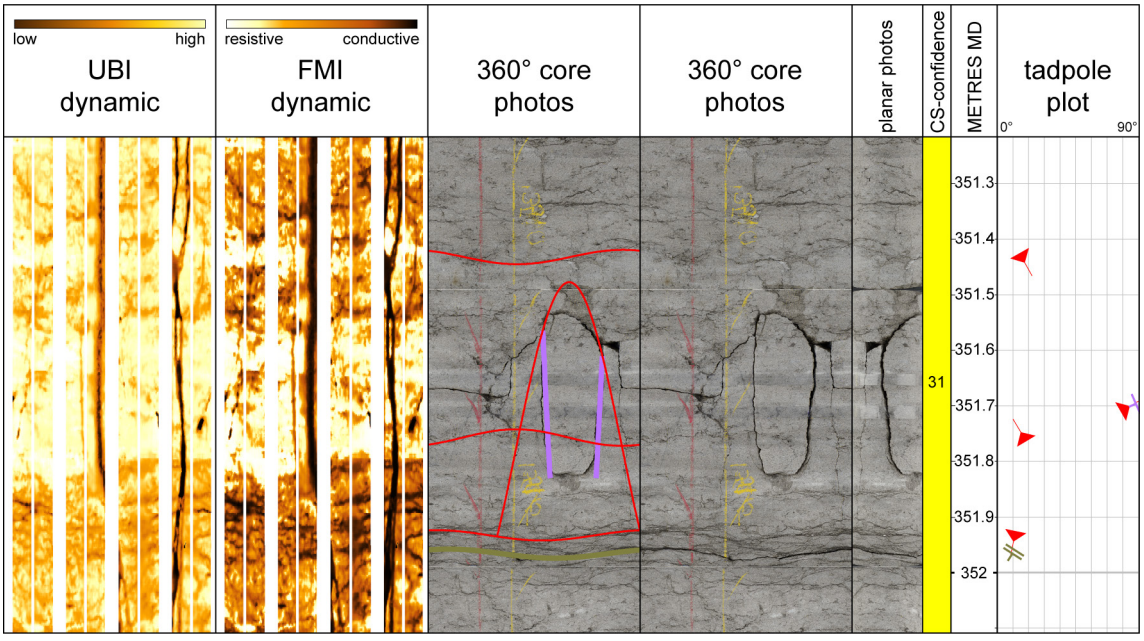

Fig. 5-1: Single joint at 351.70 m MD (log depth)

The joint surrounded by stylolites is located in the Hauptrogenstein. It appears conductive (dark) in both the FMI and UBI images (left track).

5.2 Deformation zone in the Opalinus Clay between 509.03 m and 510.74 m MD

A deformation zone was encountered in the Opalinus Clay from 509.03 m to 510.74 m MD (log depth; see Fig. 5-2). This zone is 171 cm thick and is characterised by disturbed bedding and numerous fault planes. The latter form a distinct fault zone within the specified depth interval. The deformation zone is characterised by shallow to subhorizontal bedding dipping towards the E to SE. Above and below this deformation zone the dip directions have a preferential orientation towards the SE and S with dip angles lower than 10°.

The majority of the structures interpreted within this zone are fault planes and mirror-like fault planes (n = 28). Most fault planes are mineralised with very thin synkinematic calcite fillings generally not exceeding 0.5 mm in thickness and correlating with the FMI image. They often do not crosscut the whole core and terminate on steeper fault planes. The mirror-like fault planes are not mineralised.

Striations could be measured on nearly all fault planes and mirror-like fault planes. Most of the striations are dip-slip. Within the deformation zone the fault planes and mirror-like fault planes dip predominantly towards the W (Figs. 5-3 and 5-4). Their dip angles vary from 3° to 76°. In contrast, the fault planes and mirror-like fault planes above and below the deformation zone strike in a NE-SW direction with striations dipping towards the N or S (Figs. 5-3, 5-4 and 5-5). The shear sense along the fault planes is generally reverse, except for mirror-like fault planes which tend to show a trend of normal shear sense.

A dense network of fault planes with varying dip angles and rotated bedding planes forms an additional distinct fault zone within the deformed interval; the fault zone is several cm thick and crosscuts the core from 510.26 m to 510.74 m MD (log depth). The fault zone is characterised by dip angles ranging from 40° to 60° towards the W. The fault density in this interval is high (14 faults per metre) with an internal degree of disintegration equivalent to FDC 2.

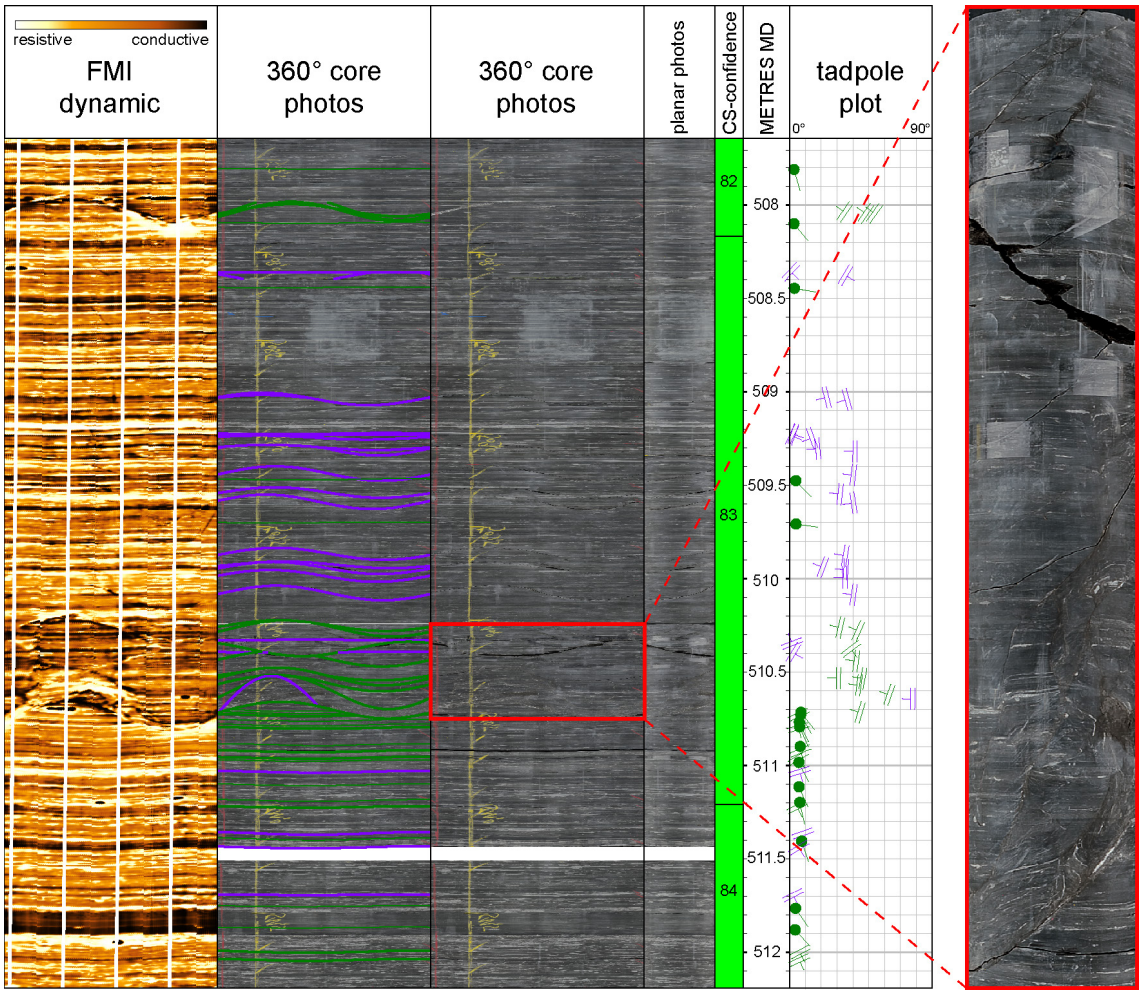

Fig. 5-2: Overview plot of the Opalinus Clay with the well visible deformation zone from 509.03 m to 510.74 m MD (log depth)

Note the fault zone on the right image from 510.26 m to 510.74 m MD (log depth).

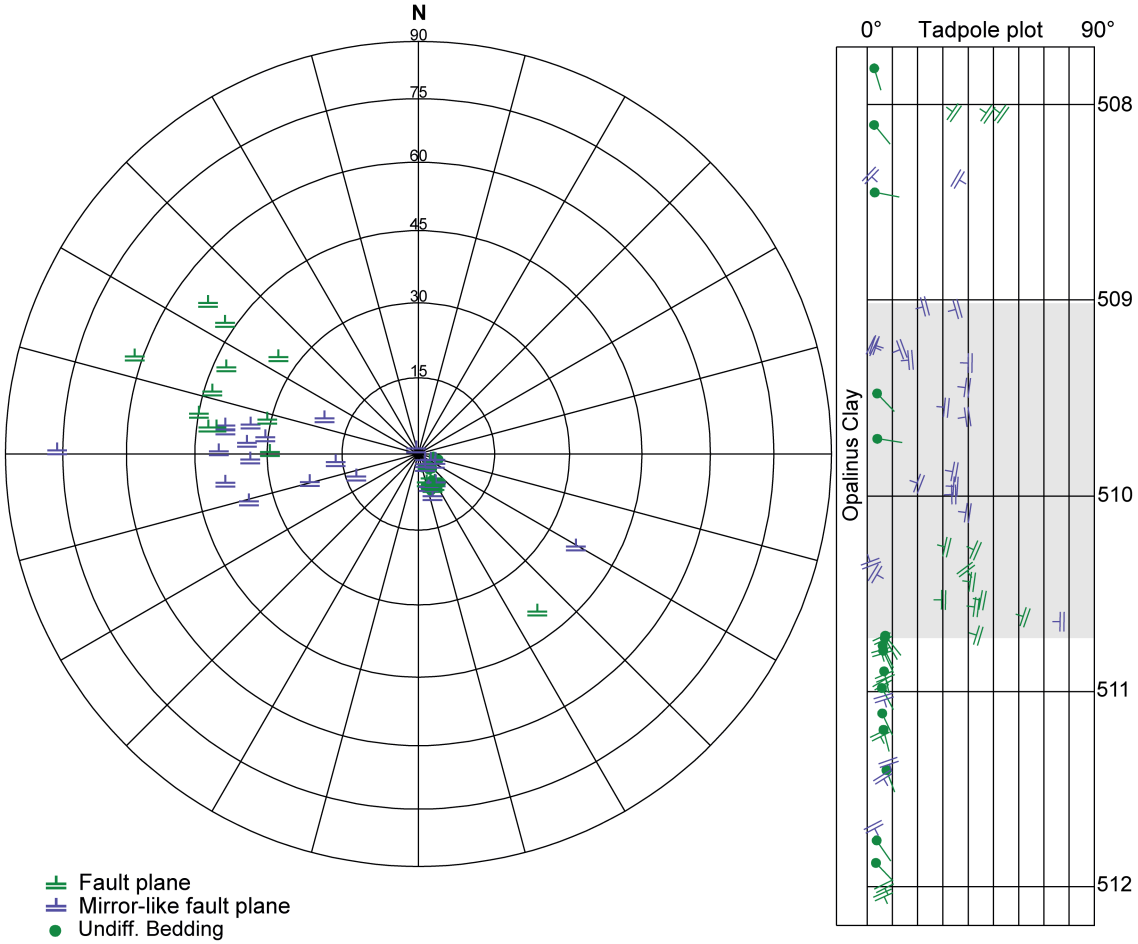

Fig. 5-3: Stereogram and depth plot of fault planes from the depth interval 507.7 m to 512.2 m MD (log depth)

Fault planes (n = 19), mirror-like fault planes (n = 24) and bedding planes (n = 16). The deformation zone is indicated by a grey bar.

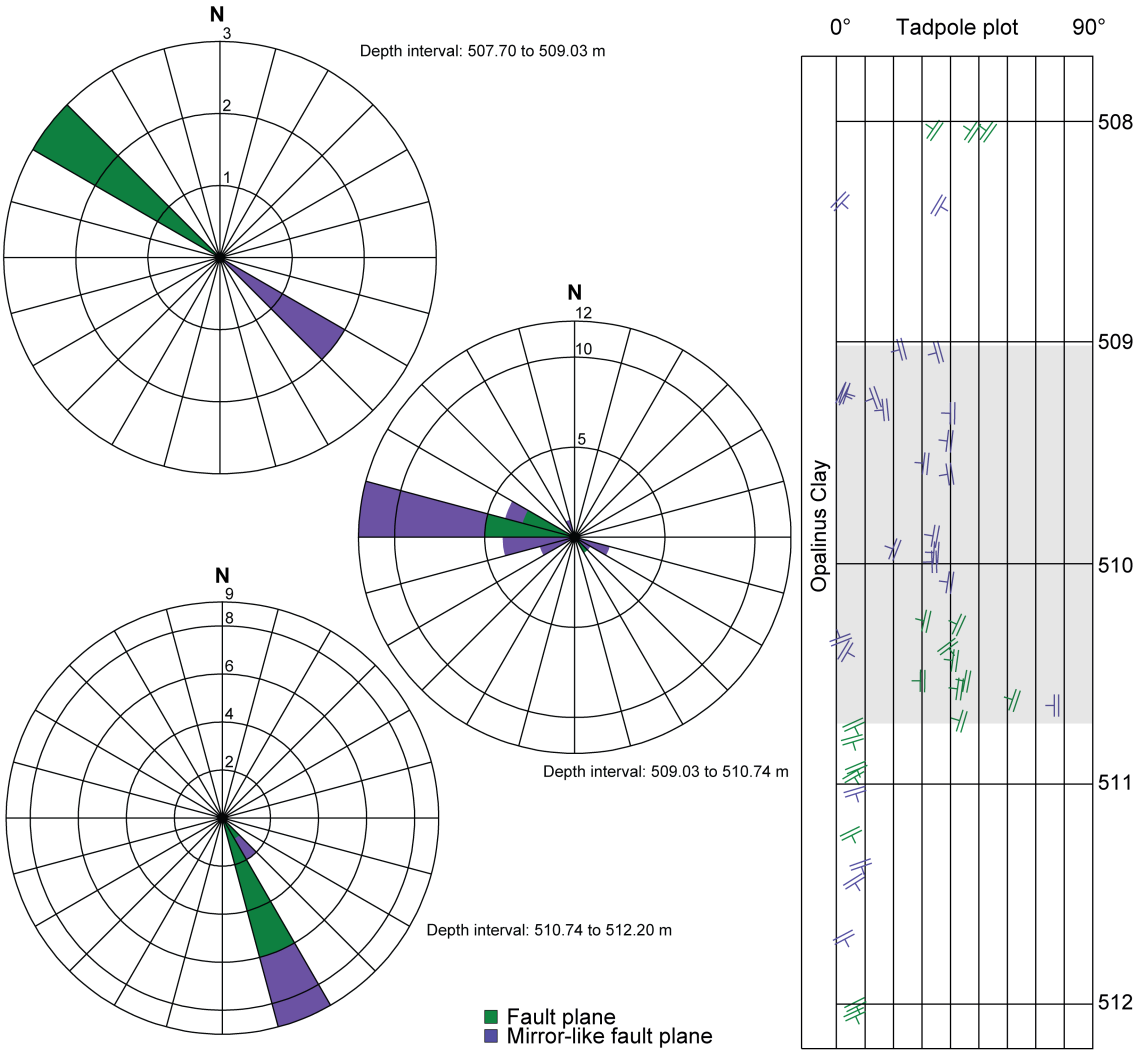

Fig. 5-4: Dip azimuth rose diagrams showing dip directions and depth plot of fault planes from the depth interval 507.7 m to 512.2 m MD (log depth)

The rose diagrams are given for the fault planes above, within and below the deformation zone from 509.03 m to 510.74 m MD (log depth). Fault planes (n = 19) and mirror-like fault planes (n = 24). The zone of deformation is indicated by a grey bar.

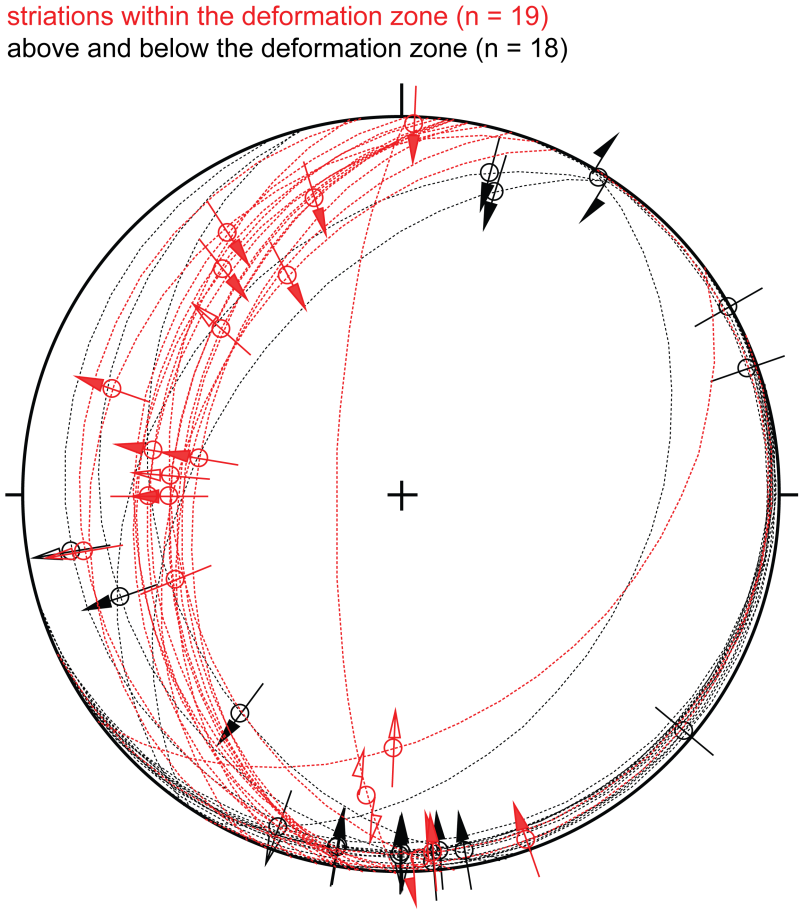

Fig. 5-5: Stereogram of fault planes and associated striations within (red) and around (black) the deformation zone

Interval investigated: from 507.7 m to 512.2 m MD (log depth); n = 37.

5.3 Deformation zone in the Opalinus Clay between 530.51 m and 533.22 m MD

A second deformation zone in the Opalinus Clay was encountered from 530.51 m to 533.22 m MD (log depth) with a fault zone between 530.51 m and 532.25 m MD (log depth; Fig. 5-6). This 271 cm-thick zone is characterised by disturbed bedding and numerous fault planes. The bedding in the Opalinus Clay is generally subhorizontal with dip directions towards the SE. From 527 m MD (log depth) downwards to the top of the deformation zone, the bedding orientation changes and shows dip azimuth values of approximately 30° to 80° and dip angles between 3° and 6°. Within the deformation zone the bedding dips steeper (dip angles between 4° and 13°) and directed towards the NNE to NE. Below the deformation zone, the bedding rotates back to the regional trend towards SE with dip angles between 3° and 4°. The abrupt changes in bedding orientation correlate with the boundaries of the deformation.

All structures interpreted within this zone are fault planes (n = 26) except for one mirror-like fault plane observed at the base. Several fault planes correlate with the FMI images, however they often do not crosscut the whole drill core. Most fault planes were intact and are mineralised with very thin fibrous or synkinematic calcite (not exceeding 1 mm in thickness; Fig. 5-7). The fibrous mineralisation is oriented perpendicular to the structure. Synkinematic calcite generally correlates with a reverse sense of shear, while fibrous calcite correlates with normal faulting.

Within the deformation zone from 530.51 m to 532.25 m MD (log depth) the fracture density is high (10 faults per metre) with an internal degree of disintegration equivalent to FDC 2

Normal faulting is observed on 13 fault planes while 6 fault planes show reverse faulting. The fault planes with normal faulting are most likely of synsedimentary origin and were reactivated later, allowing the fibrous calcite to precipitate. These fault planes show displacements of a few mm along the fault plane and often do not crosscut the core. They display a dominant dip towards SE to S with a mean of dip angles of approximately 30° (Figs. 5-8 and 5-9). In contrast to the fibrous mineralised fault planes, fault planes with synkinematic calcite show variable dip azimuths, subhorizontal dip angles and often a reverse sense of shear.

Because the majority of fault planes are intact / closed, only few striations could be measured. The striations mostly indicate dip-parallel slip (Fig. 5-10) and the majority dips towards the SE to S. The dip angles vary from 1° to 20°.

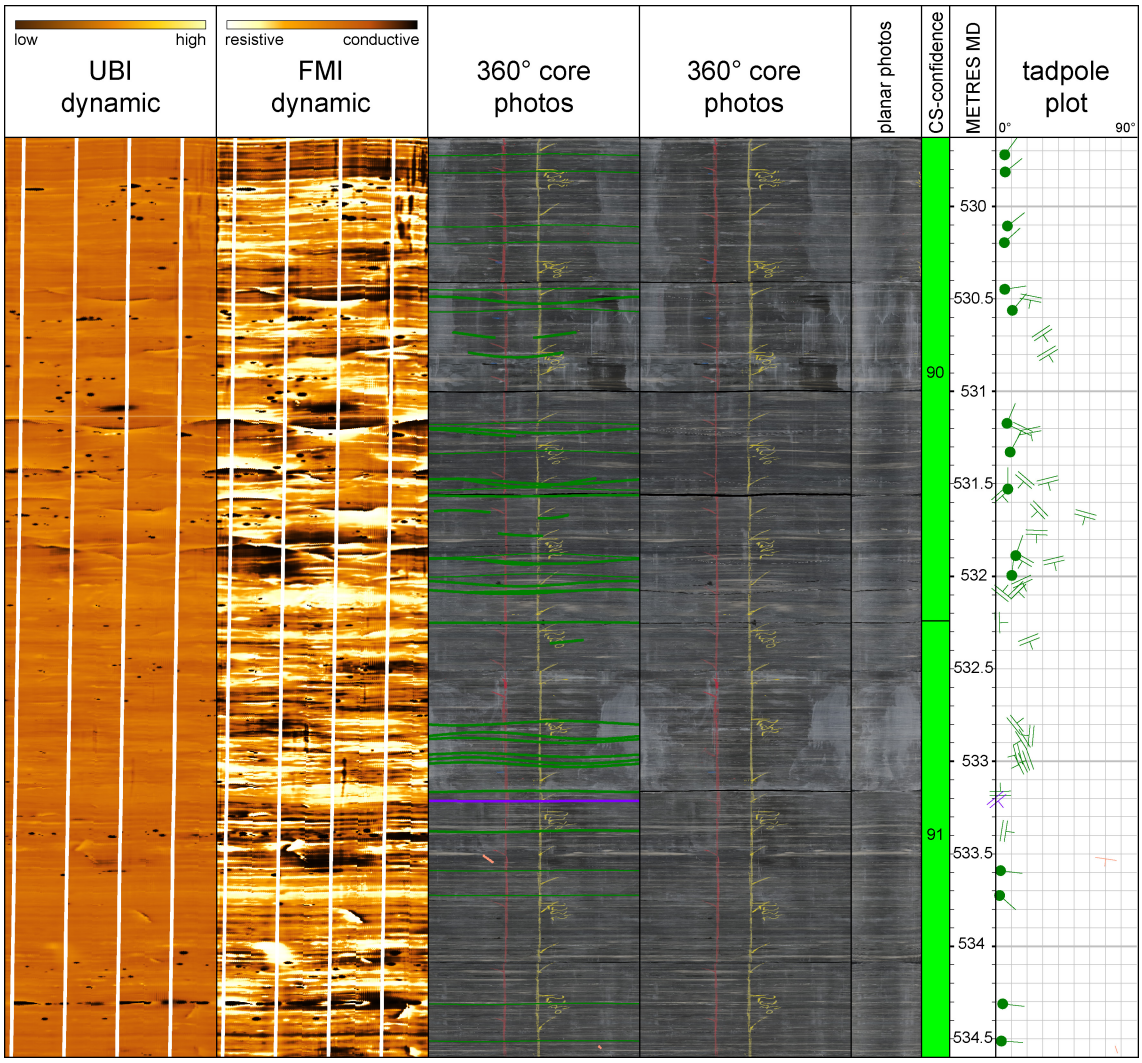

Fig. 5-6: Overview plot of the deformed Opalinus Clay from 530.51 m to 533.22 m MD (log depth)

Note the change in bedding dip azimuths within the deformation zone.

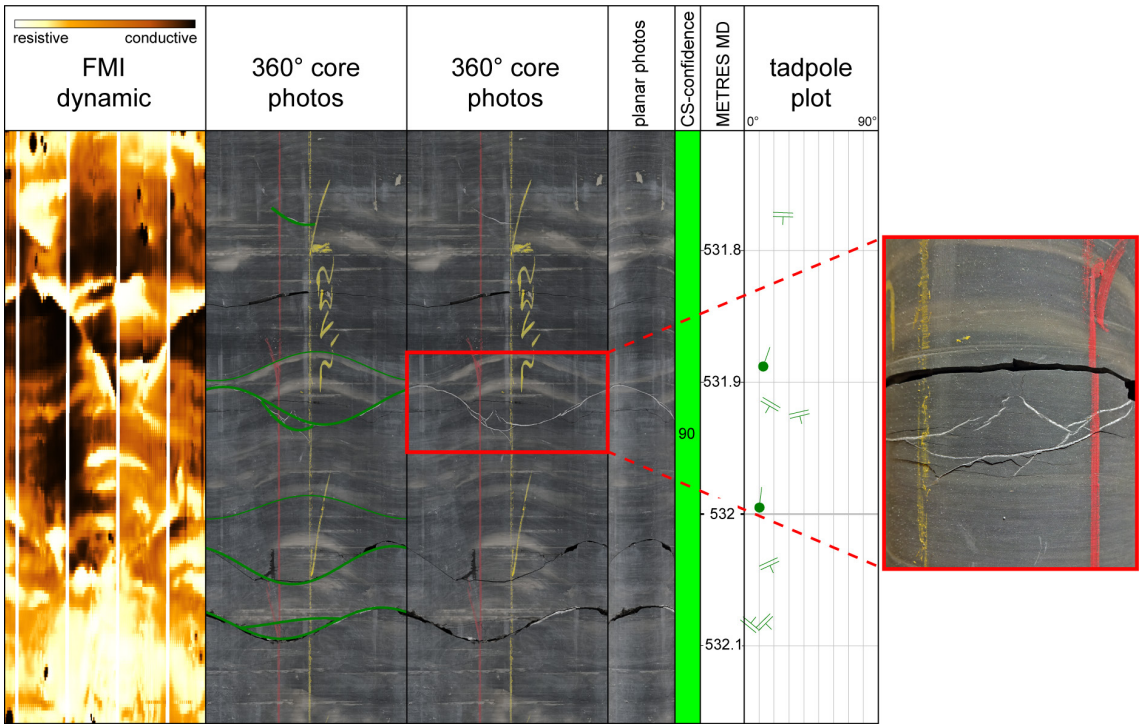

Fig. 5-7: Example of mineralised fault plane within the Opalinus Clay at 531.9 m MD (log depth)

Note the clear truncation of beds and the mm- to cm-scale displacements related to normal faults at 531.9 m MD (log depth). The 1 mm thick mineralisation is characterised by fibrous calcite crystals oriented perpendicular to the plane.

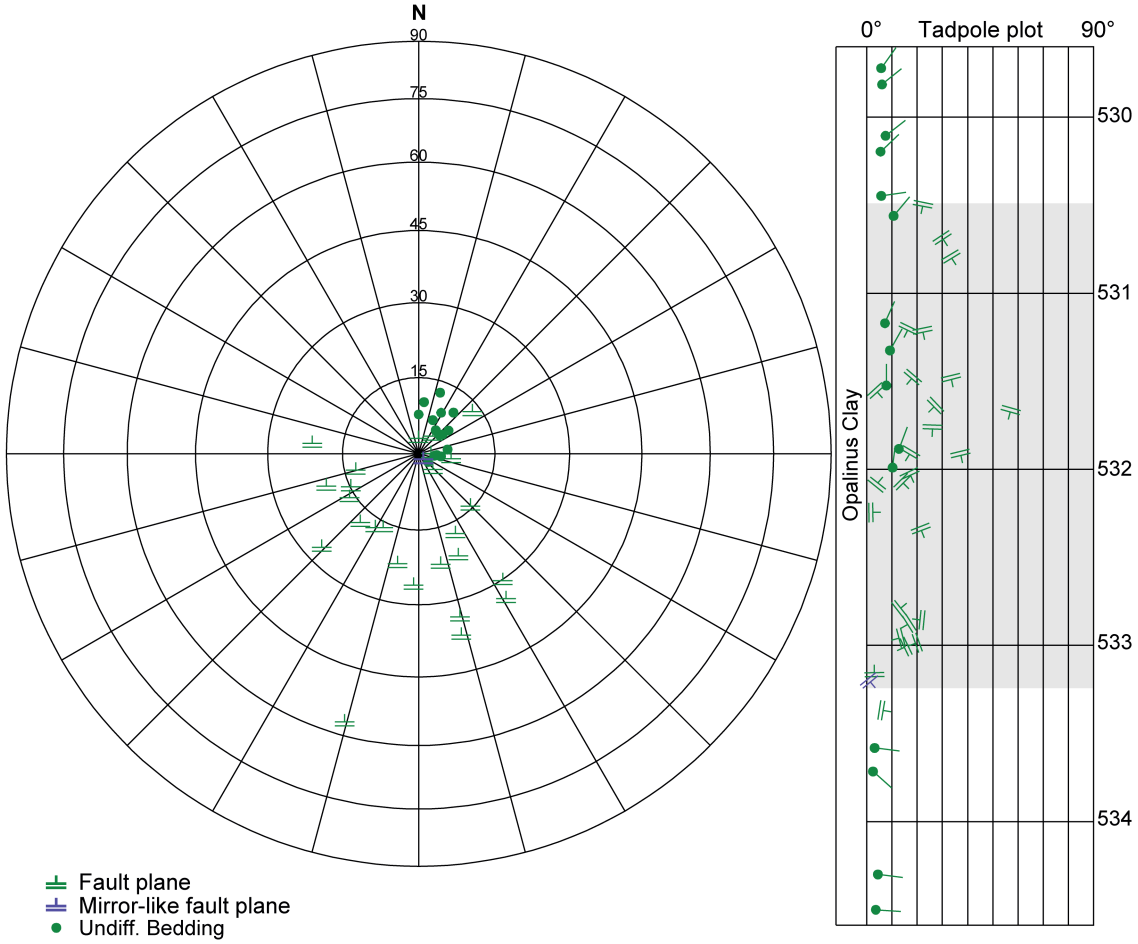

Fig. 5-8: Stereogram of fault planes and bedding around and within the deformed Opalinus Clay, from the depth interval 529.6 m to 534.6 m MD (log depth)

Fault planes (n = 26), mirror-like fault planes (n = 1) and bedding (n = 15). The zone of deformation is indicated by a grey bar.

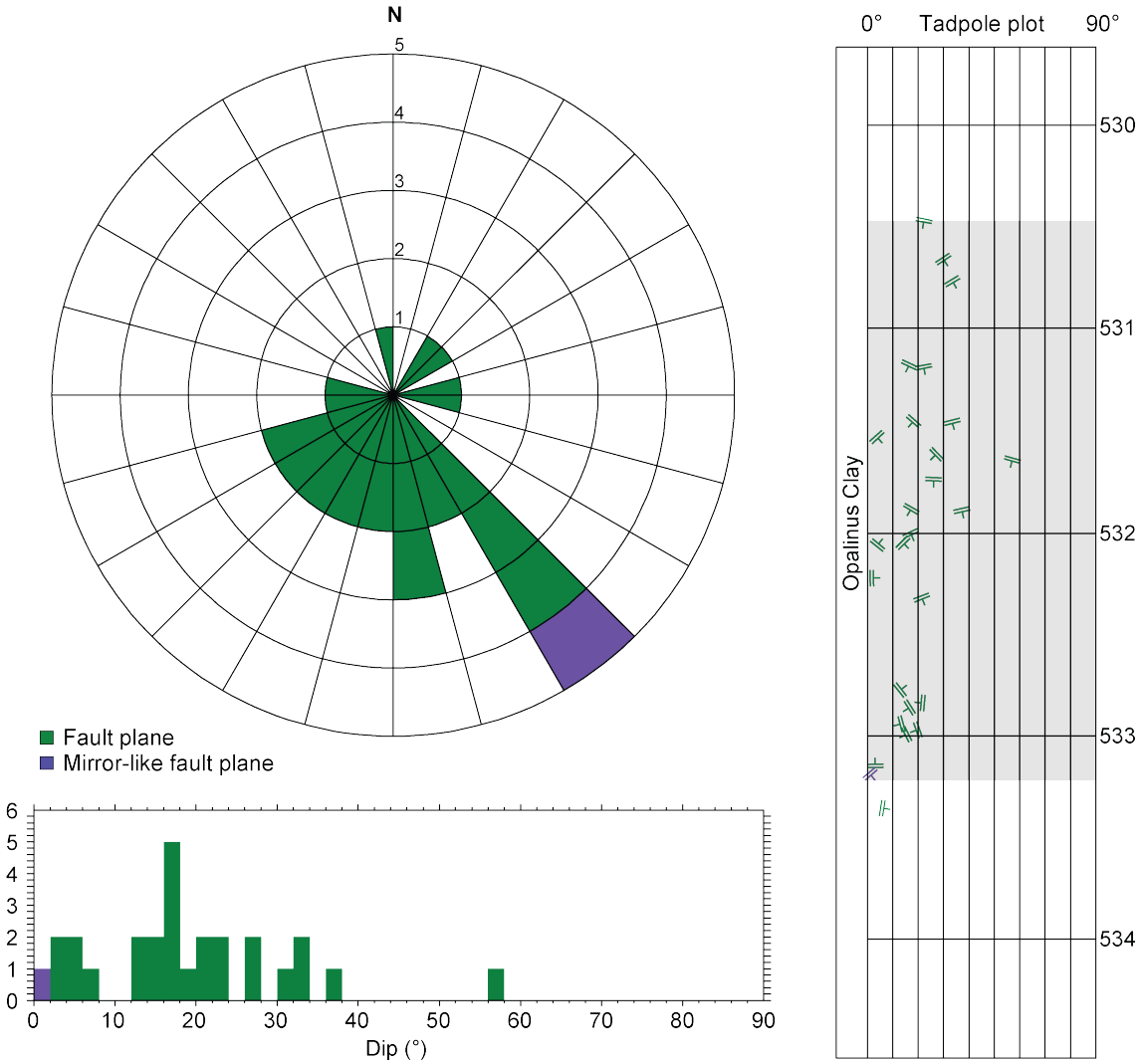

Fig. 5-9: Dip azimuth rose diagram, dip histogram and depth plot of fault planes within the deformed Opalinus Clay from the depth interval 529.6 m to 534.6 m MD (log depth)

Fault planes (n = 26), mirror-like fault planes (n = 1). The zone of deformation is indicated by a grey bar.

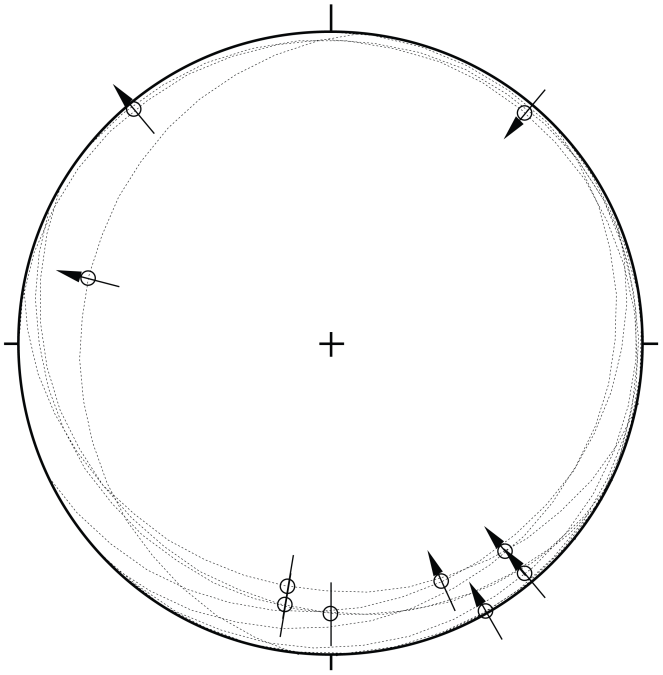

Fig. 5-10: Stereogram of fault planes and associated striations within the deformation zone
Interval investigated: from 530.51 m to 533.22 m MD (log depth); n = 11.

6 References

Barton, N. (1976): The shear strength of rock and rock joints. Int. J. Rock. Mech. Min. Sci. & Geomech. Abstr. 13/9, 255-279.

Barton, N. & Choubey, V. (1977): The shear strength of rock joints in theory and practice. Rock mechanics 10/1-2, 1-54.

Bauer, H., Schröckenfuchs, T. & Decker, K. (2016): Hydrogeological properties of fault zones in a karstified carbonate aquifer (Northern Calcareous Alps, Austria). Hydrogeology Journal 24, 1147-1170.

Ebert, A. & Decker, K. (2019): Structural Analysis Manual. Nagra Arbeitsbericht NAB 19-12.

Hancock, P.L. (1985): Brittle microtectonics: principles and practice. J. Structural Geology 7/3-4, 437-457.

Isler, A., Pasquier, F. & Huber, M. (1984): Geologische Karte der zentralen Nordschweiz 1:100'000. Herausgegeben von der Nagra und der Schweiz. Geol. Komm.

Nagra (2014): SGT Etappe 2: Vorschlag weiter zu untersuchender geologischer Standortgebiete mit zugehörigen Standortarealen für die Oberflächenanlage – Geologische Grundlagen. Dossier II – Sedimentologische und tektonische Verhältnisse. Nagra Technischer Bericht NTB 14-02.

Passchier, C.W. & Trouw, R.A.J. (1996): Microtectonics. Springer, 289 pp.

Peacock, D.C.P., Nixon, C.W., Rotevatn, A. & Sanderson, D.J. (2016): Glossary of faults and other fracture networks. J. Structural Geology 92, 12-29.

Pietsch, J. & Jordan, P. (2014): Digitales Höhenmodell Basis Quartär der Nordschweiz – Version 2013 (SGT E2) und ausgewählte Auswertungen. Nagra Arbeitsbericht NAB 14-02.